

Master Thesis

Master in Electronics, Robotics and Automation  
Engineering

Trabajo Fin de Máster

Máster Universitario en Ingeniería Electrónica,  
Robótica y Automática

Energy management system of a zero-emission  
vehicle charging station based on MPC

Sistema de gestión de energía para una estación  
de carga de vehículos cero emisiones basado en  
MPC

Author: Manuel Mora Nieto

Supervisor: Carlos Bordons Alba

**Dep. de Ingeniería de Sistemas y Automática**  
**Escuela Técnica Superior de Ingeniería**  
**Universidad de Sevilla**

Sevilla, 2021





Trabajo Fin de Máster  
Máster Universitario en Ingeniería Electrónica, Robótica y Automática

# **Energy management system of a zero-emission vehicle charging station based on MPC**

Author:

Manuel Mora Nieto

Supervisor:

Carlos Bordons Alba

Catedrático de Universidad

Dep. de Ingeniería de Sistemas y Automática

Escuela Técnica Superior de Ingeniería

Universidad de Sevilla

Sevilla, 2021



Trabajo Fin de Máster: Energy management system of a zero-emission vehicle charging station based on MPC

Author: Manuel Mora Nieto

Supervisor: Carlos Bordons Alba

El tribunal nombrado para juzgar el Proyecto arriba indicado, compuesto por los siguientes miembros:

Presidente:

Vocales:

Secretario:

Acuerdan otorgarle la calificación de:

El Secretario del Tribunal

Fecha:



*To my family*

*To my teachers and professors*





# Acknowledgments

---

It was almost half and a year when I decided to start a new *Master of Science* while I was also finishing the *Industrial Engineering Master*. It was not an easy decision but I have no doubts that I got right. Therefore, I would like to thank my family for their patience. They have been my main support during the difficult pandemic times.

Thanks also to all my colleagues in the laboratory. They have made easier the work done.

Finally, I would like to express my gratitude to my advisor Carlos. I am continuously learning from him.

*Manuel Mora Nieto*

*Student in Escuela Técnica Superior de Ingeniería, University of Seville*

*Seville, 2021*



# Abstract

---

This work is within the lines of research of the *Automática y Robótica Industrial* group from the *Ingeniería de Sistemas y Automática Department* at *University of Seville*. In particular, it aims at serving as a base for the group contribution to the zero-emission vehicle recharging station future project, which will be held by the *Excellent Research Group ENGREEN* with the collaboration of researches from the whole *Escuela Técnica Superior de Ingeniería*.

Due to environmental goals of ENGREEN, besides inspiring the use of electric and hydrogen-based vehicles, the charging station will consume renewable energy coming from solar power. The use and management of energy storage system such as hydrogen is crucial because of uncertainty in energy production and consumption. Predictive controllers, well-known as *MPC*, are used in this work for the resolution of such a complex and multi-objective energy flow problem in that system.

Throughout this report, the microgrid is simulated in different generation and consumption scenarios, showing how a scheduler MPC, using both continuous and logic variables, and a reference tracking MPC, using only continuous variables, allow for optimal and efficient solutions. The software *Simugrid*, developed by the group itself some years ago, is used over *MATLAB/Simulink* with *Yalmip* toolbox and solver *CPLEX* for the scheduler MPC and the solver *quadprog* without *Yalmip* for the reference tracking MPC. The work described above is expected to be used in the future as a starting point for a more complex and detailed management of zero-emission vehicles charging process.



# Resumen

---

Este trabajo se encuentra dentro de las líneas de investigación del grupo *Automática y Robótica Industrial* del *Departamento de Ingeniería de Sistemas y Automática* de la *Universidad de Sevilla*. En concreto, trata de sentar las bases de la aportación de dicho grupo al futuro proyecto de estación de recarga de vehículos cero emisiones que llevará a cabo la *Unidad de Excelencia ENGREEN*, con componentes de toda la *Escuela Técnica Superior de Ingeniería*.

Debido a los fines medioambientales de dicha unidad de excelencia, además de impulsar el uso del vehículo eléctrico y del basado en hidrógeno, la estación de recarga hará uso de fuentes de energía renovable como la solar. La incertidumbre en la producción y consumo de energía hace necesario el empleo de sistemas de almacenamiento de energía como el hidrógeno y su consiguiente gestión. El flujo de potencia en estos sistemas es un problema de control complejo y multiobjetivo para cuya resolución se emplean en este trabajo técnicas de control predictivo, o más conocido como *MPC*.

A lo largo de esta memoria se describen las simulaciones de la microrred con diferentes escenarios de generación y consumo, mostrando cómo un MPC planificador, usando tanto variables continuas como lógicas, y otro de seguimiento, usando sólo variables continuas, permiten obtener una solución óptima y eficiente. Para ello se usa *MATLAB/Simulink* sobre el software *SimuGrid*, desarrollado en años anteriores por el propio grupo de investigación, con el *toolbox Yalmip* y el *solver CPLEX* para el MPC planificador y el *solver quadprog* sin *Yalmip* para el MPC de seguimiento. Lo anterior pretende emplearse en un futuro como punto de partida para una gestión más compleja y detallada del proceso de recarga de vehículos cero emisiones.

## A. Introducción

El cambio climático es un problema de actualidad según el cual muchas medidas se están tomando hoy día para tratar de reducir las emisiones. Entre ellas, destacan el fomento del uso de energías renovables y la movilidad sostenible. No es de extrañar que la movilidad sostenible para coches sea uno de los campos en mayor auge y que recibe más financiación para reducir las emisiones. De hecho, según la *Agencia Europea del Medioambiente*, el coche, y en concreto el coche que transporta un solo pasajero, es el más contaminante, como se puede ver en la Figura 0-1.

Con esto, entran en juego los sistemas de almacenamiento de energía para combinarlos con la generación renovable en las conocidas como microrredes, sistemas de producción distribuida, almacenamiento híbrido y consumo de energía para pequeña y media escala. Dentro de las microrredes, está actualmente en auge el uso del hidrógeno como sistema de almacenamiento de energía. Además, en relación a la movilidad sostenible, los vehículos eléctricos e incluso vehículos basados en hidrógeno pueden ser usados como un elemento más de la microrred, tanto para su carga como para su descarga de nuevo a la microrred usando el concepto de *Vehicle-to-Grid (V2G)*.

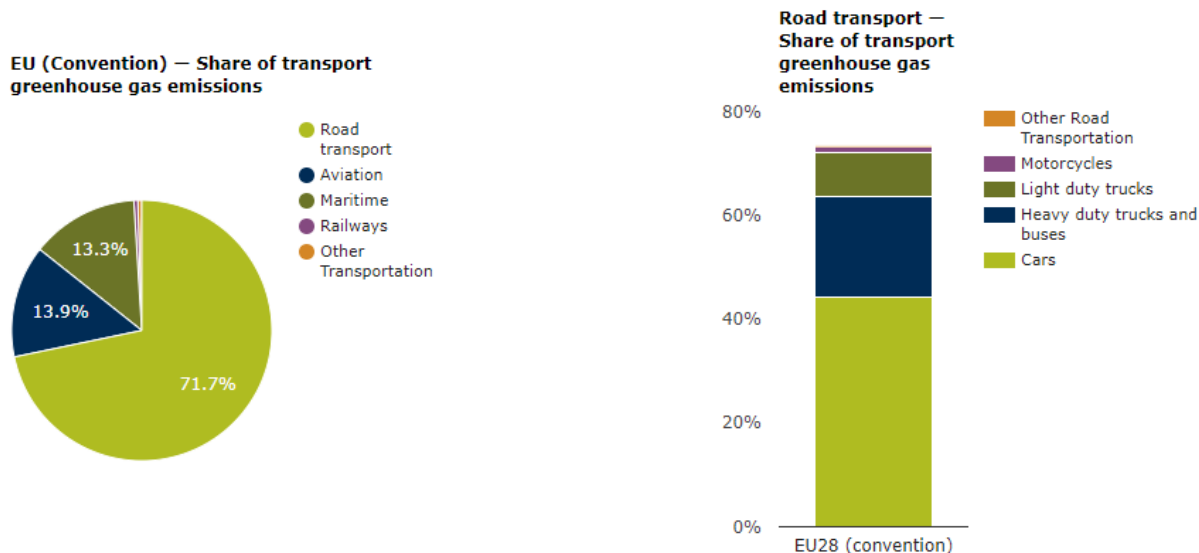


Figura 0-1. Porcentaje de emisiones de gases de efecto invernadero in el sector del transporte y detalle para el transporte por carretera (Fuente: [1])

El objetivo final de este trabajo es construir una microrred en los laboratorios de la Escuela Técnica Superior de Ingeniería de Sevilla para usarse en la recarga de vehículos de cero emisiones, incluyendo tanto vehículos eléctricos como vehículos basados en hidrógeno. Es un proyecto que aparece con una sinergia entre los departamentos de ingeniería eléctrica, energética, electrónica y de control automático, entre otros. Cada uno de ellos proporcionará su experiencia y sus equipos disponibles. La microrred estará compuesta de campos fotovoltaicos (*PV*), baterías, tecnología de hidrógeno (electrolizador, almacenamiento en hidruros metálicos y pila de combustible), supercondensador, conexión con la red eléctrica, puntos de recarga de vehículos eléctricos y puntos de recarga de vehículos basados en hidrógeno.

El objetivo de este trabajo es desarrollar una estrategia eficiente de gestión de energía para esta microrred, que será capaz de decidir el flujo de energía entre los equipos en cada instante de tiempo. Esto se hace usando dos controladores predictivos (*MPC*) que deciden el flujo de energía de una manera óptima, teniendo en cuenta las limitaciones de los equipos y los problemas de degradación. El primer controlador MPC usa las predicciones de consumo, producción y precio de la energía a cada hora para dar referencias a un segundo controlador, que actuará en una escala de tiempo del orden de segundos para corregir las desviaciones de potencia y tratar con los cambios repentinos en la producción y el consumo de energía. Estas desviaciones se verán aumentadas por una demanda extra de hidrógeno para recargar el vehículo basado en hidrógeno disponible en el laboratorio y por la demanda de potencia para el proceso de recarga de vehículos eléctricos. La salida del segundo controlador se usará en el futuro como referencias para los convertidores de potencia, los cuales actuarán en una escala de tiempo del orden de los milisegundos, pero que no han sido implementados en este trabajo.

Los controladores se prueban en simulación usando *MATLAB/Simulink* con el modelo de la microrred en *Simugrid*, una herramienta de simulación creada por el grupo de investigación de *Automatica y Robótica Industrial* hace algunos años. Para la resolución del problema de optimización, el toolbox *Yalmip* y el solver *CPLEX* se usan para el primer controlador, y el solver *quadprog* sin *Yalmip* para el segundo controlador.

Por tanto, para alcanzar los objetivos mencionados, se han llevado a cabo los siguientes pasos:

- Revisión del estado del arte, especialmente en cuanto a los campos de hidrógeno verde y estaciones de recarga de vehículos eléctricos.
- Planificación de la microrred, recogiendo toda la información necesaria de los equipos disponibles, y preparación del modelo de simulación.
- Estudio sobre estrategias de control de microrredes.
- Instalación y aprendizaje del uso del toolbox *Yalmip* con el solver *CPLEX* en *MATLAB*.

- Diseño y prueba de los controladores MPC (terciario y secundario) en simulación.
- Creación de demandas extra para la estación de carga de vehículos de cero emisiones: de hidrógeno y de potencia eléctrica.

## B. Estado del arte

Como ya se ha comentado, se lleva a cabo un estado del arte centrado, en primer lugar, en el hidrógeno verde y sus aplicaciones, incluyendo movilidad. Buena parte de la literatura usa el hidrógeno en microrredes y actualmente hay muchos proyectos activos tanto en Europa como en España en lo que se refiere a hidrógeno verde. Aún así, la tecnología de electrólisis y el proceso completo de producción de hidrógeno a partir de fuentes de energía renovable, debe mejorar en los próximos años para convertirse en una verdadera opción competitiva. Uno de los trabajos llevado a cabo hace algunos años en la Escuela Técnica Superior de Ingeniería de Sevilla fue el proyecto *Hylab*, donde se creó una microrred basada en hidrógeno para la cual se han publicado muchos trabajos de planificación y control de la misma. Buena parte de ellos se recogen en el libro que es la principal referencia para este trabajo [2] y muchos de los componentes de dicha microrred se usarán en la futura estación de recarga de vehículos cuyas bases sienta este trabajo. En cualquier caso, tanto el control del proceso de producción de hidrógeno como el control de un sistema de gestión de energía de una microrred que incluya hidrógeno, son objeto de estudio actualmente. En el caso de ese trabajo, lo segundo será llevado a cabo.

Por otro lado, el estado del arte tiene una segunda parte dedicada a movilidad sostenible, haciendo de unión con nuevas tecnologías como el hidrógeno para propulsar una movilidad con menores emisiones. Un campo emergente y de moda es la movilidad basada en vehículo eléctrico, por lo que muchos autores publican trabajos relacionados con los mismos. Como el campo de los vehículos eléctricos es muy amplio, se restringe el estado del arte a casos de integración del proceso de carga/descarga del vehículo eléctrico en una microrred, haciendo uso de energías renovables. Al igual que en otras microrredes, tanto controladores heurísticos basados en reglas simples como controladores basados en optimización, se desarrollan en la bibliografía. Los primeros son más sencillos pero están más limitados y es difícil emplearlos cuando la complejidad o tamaño del problema se elevan. Por el contrario, los controladores basados en optimización con redes de neuronas o controladores predictivos, son más complejos pero permiten llevar a cabo una resolución óptima de problemas más complejos. Es en este punto en el que aparecen los controladores predictivos o MPC, que son controladores óptimos basados en un modelo del sistema que usan una realimentación para corregir perturbaciones y posibles errores de modelado, y que se usarán a lo largo de este trabajo.

## C. Diseño de la estrategia de control

En primer lugar, es necesario describir el sistema y obtener un modelo del mismo. En la Figura 0-2 se puede ver la configuración de la microrred. En concreto, está formada por: campos fotovoltaicos, banco de baterías, electrolizador PEM, almacenamiento de hidrógeno en hidruros metálicos, pila de combustible PEM, supercondensador, cargas de consumo eléctrico, puntos de recarga de vehículo eléctrico (sin implementación del V2G) y vehículo de hidrógeno y conexión con la red eléctrica. Cada elemento lleva asociado unos convertidores de potencia cuyo diseño y control se escapan del alcance de este trabajo.

El modelo del sistema incluirá tanto las ecuaciones en espacio de estado como la ecuación del balance de potencias en la microrred. Para el primer caso, debido a los tiempos característicos de las dinámicas de todos los elementos de la microrred, el estado viene dado por el porcentaje de capacidad del almacenamiento en baterías, de hidrógeno y en el supercondensador, que son los elementos con dinámica más lenta. Linealizando los modelos usados en simulación para dichos equipos de almacenamiento y, llevando a cabo una serie de desarrollos matemáticos, se concluye que el modelo en espacio de estados del sistema viene dado por las ecuaciones:

$$SOC_{bat}(t + 1) = SOC_{bat}(t) + \frac{\eta_{bat,ch} T_s}{C_{max,bat}} P_{bat,ch}(t) - \frac{T_s}{\eta_{bat,disc} C_{max,bat}} P_{bat,disc}(t) \quad (0-1)$$

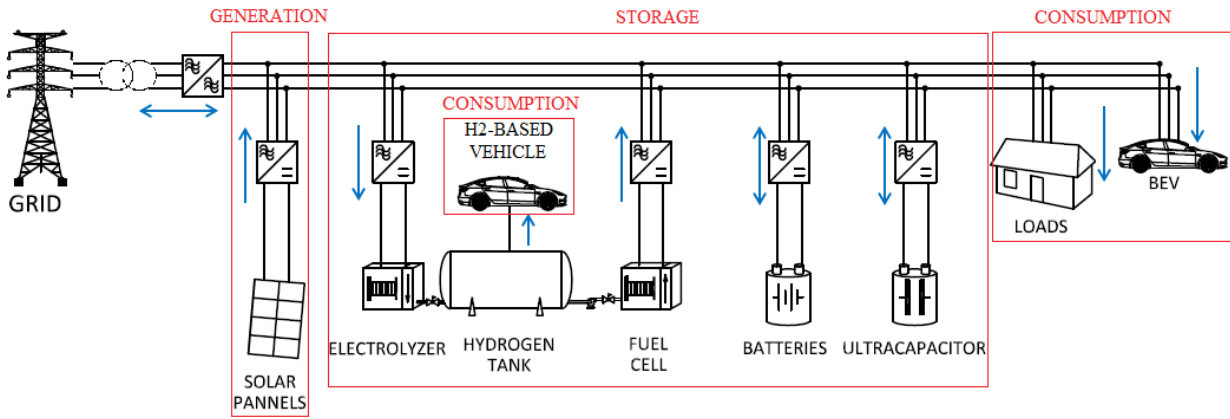


Figura 0-2 Esquema de la microred (Imagen modifica a partir de la original de [2])

$$LOH(t+1) = LOH(t) + 100 \frac{\eta_{ez} T_s}{V_{max}} P_{ez}(t) \delta_{ez}(t) - 100 \frac{T_s}{\eta_{fc} V_{max}} P_{fc}(t) \delta_{fc}(t) \quad (0-2)$$

$$SOC_{uc}(t+1) = SOC_{uc}(t) + \frac{\eta_{uc,ch} T_s}{C_{max,uc}} P_{uc,ch}(t) - \frac{T_s}{\eta_{uc,disc} C_{max,uc}} P_{uc,disc}(t) \quad (0-3)$$

Por su parte, el balance de potencias:

$$P_{grid}(t) + P_{bat}(t) + P_{uc}(t) + P_{fc}(t) - P_{ez}(t) + d(t) = 0 \quad (0-4)$$

Siendo  $d(t)$  la perturbación medible del sistema, obtenida como la generación menos la demanda (incluida la de recarga de vehículos eléctricos).

Una vez que se tiene el modelo del sistema, se puede diseñar la estrategia de control. El esquema de la misma se basa en la estructura basada en capas jerárquicas típicas de un sistema de control, donde un controlador terciario lleva a cabo una planificación económica teniendo en cuenta aspectos de operación y degradación de los equipos, para enviar referencias cada hora a un controlador secundario que actúa en un tiempo de muestreo del orden de segundos, y que se encarga del seguimiento de la planificación enviada por el controlador terciario. Además, este controlador secundario también se ocupa de aspectos operacionales y relacionados con el mantenimiento de los equipos. Entre otras diferencias, el controlador secundario incluye el supercondensador (el terciario no lo incluye) debido a que es un dispositivo capaz de actuar de forma rápida amortiguando los picos de potencia en cambios bruscos.

Esta estrategia puede verse en la Figura 0-3. Como se puede observar, el controlador terciario recibe entradas procedentes de las predicciones de consumo, generación y precio de la energía y de las medidas de los niveles de energía en sus almacenamientos. Como salida, proporciona la planificación para el controlador secundario. Dicho controlador secundario, además de la planificación procedente del controlador terciario, recibe medidas de la potencia generada y consumida real (incluyendo la de carga de vehículos eléctricos) y, de nuevo, de los niveles de almacenamiento de energía. Su salida son las potencias de referencia para los convertidores de potencia que no han sido implementados en este trabajo.

Para el diseño del controlador terciario, tanto variables lógicas como continuas se usarán, por lo que es necesario convertir el sistema a un *Mixed Logical Dynamical*, *MLD*. En estos sistemas, las variables binarias y sus relaciones lógicas se definen, para luego transformar dichas relaciones en desigualdades lineales como muestra la Tabla 0-1, y que serán añadidas como restricciones al problema de optimización. También se definen variables mixtas, compuestas por operaciones matemáticas que involucran ambos tipos de variable. El modelo en espacio de estados del sistema debe quedar descrito como función del propio estado, las acciones de control, las variables lógicas y las variables mixtas. Esas tres últimas serán las variables de decisión en el



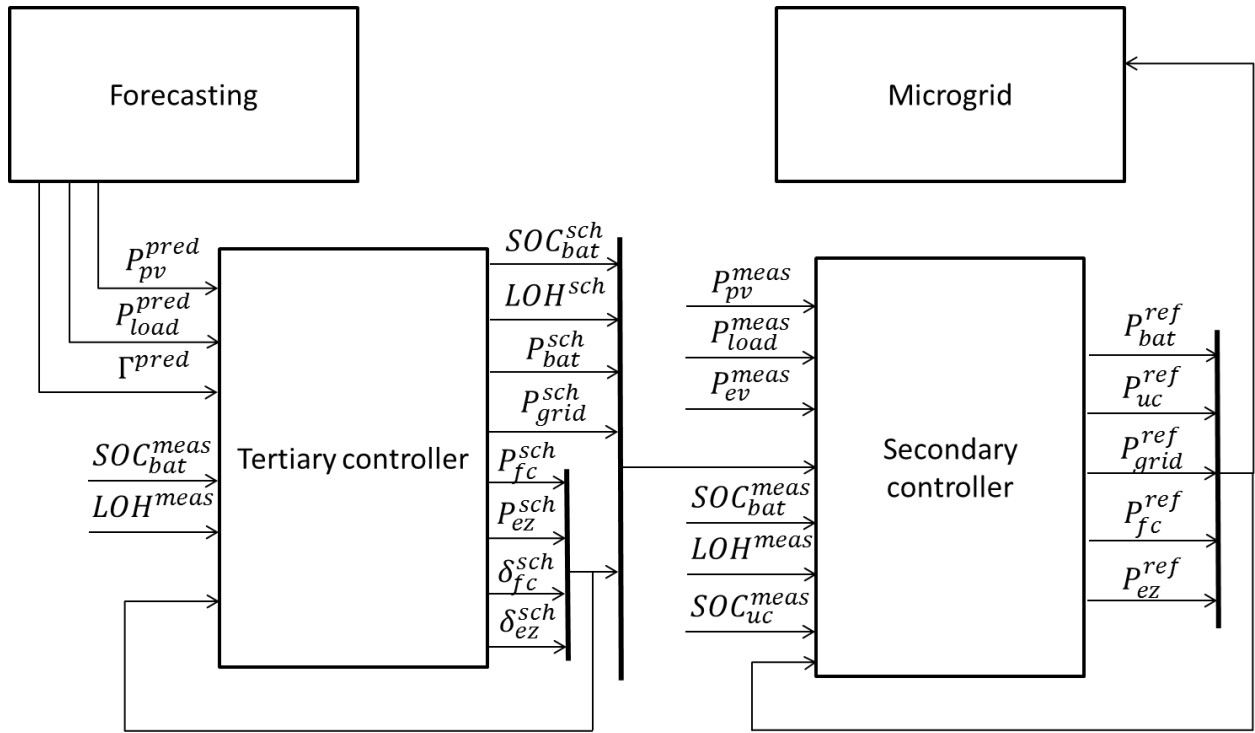


Figura 0-3. Estrategia de control

problema de optimización. Una vez que se tiene el sistema MLD descrito y con las nuevas restricciones a añadir, se tiene un problema *Mixed Integer Programming*, *MIP*, que al ser las restricciones lineales, será un *Mixed Integer Linear Programming*, *MILP* si la función de coste es lineal, o un *Mixed Integer Quadratic Programming*, *MIQP* si la función de coste es cuadrática. Como estos problemas son más difíciles de resolver, se suelen emplear técnicas conocidas como *branch and bound* para ir reduciendo el número de casos posibles en el problema de optimización.

	Relation	Logic	MLD inequalities
P1	AND ( $\wedge$ )	$S_3 \Leftrightarrow (S_1 \wedge S_2)$	$-\infty \leq -\delta_1 + \delta_3 \leq 0$ $-\infty \leq -\delta_2 + \delta_3 \leq 0$ $-\infty \leq \delta_1 + \delta_2 - \delta_3 \leq 1$
P2	OR ( $\vee$ )	$S_1 \vee S_2$	$1 \leq \delta_1 + \delta_2 \leq 2$
P3	NOT ( $\sim$ )	$S_2 \equiv \sim S_1$	$1 \leq \delta_1 + \delta_2 \leq 1$
P4	IMPLY ( $\Rightarrow$ )	$[a^T x \leq 0] \Rightarrow [\delta = 1]$	$\varepsilon \leq a^T x - (m - \varepsilon)\delta \leq \infty$
P5	IMPLY ( $\Rightarrow$ )	$[\delta = 1] \Rightarrow [a^T x \leq 0]$	$-\infty \leq a^T x + M\delta \leq M$
P6	IFF ( $\Leftrightarrow$ )	$[a^T x \leq 0] \Leftrightarrow [\delta = 1]$	$\varepsilon \leq a^T x - (m - \varepsilon)\delta \leq \infty$ $-\infty \leq a^T x + M\delta \leq M$
P7	Mixed product	$z = \delta \cdot a^T x$	$-\infty \leq z - M\delta \leq 0$ $0 \leq z - m\delta \leq \infty$ $-\infty \leq z - a^T x + m(1 - \delta) \leq 0$ $0 \leq z - a^T x + M(1 - \delta) \leq \infty$

Tabla 0-1. Relaciones lógicas en un sistema y sus correspondiente desigualdades lineales (Tabla tomada directamente de [2])

Siendo las variables de decisión del problema de optimización para el controlador terciario las siguientes:

$$u(t_k) = \begin{bmatrix} P_{bat}(t_k) \\ P_{fc}(t_k) \\ P_{ez}(t_k) \\ P_{grid}(t_k) \end{bmatrix} \quad \delta(t_k) = \begin{bmatrix} \delta_{bat,ch}(t_k) \\ \delta_{bat,disc}(t_k) \\ \delta_{fc}(t_k) \\ \delta_{ez}(t_k) \\ \delta_{sale}(t_k) \\ \delta_{pur}(t_k) \\ \sigma_{fc}^{on}(t_k) \\ \sigma_{ez}^{on}(t_k) \\ \chi_{fc}(t_k) \\ \chi_{ez}(t_k) \end{bmatrix} \quad z(t_k) = \begin{bmatrix} P_{bat,ch}(t_k) \\ P_{bat,disc}(t_k) \\ z_{fc}(t_k) \\ z_{ez}(t_k) \\ P_{sale}(t_k) \\ P_{pur}(t_k) \\ \theta_{fc}(t_k) \\ \theta_{ez}(t_k) \end{bmatrix} \quad (0-5)$$

Y tras un largo desarrollo matemático cuyo detalle puede verse en la versión completa de este trabajo en inglés, el problema MIQP que define al controlador secundario viene recogido en la siguiente caja.

$$\begin{aligned} \min_u J(t) = & \sum_{k=1}^{SH} \left( \left( -\Gamma_{sale}^{pred}(t_k|t) P_{sale}(t_k|t) + \Gamma_{pur}^{pred}(t_k|t) P_{pur}(t_k|t) \right) T_s \right. \\ & + \frac{CC_{bat}}{2 \text{Cycles}_{bat}} \left( P_{bat,ch}(t_k|t) + P_{bat,disc}(t_k|t) \right) T_s \\ & + \left( Cost_{degr,ch} P_{bat,ch}^2(t_k|t) + Cost_{degr,disc} P_{bat,disc}^2(t_k|t) \right) T_s \\ & + T_s \left( \frac{CC_{fc}}{\text{Hours}_{fc}} + Cost_{o\&m,fc} \right) \delta_{fc}(t_k|t) + Cost_{start,fc} \sigma_{fc}^{on}(t_k|t) \\ & + Cost_{degr,fc} \theta_{fc}^2(t_k|t) + T_s \left( \frac{CC_{ez}}{\text{Hours}_{ez}} + Cost_{o\&m,ez} \right) \delta_{ez}(t_k|t) \\ & \left. + Cost_{start,ez} \sigma_{ez}^{on}(t_k|t) + Cost_{degr,ez} \theta_{ez}^2(t_k|t) \right) \end{aligned}$$

$$\begin{aligned} s. a. \quad \begin{bmatrix} SOC_{bat}(t_k+1) \\ LOH(t_k+1) \end{bmatrix} &= \begin{bmatrix} 1 & 0 \\ 0 & 1 \end{bmatrix} \begin{bmatrix} SOC_{bat}(t_k) \\ LOH(t_k) \end{bmatrix} + \begin{bmatrix} 0 & \dots & 0 \\ 0 & \dots & 0 \end{bmatrix}_{(2,4)} u(t_k) + \\ \begin{bmatrix} 0 & \dots & 0 \\ 0 & \dots & 0 \end{bmatrix}_{(2,10)} \delta(t_k) &+ \begin{bmatrix} K_{bat,ch} & -K_{bat,disc} & 0 & 0 & 0 & 0 & 0 & 0 \\ 0 & 0 & -K_{fc} & K_{ez} & 0 & 0 & 0 & 0 \end{bmatrix} z(t_k) \end{aligned}$$

$$\begin{bmatrix} y_1(t_k) \\ y_2(t_k) \end{bmatrix} = \begin{bmatrix} 1 & 0 \\ 0 & 1 \end{bmatrix} \begin{bmatrix} SOC_{bat}(t_k) \\ LOH(t_k) \end{bmatrix}$$

$$P_{pv}^{pred}(t_k|t) + P_{grid}(t_k) + P_{bat}(t_k) + z_{fc}(t_k) - z_{ez}(t_k) - P_{load}^{pred}(t_k|t) = 0$$

$$P_i^{min} \leq P_i(t_k) \leq P_i^{max} \quad |_{i=bat,fc,ez,grid}$$

$$SOC_{bat}^{min} \leq SOC_{bat}(t_k) \leq SOC_{bat}^{max}$$

$$LOH^{min} \leq LOH(t_k) \leq LOH^{max}$$

$$0 \leq \delta_i(t_k) \leq 1 \quad |_{i=fc,ez}$$

$$P_{grid}(t_k) = P_{pur}(t_k) - P_{sale}(t_k), \quad P_{pur}(t_k) \geq 0, P_{sale}(t_k) \geq 0$$

$$\delta_{pur}(t_k) + \delta_{sale}(t_k) = 1$$

$$\begin{aligned}
& P_{grid}^{min} \delta_{pur}(t_k) \leq P_{pur}(t_k) \leq P_{grid}^{max} \delta_{pur}(t_k) \\
& P_{grid}(t_k) - P_{grid}^{max} (1 - \delta_{pur}(t_k)) \leq P_{pur}(t_k) \leq P_{grid}(t_k) - P_{grid}^{min} (1 - \delta_{pur}(t_k)) \\
& \epsilon + (P_{grid}^{min} - \epsilon) \delta_{sale}(t_k) \leq P_{grid}(t_k) \leq P_{grid}^{max} (1 - \delta_{sale}(t_k)) \\
& P_{bat}(t_k) = P_{bat,disc}(t_k) - P_{bat,ch}(t_k), \quad P_{bat,disc}(t_k) \geq 0, P_{bat,ch}(t_k) \geq 0 \\
& \delta_{bat,disc}(t_k) + \delta_{bat,ch}(t_k) = 1 \\
& P_{bat}^{min} \delta_{bat,disc}(t_k) \leq P_{bat,disc}(t_k) \leq P_{bat}^{max} \delta_{bat,disc}(t_k) \\
& P_{bat}(t_k) - P_{bat}^{max} (1 - \delta_{bat,disc}(t_k)) \leq P_{bat,disc}(t_k) \leq P_{bat}(t_k) - P_{bat}^{min} (1 - \delta_{bat,disc}(t_k)) \\
& \epsilon + (P_{bat}^{min} - \epsilon) \delta_{bat,ch}(t_k) \leq P_{bat}(t_k) \leq P_{bat}^{max} (1 - \delta_{bat,ch}(t_k)) \\
& 0 \leq \delta_{fc}(t_k) + \delta_{ez}(t_k) \leq 1 \\
& P_i^{min} \delta_i(t_k) \leq z_i(t_k) \leq P_i^{max} \delta_i(t_k), \quad i = fc, ez \\
& P_i(t_k) - P_i^{max} (1 - \delta_i(t_k)) \leq z_i(t_k) \leq P_i(t_k) - P_i^{min} (1 - \delta_i(t_k)), \quad i = fc, ez \\
& -\infty \leq -\delta_i(t_k) + \sigma_i^{on}(t_k) \leq 0, \quad i = fc, ez \\
& -\infty \leq -(1 - \delta_i(t_k - 1)) + \sigma_i^{on}(t_k) \leq 0, \quad i = fc, ez \\
& -\infty \leq \delta_i(t_k) + (1 - \delta_i(t_k - 1)) - \sigma_i^{on}(t_k) \leq 1, \quad i = fc, ez \\
& -\infty \leq -\delta_i(t_k) + \chi_i(t_k) \leq 0, \quad i = fc, ez \\
& -\infty \leq -\delta_i(t_k - 1) + \chi_i(t_k) \leq 0, \quad i = fc, ez \\
& -\infty \leq \delta_i(t_k) + \delta_i(t_k - 1) - \chi_i(t_k) \leq 1, \quad i = fc, ez \\
& 0 \leq \chi_{fc}(t_k) + \chi_{ez}(t_k) \leq 1 \\
& \Delta P_i^{min} \chi_i(t_k) \leq \theta_i(t_k) \leq \Delta P_i^{max} \chi_i(t_k), \quad i = fc, ez \\
& \Delta P_i(t_k) - \Delta P_i^{max} (1 - \chi_i(t_k)) \leq \theta_i(t_k) \leq \Delta P_i(t_k) - \Delta P_i^{min} (1 - \chi_i(t_k)), \quad i = fc, ez
\end{aligned}$$

Por su parte, el controlador secundario, como se ha dicho, trata de seguir la planificación establecida por el controlador terciario, además de buscar el correcto funcionamiento de los equipos. En este caso sólo se usarán variables continuas, por lo que se tiene un problema de programación cuadrática que puede fácilmente resolver con la función propia de *MATLAB* denominada *quadprog*.

Definiendo las acciones de control y sus variaciones (estas últimas serán las variables de decisión del problema de optimización) como:

$$u(t_k) = \begin{bmatrix} P_{H_2}(t_k) \\ P_{grid}(t_k) \\ P_{uc}(t_k) \end{bmatrix} \quad \Delta u(t_k) = \begin{bmatrix} \Delta P_{H_2}(t_k) \\ \Delta P_{grid}(t_k) \\ \Delta P_{uc}(t_k) \end{bmatrix} = \begin{bmatrix} P_{H_2}(t_k) \\ P_{grid}(t_k) \\ P_{uc}(t_k) \end{bmatrix} - \begin{bmatrix} P_{H_2}(t_k - 1) \\ P_{grid}(t_k - 1) \\ P_{uc}(t_k - 1) \end{bmatrix} \quad (0-6)$$

Y, de nuevo, tras una larga deducción que puede verse en la versión completa en inglés, el problema de optimización para el controlador secundario queda recogido en la siguiente tabla.

$$\min_{\Delta u} \frac{1}{2} \Delta u^T H_{qp} \Delta u + B_{qp}^T \Delta u$$

$$s. t. R \Delta u \leq c$$

Where:

$$H_{qp} = 2(T^T \alpha T + \lambda + H^T \delta H + T^T \alpha_{4u2} T + \lambda_{4u2} + T^T \gamma T + T^T \mathbf{aux}_u^T \gamma_{bat} \mathbf{aux}_u T)$$

$$B_{qp} = 2 \left( T^T \alpha (\mathbf{1}_{N_c m, m} u(t_k - 1)) + H^T \delta (F \hat{x}(t) - w) \right) + 2 \left( (\mathbf{1}_{N_c m, m} u(t_k - 1))^T \alpha_{4u2} T + \hat{x}^T(t_k) \alpha_{4xu} T + 2 \Delta d(t_k) \lambda_{4xu, small} \right)^T + 2 \left( (\mathbf{1}_{N_c m, m} u(t_k - 1) - \mathbf{u}^{sch})^T \gamma T \right)^T + 2 \left( (\mathbf{aux}_u \mathbf{1}_{N_c m, m} u(t_k - 1) + \mathbf{aux}_x \hat{x}(t_k) - \mathbf{P}_{bat}^{sch})^T \gamma_{bat} \mathbf{aux}_u T \right)^T$$

$$R = \begin{bmatrix} I_{N_c m, N_c m} \\ -I_{N_c m, N_c m} \\ T \\ -T \\ H \\ -H \\ \mathbf{aux}_u T \\ -\mathbf{aux}_u T \\ \mathbf{aux}_u \\ -\mathbf{aux}_u \end{bmatrix}$$

$$c = \begin{bmatrix} \mathbf{1}_{N_c m, m} \Delta u_{max} \\ -\mathbf{1}_{N_c m, m} \Delta u_{min} \\ \mathbf{1}_{N_c m, m} u_{max} - \mathbf{1}_{N_c m, m} u(t_k - 1) \\ -\mathbf{1}_{N_c m, m} u_{min} + \mathbf{1}_{N_c m, m} u(t_k - 1) \\ \mathbf{1}_{N_p p, p} y_{max} - F \hat{x}(t) \\ -\mathbf{1}_{N_p p, p} y_{min} + F \hat{x}(t) \\ \mathbf{P}_{bat}^{max} - \mathbf{1}_{N_c m, m} u(t_k - 1) - \mathbf{aux}_x \hat{x}(t_k) \\ -\mathbf{P}_{bat}^{min} + \mathbf{aux}_u \mathbf{1}_{N_c m, m} u(t_k - 1) + \mathbf{aux}_x \hat{x}(t_k) \\ \Delta \mathbf{P}_{bat}^{max} + \begin{bmatrix} d(t_k) - d(t_k - 1) \\ 0 \\ \vdots \\ 0 \end{bmatrix} \\ -\Delta \mathbf{P}_{bat}^{min} - \begin{bmatrix} d(t_k) - d(t_k - 1) \\ 0 \\ \vdots \\ 0 \end{bmatrix} \end{bmatrix}$$

Para la simulación de la microrred se usa, como ya se ha comentado previamente, la librería *Simugrid* de *MATLAB/Simulink*. En esta librería, los componentes típicos de una microrred son modelados con el objetivo de usar esos modelos en tareas de control, y se implementan en Simulink en función de algunos parámetros configurables que pueden obtenerse de los fabricantes o a través de técnicas de indentificación de modelos y parámetros con equipos reales. Estos modelos se han validado y usado en otros proyectos y publicaciones. Como ejemplo, el diagram Simugrid diagram for this work is shown in Figura 0-4.

En el aspecto software, a lo anterior lo complementan el *toolbox Yalmip* con el *solver CPLEX* usado en el controlador terciario y el *solver quadprog* como una función propia de *MATLAB* para el controlador secundario. El segundo caso es sencillo y directo de aplicar. Para el primero, tanto Yalmip como CPLEX requieren de unos pasos previos de instalación y configuración software, que son recogidos en el texto completo de este trabajo en inglés. Además, para usar Yalmip, que es muy adecuado para problemas de optimización en el ámbito del control automático como los MPCs, es necesario conocer que, típicamente, hay que seguir una serie de pasos:

- 1- Definir las variables de decisión del problema de optimización usando *sdpvar*, o *binvar* para variables binarias. Estas serán usadas como variables simbólicas en la definición del problema.
- 2- Definir la función de coste y restricciones siguiendo la sintaxis propia de Yalmip.
- 3- Decidir y establece cuáles van a ser las entradas y salidas del problema de optimización.

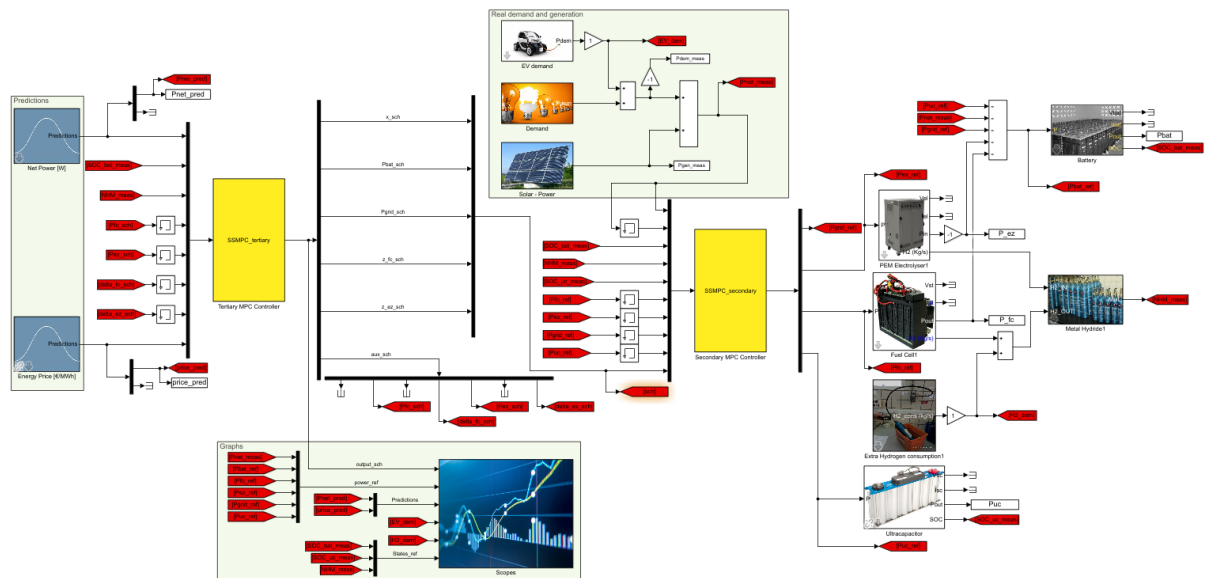


Figura 0-4. Diagrama SimuGrid completo

- 4- Usar el commando *optimizer* para definir una sólo vez el problema como un objeto. Este comando recibe como entrada, en el siguiente orden: *restricciones*, *función de coste*, *opciones*, *entradas*, *salidas*. En las *opciones*, el solver se puede cambiar; por ejemplo, para usar CPLEX, se debe enviar el argumento *sdpssettings('solver', 'cplex')* en el campo de *opciones*.
- 5- Llamar al objeto que contiene el problema de optimización proporcionándole las entradas requeridas para resolverlo.

## D. Resultados

Los controladores han sido probados en simulación con pruebas de un día de duración (simulado) en diferentes situaciones. En primer lugar, el controlador terciario se prueba por separado para comprobar su correcto funcionamiento, así como la evolución adecuada tanto de las variables lógicas como continuas. Se hacen pruebas en el modo conectado a red para días soleado y nublado, cuyos resultados de potencias y nivel de almacenamiento de energía se muestran en la Figura 0-5 y la Figura 0-6, respectivamente. Los resultados son satisfactorios, buscando la maximización del beneficio económico vendiendo a red en los momentos de mayor precio de la energía (en torno a las horas 11 y 20). Además, se minimizan los arranques del electrolizador y la pila, así como se protegen los equipos de altas cargas de potencia y variaciones. En el caso del día nublado, se tiene que hacer un mayor uso de la red comprando energía para poder suplir la demanda.

Como en ambas simulaciones no se observa el funcionamiento del hidrógeno, ya que su arranque es costoso económicamente y en cuanto a aspectos operacionales, se llevan a cabo dos simulaciones más. La primera de ellas, mostrada en la Figura 0-7, se corresponde con el modo conectado a red en un día soleado con demanda casi nula, como podría ser un fin de semana en el campus universitario. Por tanto, hay mucho exceso de energía y no todo puede ser almacenado en la batería o vendido a la red, por lo que el electrolizador arranca y almacena algo de energía.

La última simulación hecha para el controlador terciario sólo se corresponde con una día soleado en el caso de microred aislada, por lo que en este caso el electrolizador, así como la batería y la pila de combustible se usa con más frecuencia e intercambiando más energía. Los resultados puede verse en la Figura 0-8, obteniendo similares conclusiones que en los casos anteriores.

Por su parte, para probar el sistema completo, dos simulaciones se han llevado cabo, ambas en modo conectado a red. La primera de ellas corresponde a un día soleado como el que se simuló en el primer caso del controlador terciario. Las potencias resultado del controlador terciario (arriba) y secundario (abajo) se muestran en la Figura 0-9. Los niveles de almacenamiento de energía, por su parte, se muestran en la Figura 0-10 para lo planificado por el controlador terciario (arriba) y para las medidas tomadas directamente de los

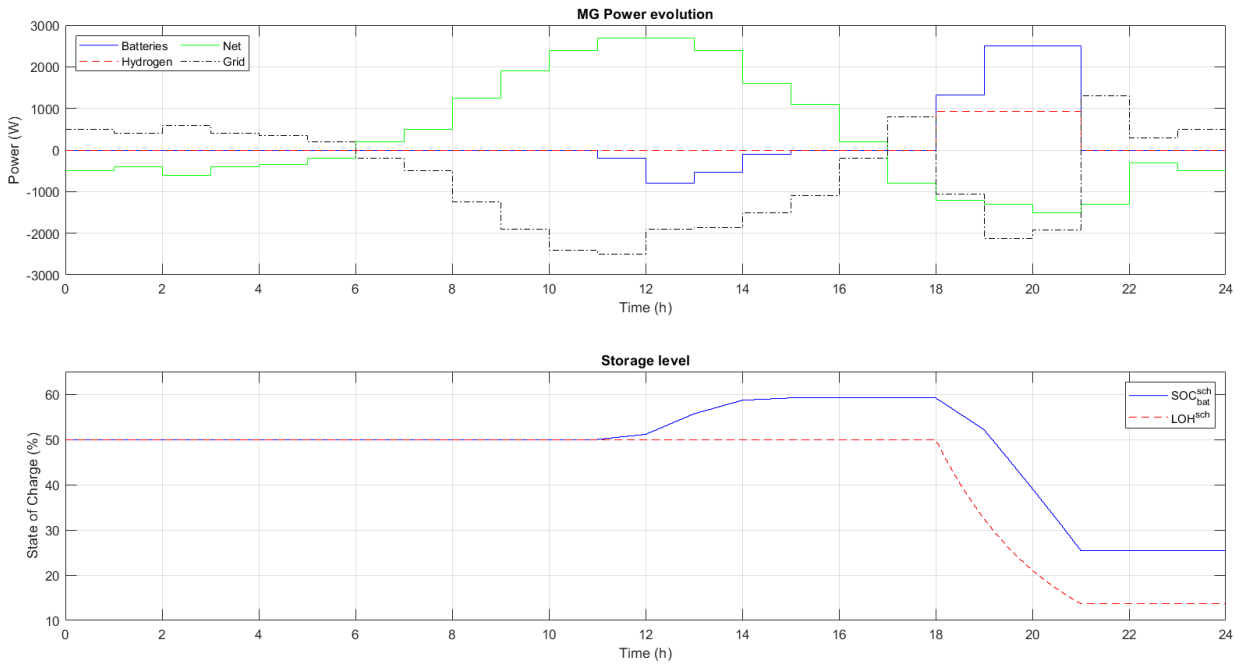


Figura 0-5. Evolución de las potencias y los niveles de almacenamiento para el caso conectado a red y día soleado

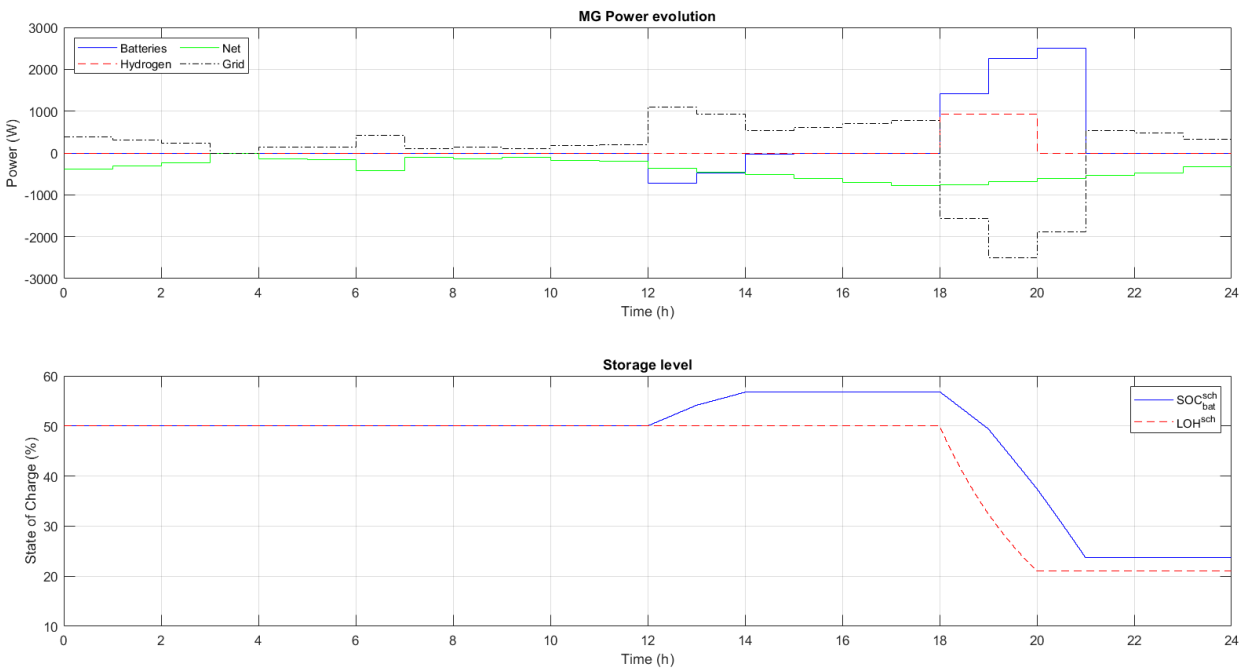


Figura 0-6. Evolución de las potencias y los niveles de almacenamiento para el caso conectado a red y día nublado

equipos (abajo). Se puede ver cómo el controlador secundario trata de seguir las referencias tanto de estado como de potencia para todos los equipos, a pesar de que la potencia neta difiere en el caso real, y más por la inclusión de demanda eléctrica para carga de vehículos eléctricos y demanda extra de hidrógeno. Además, otros aspectos como las variaciones suaves en electrolizador y pila de combustible también se cuidan. También es importante destacar cómo el supercondensador absorbe las variaciones rápidas de potencia cada vez que se produce un cambio brusco y cómo lo hace por poco tiempo, lo que encaja con el hecho de que tenga alta potencia específica pero baja energía específica.

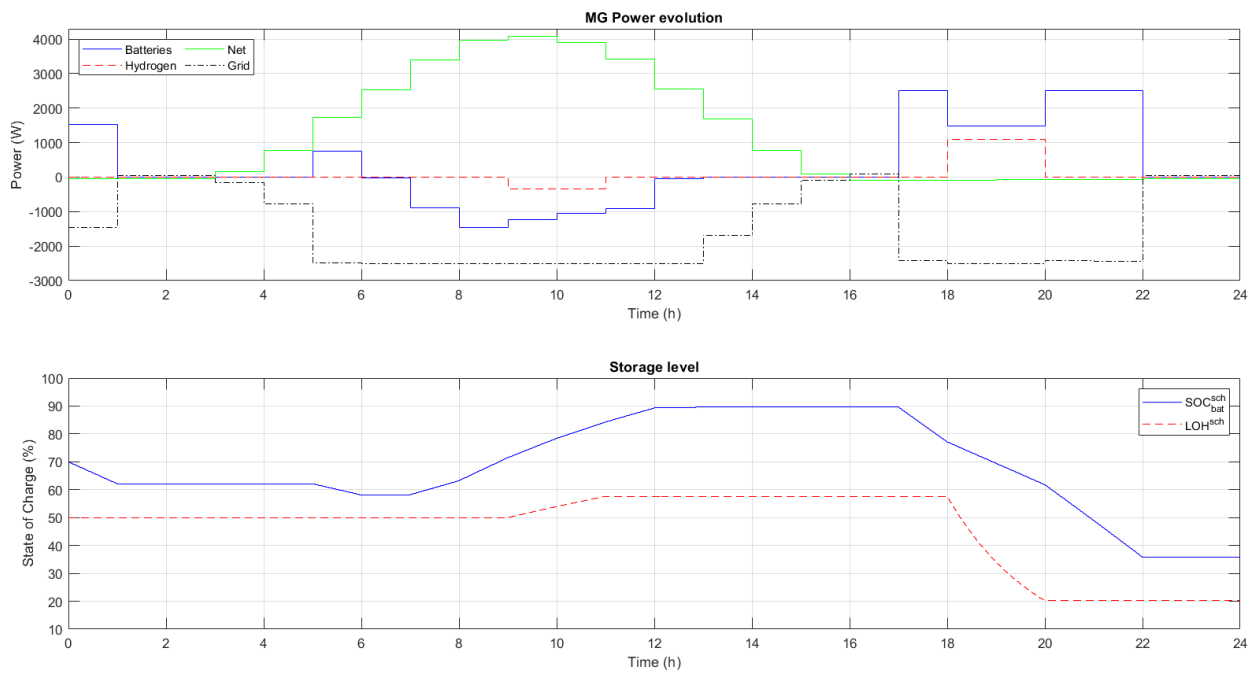


Figura 0-7. Evolución de las potencias y los niveles de almacenamiento para el caso conectado a red en día soleado con demanda casi nula

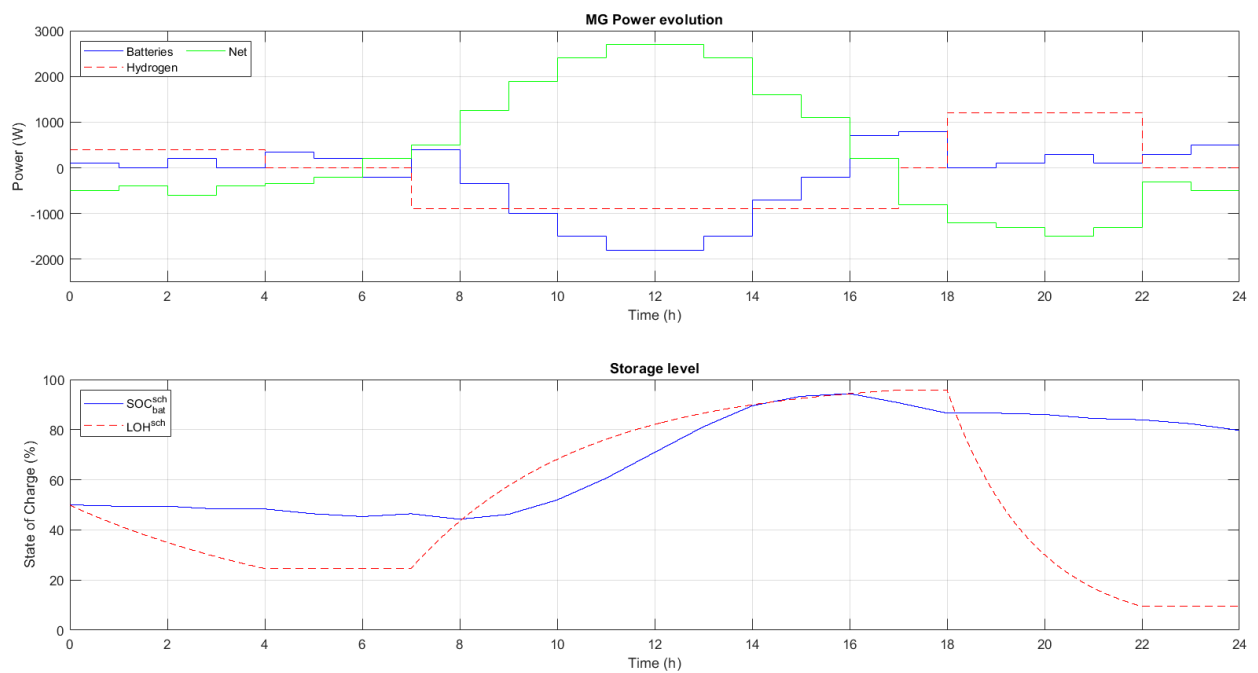


Figura 0-8. Evolución de las potencias y los niveles de almacenamiento para el caso de microred aislada en día soleado

La otra simulación hecha para el sistema completo se corresponde con un día nublado como el probado para el controlador terciario. La evolución de las potencias y de los niveles de almacenamiento de energía pueden verse en la Figura 0-11 y la Figura 0-12, respectivamente, como en el caso de la simulación anterior. En este caso es necesario comprar más energía de la red, ya que no hay tanto exceso de producción como para venderla, por lo que el beneficio económico se verá mermado en aras de cumplir con los requerimientos de la demanda con la generación y almacenamiento disponibles. Conclusiones similares se pueden sacar, por lo que se consideran satisfactorias las pruebas hechas y válidos los controladores diseñados.

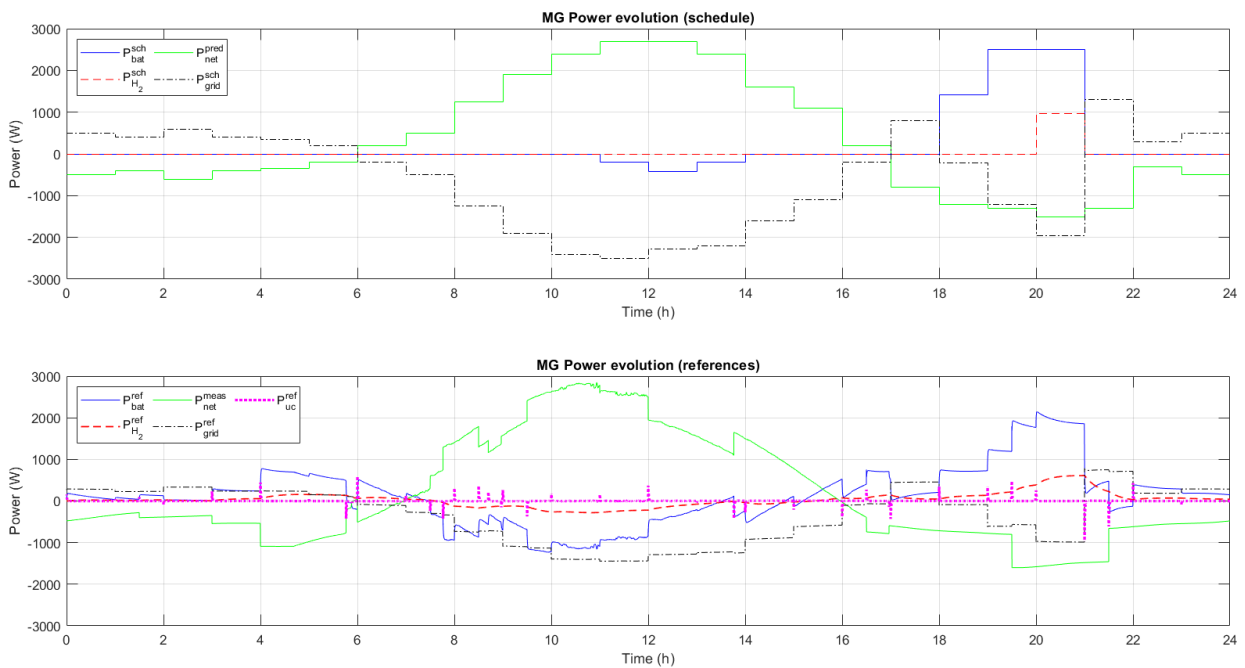


Figura 0-9. Evolución de las potencias en el caso conectado a red y día soleado. Arriba: potencia planificada por el controlador terciario; abajo: referencias de potencia dadas por el controlador secundario

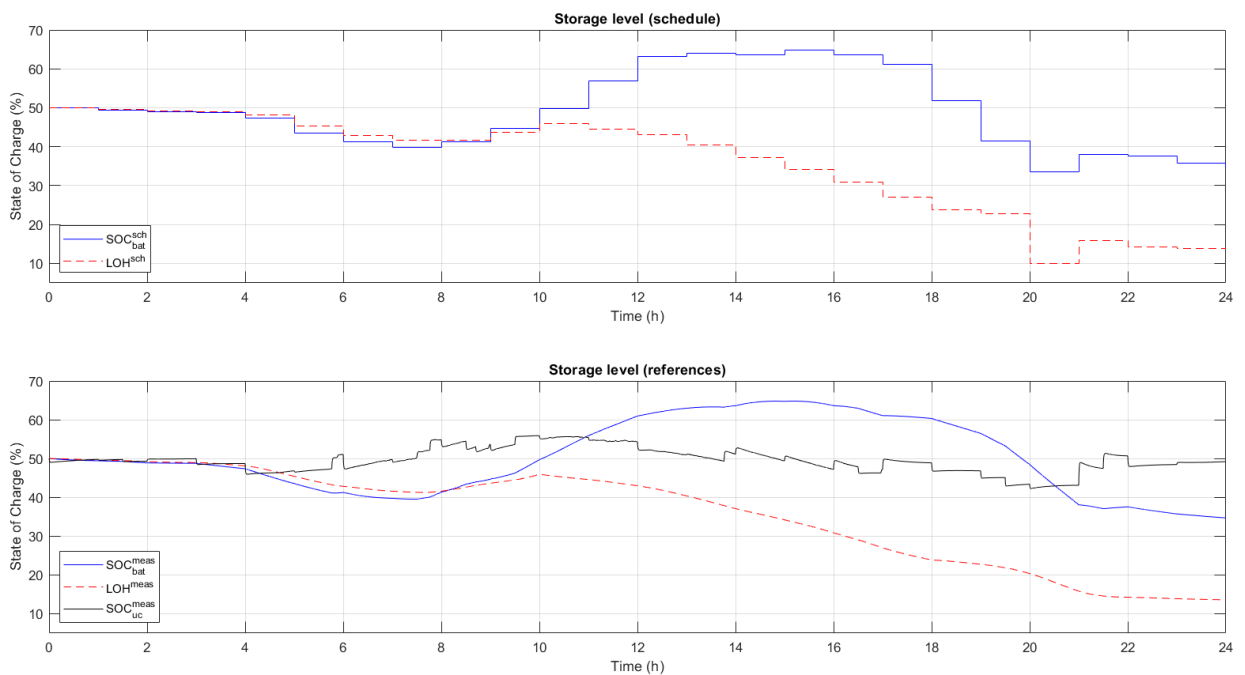


Figura 0-10. Evolución de los niveles de almacenamiento en el caso conectado a red y día soleado. Arriba: potencia planificada por el controlador terciario; abajo: referencias de potencia dadas por el controlador secundario

## E. Conclusiones

Una vez que los controladores se han diseñado y los resultados de simulación se han analizado, se puede recapitular y extraer algunas conclusiones. Además, los puntos débiles y el posible trabajo futuro se describen para mejorar la estrategia de control y progresar hacia la implementación en la planta real de la microred para



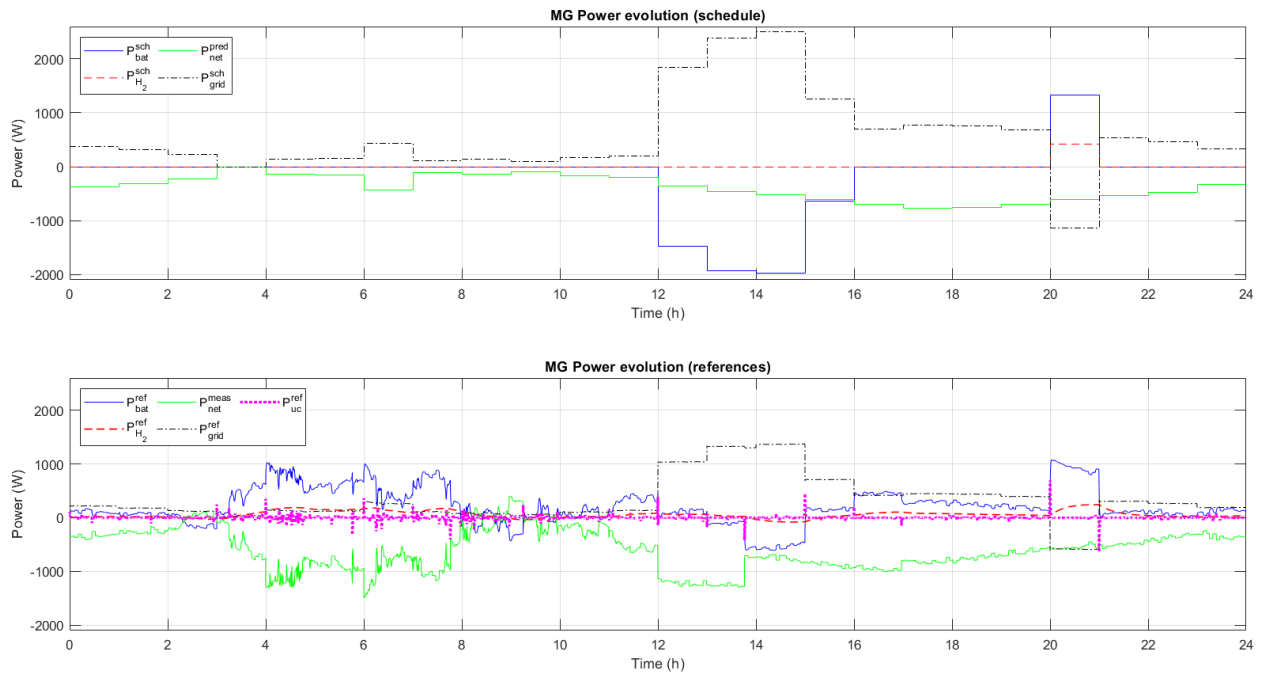


Figura 0-11. Evolución de las potencias en el caso conectado a red y día nublado. Arriba: potencia planificada por el controlador terciario; abajo: referencias de potencia dadas por el controlador secundario

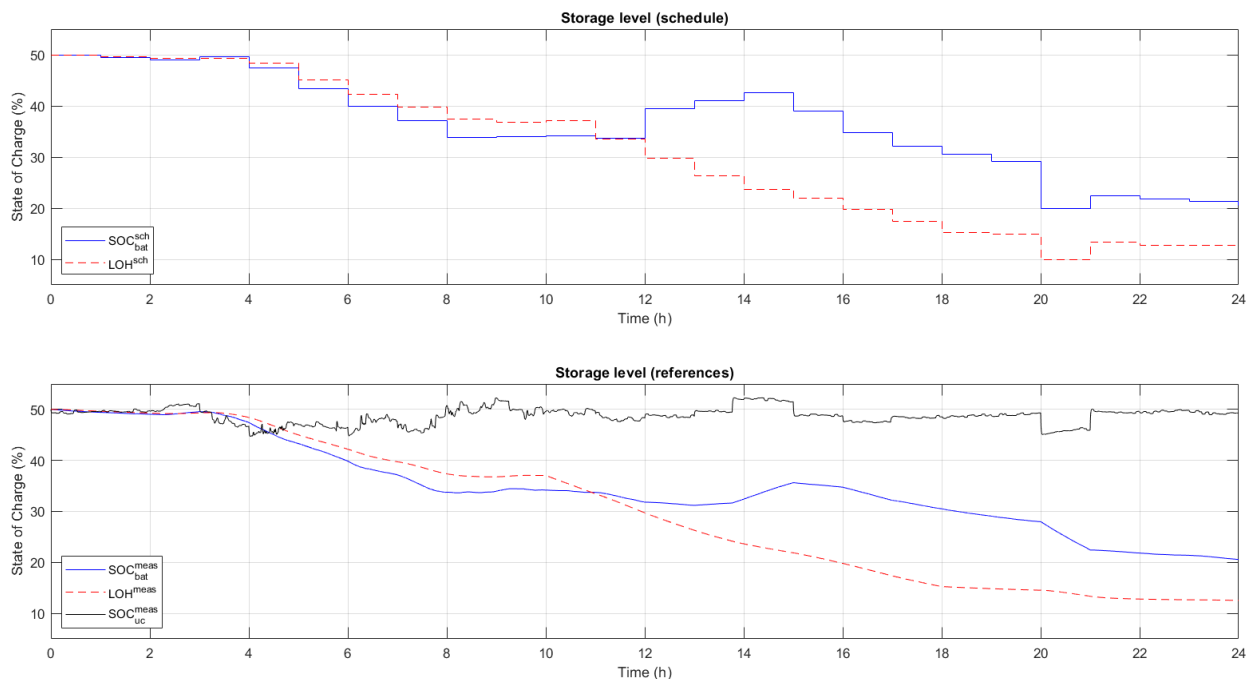


Figura 0-12. Evolución de los niveles de almacenamiento en el caso conectado a red y día soleado. Arriba: potencia planificada por el controlador terciario; abajo: referencias de potencia dadas por el controlador secundario

carga de vehículos de cero emisiones.

Una microrred para estación de carga de vehículos de cero emisiones se ha descrito y modelado en este trabajo para diseñar una estrategia de control óptimo basada en técnicas de MPC. Dos controladores se han diseñado y probado en simulación usando MATLAB/Simulink: un controlador terciario para la optimización de aspectos económicos, de operación y degradación en un problema MIQP (usando Yalmip y CPLEX), que proporciona

cada hora la planificación a un controlador secundario; y este controlador secundario que actúa cada segundo resolviendo un problema QP (usando quadprog) para seguir de manera óptima la planificación impuesta por el controlador terciario y para vigilar que los equipos no exceden sus limitaciones.

Varias simulaciones se han llevado a cabo para probar los controladores. Primero, simulaciones tanto en modo conectado a red (con días soleado y nublado, así como día soleado con demanda casi nula) como en modo aislado se han hecho para probar el controlador terciario y para observar más detalladamente el comportamiento de las variables binarias. Tras esto, el sistema completo con ambos controladores se prueba bajo las condiciones de caso conectado a red, tanto en día soleado como en día nublado.

El diseño de los controladores da Buenos resultados para todas las simulaciones hechas, con el controlador terciario tratando de maximizar el beneficio económico de la microred mientras trata de aprovechar la vida útil de sus componentes, y con el controlador secundario amortiguando las diferencias entre la planificación basadas en predicciones y la situación real, donde pueden existir muchos cambios. Estos cambios pueden darse en: potencia generada real, potencia demandada real y precio real de la energía, así como grandes variaciones debido a las demandas extra de potencia para la carga de vehículos eléctricos (que no ha sido considerado en las predicciones) y de hidrógeno que hace disminuir la cantidad de hidrógeno almacenado. Para esta tarea, el supercondensador juega un papel crucial absorbiendo los cambios rápidos de potencia de otros equipos o debidos a nuevos eventos. Esto es posible debido a la alta potencia específica del supercondensador. Sin embargo, para cantidades mayores de desviaciones de potencia, la batería y después el hidrógeno se suelen usar, porque el supercondensador tiene una energía específica baja.

Por tanto, se ha demostrado que el uso de controladores predictivos es adecuado para tener un sistema de gestión de energía óptimo en una microred, tratando con un gran número de variables, restricciones, y tamaño del problema. Estos controladores ofrecen una gran variedad de posibilidades para diseñar el sistema con requisitos concretos. Además, el uso de dos controladores conectados como en una estructura de control jerárquica en capas típica en la industria de procesos parece ser adecuado, siendo ambos controladores compaginados.

Otro aspecto importante es el uso de sistemas de almacenamiento de energía híbridos. El uso de baterías, almacenamiento de hidrógeno y el supercondensador permite al EMS establecer una mejor estrategia de optimización. Los inconvenientes de uno de estos equipos se complementan con las ventajas de los otros. Como ejemplo, el almacenamiento de hidrógeno tiene una alta energía específica pero una baja potencia específica, y lo contrario para el supercondensador. Por tanto, cuando ocurran variaciones de potencia instantánea, el supercondensador actuará, y para almacenamientos o suministros de energía durante más tiempo y en más cantidad, la tecnología del hidrógeno debe ser usada. Además, la tecnología del hidrógeno sufre si se aplican grandes variaciones de potencia, por lo que el proceso de arranque se intenta minimizar con el controlador secundario y las variaciones de potencia en el hidrógeno se limitan.

Además de las ventajas que se han extraído de los resultados analizados, existen algunos inconvenientes. En primer lugar, como se ha comentado a lo largo de la memoria, cuando la microred está en modo aislado, la planificación de la misma tiene que hacerse con un mayor horizonte temporal (por ejemplo una semana) para dimensionar mejor los equipos o para planificar mejor los intercambios de potencia con otras microredes o con la red eléctrica asumiendo que el modo aislado se puede cambiar a un modo conectado. Si este aspecto no se tiene en cuenta, podría haber situaciones en el modo aislado donde los sistemas de almacenamiento de energía estén llenos y haya un excedente de producción de energía. Esta situación también puede ocurrir en el modo conectado a red, pero la red proporciona mayor flexibilidad a la microred, a pesar de que no es recomendable debido a las penalizaciones económicas si la potencia programada para intercambiar con la red no se cumple.

Un aspecto importante para mejorar el desempeño de la estrategia de control es el hecho de que un controlador secundario con variables continuas y lógicas puede desarrollarse. En este trabajo, por simplicidad y para menores duraciones de simulación, un controlador secundario con sólo variables continuas se ha diseñado. Aunque es un controlador completo, que considera muchas limitaciones de los equipos y algunos requisitos de desempeño, no permite considerar el proceso de arranque de la tecnología del hidrógeno (electrolizador y pila de combustible) para minimizarlo. Por tanto, en algunas simulaciones del controlador secundario, se puede ver que este aspecto no ha sido tenido en cuenta en este trabajo.

Otro aspecto que puede ser considerado en el futuro para mejorar esta aplicación es la mejor gestión de la demanda de vehículos eléctricos. Nuevos perfiles de demanda de potencia para vehículos eléctricos pueden añadirse y probarse, o incluso modelos de demanda basados en distribuciones Gausianas pueden desarrollarse.

Además, implementar una estrategia V2G aumentaría la flexibilidad de la microred y esto necesitará una gestión de la carga de vehículos eléctricos específica que incluya tanto variables binarias como continuas, tal y como se hace en el trabajo de [3].

Finalmente, como se mencionó al principio de esta memoria, se quiere que este proyecto se lleve a cabo en una planta real. Para esta materialización, algunas tareas más tienen que hacerse. Entre otras, las predicciones del consumo, la producción y el precio de la energía deben ser implementadas con algunos modelos de predicción, los convertidores electrónicos de potencia deben ser considerados y controlados, y más situaciones deben probarse. Además, como alguno de los equipos fueron usados en proyectos antiguos, nuevos experimentos deberían hacerse para comprobar que los parámetros de los modelos permanecen tal y como se han considerado.



# Índice

---

<b>Acknowledgments</b>	<b>vii</b>
<b>Abstract</b>	<b>ix</b>
<b>Resumen</b>	<b>xi</b>
<i>A. Introducción</i>	<i>xi</i>
<i>B. Estado del arte</i>	<i>xiii</i>
<i>C. Diseño de la estrategia de control</i>	<i>xiii</i>
<i>D. Resultados</i>	<i>xix</i>
<i>E. Conclusiones</i>	<i>xxii</i>
<b>Índice</b>	<b>xxvii</b>
<b>Índice de Tablas</b>	<b>xxix</b>
<b>Índice de Figuras</b>	<b>xxxii</b>
<b>1 Introduction</b>	<b>1</b>
1.1 <i>Context and objectives</i>	2
1.2 <i>Methodology</i>	3
<b>2 State-of-Art</b>	<b>5</b>
<b>3 Control strategy design</b>	<b>15</b>
3.1 <i>System description and modeling</i>	15
3.2 <i>Controller design</i>	18
3.2.1 <i>Mixed Logical Dynamical Systems</i>	19
3.2.2 <i>Tertiary controller</i>	20
3.2.3 <i>Secondary controller</i>	28
3.3 <i>Software simulation tools</i>	42
3.3.1 <i>Simugrid</i>	42
3.3.2 <i>Yalmip and CPLEX</i>	45
<b>4 Results</b>	<b>47</b>
4.1 <i>Tertiary controller</i>	47
4.2 <i>Secondary controller</i>	56
<b>5 Conclusions</b>	<b>61</b>
5.1 <i>Conclusions</i>	61
5.2 <i>Limitations and future work</i>	62
<b>References</b>	<b>63</b>
<b>Nomenclature</b>	<b>71</b>



# ÍNDICE DE TABLAS

---

Table 1. Main current European projects for green H <sub>2</sub> production and uses	6
Table 2. Main current Spanish projects for green H <sub>2</sub> production and uses	8
Table 3. Summary of control strategies related to electrolyzers	11
Table 4. Parameters for dynamics equations	18
Table 5. Logical relations in a system and their corresponding linear inequalities (Table directly taken from [12]). Nomenclature: $\delta$ (binary variable), $S$ (statement represented by $\delta$ ), $a$ (vector of parameters), $x$ (continuous variable), $\epsilon > 0$ (small tolerance)	20
Table 6. Parameters for battery cost function (Taken from [12])	23
Table 7. Parameters for hydrogen cost function (Taken from [12])	25
Table 8. Parameters for battery Simugrid block	43
Table 9. Parameters for ultracapacitor Simugrid block	43
Table 10. Parameters for electrolyzer Simugrid block (referred to the cell)	44
Table 11. Parameters for fuel cell Simugrid block (referred to the cell)	44
Table 12. Parameters for metal hydride Simugrid block	44
Table 13. Data for the EVs charging	56
Table 14. Secondary controller cost function weighting terms for the grid-connected case	58





# ÍNDICE DE FIGURAS

---

Figure 1. Greenhouse gas emissions in mobility sector in <i>EU</i> (Source: [4])	1
Figure 2. Percentages of greenhouse gas emissions in transport sector and detailed share for road transport (Source: [6])	2
Figure 3. Scheme of the microgrid (Modified image from the original of [12])	16
Figure 4. Control strategy	19
Figure 5. Tertiary controller	21
Figure 6. Secondary controller	29
Figure 7. Simµgrid complete diagram	42
Figure 8. Day-ahead market energy price	47
Figure 9. Power evolution and storage level in the sunny and grid-connected case	48
Figure 10. Hydrogen control, binary and auxiliary variables in the sunny and grid-connected case	49
Figure 11. Battery control, binary and auxiliary variables in the sunny and grid-connected case	49
Figure 12. Grid control, binary and auxiliary variables in the sunny and grid-connected case	50
Figure 13. Power evolution and storage level in the cloudy and grid-connected case	50
Figure 14. Hydrogen control, binary and auxiliary variables in the cloudy and grid-connected case	51
Figure 15. Battery control, binary and auxiliary variables in the cloudy and grid-connected case	51
Figure 16. Grid control, binary and auxiliary variables in the cloudy and grid-connected case	52
Figure 17. Power evolution and storage level in the sunny and nearly-zero demand day and in grid-connected case	52
Figure 18. Hydrogen control, binary and auxiliary variables in the sunny and nearly-zero demand day and in grid-connected case	53
Figure 19. Battery control, binary and auxiliary variables in the sunny and nearly-zero demand day and in grid-connected case	53
Figure 20. Grid control, binary and auxiliary variables in the sunny and nearly-zero demand day and in grid-connected case	54
Figure 21. Power evolution and storage level in the sunny and islanded case	54
Figure 22. Hydrogen control, binary and auxiliary variables in the sunny and islanded case	55
Figure 23. Battery control, binary and auxiliary variables in the sunny and islanded case	55
Figure 24. EVs charging power demand profile	56
Figure 25. Extra hydrogen consumption profile	57
Figure 26. Power evolution in the sunny and grid-connected case. At the top: power schedule given by the tertiary controller; at the bottom: power reference given by the secondary controller	59

Figure 27. Storage level in the sunny and grid-connected case. At the top: storage level schedule given by the tertiary controller; at the bottom: real storage level measured from the equipment	59
Figure 28. Power evolution in the cloudy and grid-connected case. At the top: power schedule given by the tertiary controller; at the bottom: power reference given by the secondary controller	60
Figure 29. Storage level in the cloudy and grid-connected case. At the top: storage level schedule given by the tertiary controller; at the bottom: real storage level measured from the equipment	60

# 1 INTRODUCTION

It is well-known nowadays that our planet is suffering a climate change process, whose consequences are expected to be catastrophic if no urgent and drastic actions are taken. In fact, recently, the 2021 United Nations Framework Convention on Climate Change, UNFCCC, has held the 26<sup>th</sup> Conference of the Parties, COP26, in Glasgow [4]. There, the 197 parties agreed in reducing emissions in order to limit the increase in Earth temperature to 1.5 degrees. Similarly, the European Commission launched the European Green Deal in 2019 [5], whose main objective is to reach climate neutrality in 2050; i.e. no greenhouse gases would be emitted.

The previous reasons explain why an important part of European funds in the programme *Horizon Europe* after *COVID19* crisis are going to be allocated to support sustainable and *green* projects. In *Horizon Europe Programme* [6], some project topics to be funded are climate change, *UN's sustainable Development Goals* (there are 3 interesting from a total of 17: *Affordable and Clean Energy*, *Sustainable Cities and Communities*, and *Climate Action*), and improvements and growth of European technology and industry. One of the main areas in this programme is the *Pillar II (Global Challenges & European Industrial Competitiveness)*, which has 6 *Clusters*. One of those clusters is *Climate, Energy & Mobility*. About 53.4% of the budget will be allocated for that *Pillar II*, where 15.123 billion€ will be for *Cluster 5 – Climate, Energy & Mobility* (including 1.35 billion€ from *Next Generation Europe, NGEU*). In *Horizon 2020*, 30% of investments were destined to climate change. Digitalization is also present in *Cluster 4 – Digital, Industry & Space*, so projects combining environmental sustainability and digitalization as a key tool will have high priority in the following years.

As it has been told yet, an important topic in climate change is mobility. The *European Environment Agency* showed in 2021 that, in general, greenhouse gas emissions (*GHG*) in mobility sector are increasing, unlike in other sectors [7]. Figure 1 shows the change in emission levels since and with respect to 1990, and it can be observed how aviation, maritime and road transport emissions were increasing until *COVID19* crisis. This graph also predicts the future change in emission considering policy measures in *EU Member States* (with existing measures, *WEM*) and including national planned policies (with additional measures, *WAM*). It can be seen that in maritime and aviation sector there is a need for more severe measures, but in road transport it seems that emissions will decrease if planned measures are accomplished.

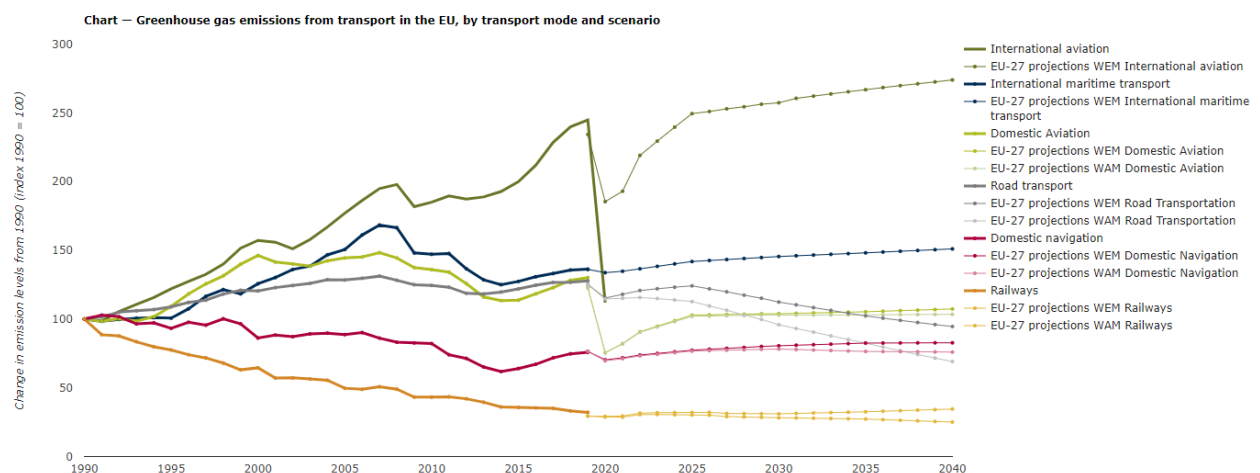


Figure 1. Greenhouse gas emissions in mobility sector in EU (Source: [7])

Looking at graphs in Figure 2, one can deduce why road transport is the one where more actions are scheduled to be done, since it is the main emitter of greenhouse gases. Cars are the principal contributors of those emissions in road transport. It is also known that when emissions comparisons are made per passenger and kilometer, aviation emissions are really high [8]. However, the less environmentally-friendly could be a one passenger car. So the growing interest in zero-emissions vehicles nowadays is reasonable.

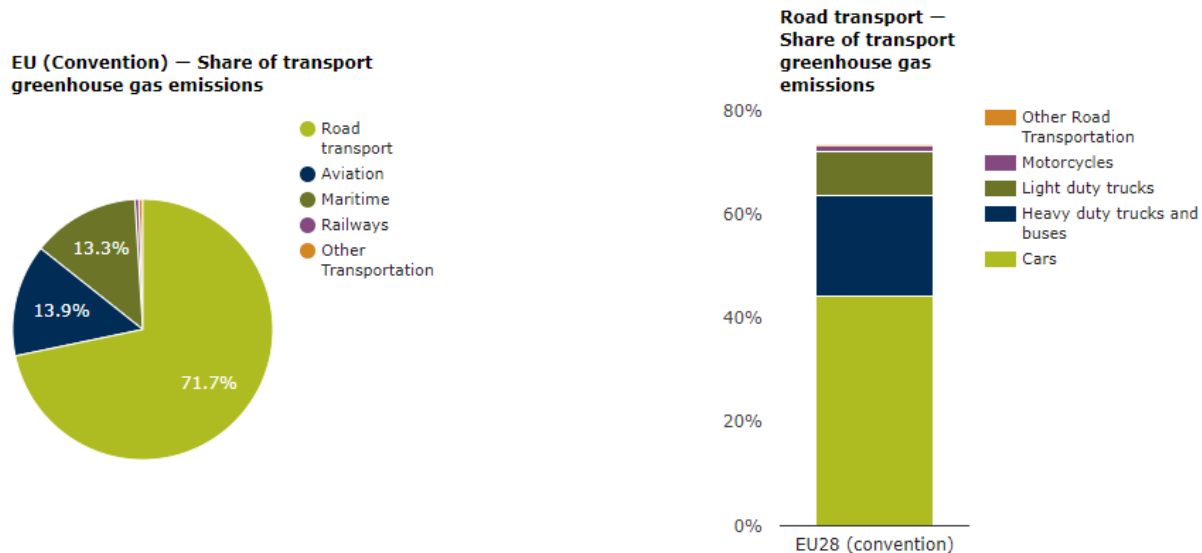


Figure 2. Percentages of greenhouse gas emissions in transport sector and detailed share for road transport (Source: [1])

Mobility emissions represent about 25% of total greenhouse gases emissions and road transport are a huge percentage of it [9]. So, in spite of encouragement to use rail transport to decarbonize, it is clear that also a change in paradigm of road mobility should be carried out if *EU 2030* and *2050* targets with respect to emissions want to be reached.

In the described context, renewable energy production and electric mobility must play a crucial role in the decarbonisation and energy transition. But both have the problem of intermittence, since the first one depends on meteorological conditions and the second one, on people behaviour as in classical energy consumption. Energy production and consumption prediction and energy storage systems, *ESS*, help in coping with such variability. In 2021, *Spanish Government* has launched its own *Energy Storage Strategy*, where energy storage system such as batteries, hydrogen and supercapacitors are highly considered [10]. A strategic roadmap for encouraging *ESS* use is developed, including an external and independent roadmap for hydrogen, which is considered one the most promising energy vector [11]. The Spanish budget for 2022 includes 2184.6 M€ for sustainable mobility and 1646 M€ for energy transition [12]. Moreover, renewable energies and sustainable mobility are the topics where more funds from *NGEU* will be allocated in Spain [13].

Here is where the concept of microgrid appears. Microgrids are production energy systems which are composed of energy production and storage equipment for short and medium scale consumption [2]. They work in an independent manner and can be connected to the main grid or other microgrids, helping in the balance and stability problem of the electrical network.

## 1.1 Context and objectives

The entire described above serve as an impulse to this work. The final objective is to build a microgrid in the laboratory facilities to be used for zero-emissions vehicle recharging, including both electric and hydrogen-based vehicles. This is a project which appears as a synergy between electrical, energy, electronic and automatic control departments, among others. Each of these contributors will provide their experience and available equipment. The microgrid will be composed of photovoltaic (*PI*) field, batteries, hydrogen technology (electrolyzer, metal hydride storage and fuel cell), ultracapacitor, connection with the main grid,

electric vehicle charging points and hydrogen-based vehicle recharging points.

The goal of this work is to develop an efficient energy management strategy for that microgrid, which will be able to decide the energy flow between equipment in every time instant. This is done using two MPC controllers deciding the energy flow in an optimal way, taking into account equipment limitations and degradation problems. The first MPC-controller uses energy consumption, production and price forecasts every hour to give references to the second controller, which will act in a timescale of seconds correcting power deviations and coping with instantaneous changes in energy consumption and production. These deviations will be increased by an extra hydrogen demand for recharging a hydrogen vehicle available in the laboratory and by the electric power demanded by electric vehicle charging process. The output of the second controller will be used in the future as references to the electronic power converters, which will act in the milliseconds scale, but they are not implemented in this work.

The controllers are tested in simulation using *MATLAB/Simulink* with the model of the microgrid built from *Simugrid*, a simulation tool developed by the *Automatica y Robótica Industrial* research group some years ago. For solving the optimization problem, *Yalmip* toolbox and solver *CPLEX* are used for the first controller, and solver *quadprog* without *Yalmip* for the second controller.

## 1.2 Metodology

To achieve the mentioned objectives, the following steps have been carried out:

- *State-of-Art* review, especially in the green hydrogen and electric vehicle charging station fields.
- Microgrid planning, gathering available equipment information, and simulation model setting up.
- Study about microgrid control strategies.
- Install and learn how to use *Yalmip* toolbox and solver *CPLEX* in *MATLAB*.
- MPC-controllers (tertiary and secondary) design and testing in simulation.
- Creation of extra demand for zero-emission car charging station: hydrogen and electric power.

So, this report is organized as follows. This introduction is followed by the state-of-art, mainly focused on hydrogen technology and electric vehicle charging process in microgrids. Section 3 is the most important since it is dedicated to controllers design. The control strategy is described and equations for both of them gathered, explaining how to implement it in simulation. In this section, some brief instructions for including *Yalmip* and *CPLEX* in *MATLAB* are given, as well as some hints to implement the secondary controller with *quadprog*. Results from the different simulations carried out are exposed and analyzed in section 4. Different scenarios are tested including sunny and cloudy days. Finally, conclusions from the previous sections are shown in section 5, where future works are mentioned in order to continue with this project.



## 2 STATE-OF-ART

---

Literature about renewable energy has been widely developed and one can read about lot of projects and publications working on the microgrid field. Advantages of proper microgrid control have been discussed and efforts are focused on this topic. The main reference for this work is [2], where the concept of microgrid is describe and analized, deriving the need for control and developing some advances control techniques using MPC. In that contemporary work one can see the huge amount of related literature which has been developed so far.

Building-up a microgrid is a task which has been extensely done yet. Due to some of the equipment used were part of the *Hylab* laboratory in the University of Seville, two interesting works are [14] and [15]. In the first one, the authors show how Hylab microgrid was set up in order to use it in the future with control purposes. It pretends to cover an initial phase in microgrid control: the correct modelling, characterization and building of the microgrid. In the second one, Hylab components (*PV* panels, *PEM* electrolyzer and fuel cell, metal hydride tank and battery) are modelled and validated in the real plant with the aim at considering dynamics and being as simple as possible. The models are of interest for control purposes. Some data and parameters for doing simulations in Simulink are taken in this work from these two papers.

Microgrids with hybrid energy storage systems seem to be adequate for taking advantages of different technologies. In this context, hydrogen is getting more and more importance. Electrolyzers are chemical devices which use *DC* current and water in order to produce hydrogen, so if the *DC* electricity comes from renewable energies, the process will be green. Then, hydrogen is stored in tanks for later use in fuel cells, where it is again converted to *DC* current to supply the microgrid.

The use of green hydrogen is extensive and it is expected to be greater in next years. Hydrogen can be used [11] as raw material in refineries, steel production or chemical industries, in sectorial integration absorbing and storing energy excess from renewable energies or being mixed in gas infrastructures, as fuel cell combined with batteries in mobility (cars, vehicles or heavy-duty transports) where an inverse electrolysis process is needed to produce electricity and the unique residual product is water. Other uses such as power supply or heating in buildings are being investigated.

As there are important technological developments in fields like fuel cells or electrolyzers which make green hydrogen feasible, and advantages and uses are really interesting, companies, governments and research centers have been putting an intensive effort on improving these technologies. In particular, there are drawbacks which have not allowed green hydrogen to be fully developed [16]. In that way, it is necessary to make green hydrogen technology more costly and energy efficient. The process from electricity-to-hydrogen has an efficiency of about 50% [10].

So we are now in a context where lots of projects are being developed in order to demonstrate in real plants the feasibility of green hydrogen production via water electrolysis for different uses. The current situation is the development of *PEM* (sometimes alkaline) electrolyzers-based plants in the *MW*-scale production, with the goal of reaching *GW* by 2030. In Europe green hydrogen seems to be a trend in North-Western countries such as Netherlands, Northern Germany or Norway, which are more intensive in green hydrogen production, typically taking electricity from wind sources instead of solar ones. The most important and present projects in Europe are summarized in Table 1. As they are projects in course, some data are not available yet and even there is no an official website.

In Spain there is a recently intensive activity because of the strategy adopted by Spanish Government, which has published a *Hydrogen roadmap* [11]. This plan relies on green hydrogen production and storage (as other storage methods as detailed in [10]) in order to recover from *COVID-19* crisis. It can be observed a change with respect to European projects in the energy source. Climatological conditions in Spain made possible more solar-to-hydrogen production than in North Europe, so the government aims at positioning Spain in the top of

Project	Location	Description / Goal	Cap. MW	Prod. tons	Source	Main use <sup>(5)</sup>	Date <sup>(2)</sup>	Companies
[17] H24ALL	Spain	Construct a high-pressure alkaline electrolyzer which can work in a 100 MW green H <sub>2</sub> production plant Produce at 3 €/kgH <sub>2</sub>	100	- <sup>(1)</sup>	- <sup>(1)</sup>		Jan 2021	Repsol, 14 partners from Belgium, Denmark, Germany, Norway, Spain, Turkey
[18] FCH2RAIL	Belgium, Germany, Spain, Portugal	Zero-emissions trains fed by aerial grid and a fuel cell system (with both H <sub>2</sub> fuel cell and batteries) Alternative to diesel trains and in zones where it is difficult to electrify Trying to take advantages of fuel cell heat for the train air-conditioning	- <sup>(3)</sup>	- <sup>(3)</sup>	- <sup>(3)</sup>	Fuel Cell for trains	Jan 2021	Toyota, Renfe, ADIF, CAF, partners from Belgium, Germany, Spain and Portugal
[19] Lingen Green Hydrogen	Germany	Green H <sub>2</sub> production Improve electrolyzer efficiency	50	9000 year	Wind	Refinery	Nov 2020	BP, Ørsted
[20] NortH2	Netherlands	Green H <sub>2</sub> production	1, 4, +10 GW <sup>(4)</sup>	1·10 <sup>9</sup> year	Offshore wind	Industry	Feb 2020	Gasunie, Groningen Seaports, Shell Nederland, Equinor, RWE
[21] Djewels	Netherlands	Development of a high pressure alkaline electrolyzer	20	3000 year	Wind or solar	Methanol production	Jan 2020	Nouryon, Gasunie, McPhy, BioMCN, DeNora, Hincio
[22] ITM Linde Electrolysis GmbH	Germany	Green H <sub>2</sub> production with the largest PEM electrolyzer in the world (24 MW)	24	- <sup>(1)</sup>	- <sup>(1)</sup>	Industry	<sup>(6)</sup> 2 <sup>nd</sup> half 2022	Joint venture between Linde and ITM Power
[23] Green Hydrogen	France	Green H <sub>2</sub> production in a new electrolyzer plant	200	28000 year	Wind or solar	Industry and mobility	Jan 2021	Air Liquide, H2V Normandy
[24] MassHylia	France	Green H <sub>2</sub> production Optimal management in the integration between different solar fields and the H <sub>2</sub> uses	40	5 day	Solar	Biorefinery	<sup>(7)</sup> Jan 2021	Total, Engie
[25] Hybridge	Germany	Studying green H <sub>2</sub> production with both PEM and alkaline electrolyzers Trying to adapt gas transportation infrastructures to H <sub>2</sub>	100	- <sup>(1)</sup>	Wind or solar	Mobility, heating, etc.	<sup>(6)</sup> 2023	Amprion, Open Grid Europe
[26] BP Rotterdam Refinery	Netherlands	Green H <sub>2</sub> production	250	45000 year	Offshore wind	Refinery	<sup>(8)</sup> 2022	BP, Nouryon, Port of Rotterdam
[27] REFHYNE	Germany	Green H <sub>2</sub> production with PEM electrolyzer	10	1300 year	Wind or solar	Refinery. Exploring industry, power generation, heating, mobility	<sup>(9)</sup> Jan 2018	Shell, ITM Power
[28] H2Future	Austria	Green H <sub>2</sub> production with PEM electrolyzer	6	1200 m <sup>3</sup> /h	Wind or solar	Steel production plant	Jan 2017 Nov 2019 (Prod)	Verbund, voestalpine, Siemens, Austrian Power Grid, TNO, K1-MET
[29] ELEMENT ONE	Germany	Power-to-gas pilot plant Focus on electricity and gas grids connection, especially in the storage with gas transmission infrastructures	100	- <sup>(1)</sup>	Wind	Methane production (industry), mobility	<sup>(10)</sup> Oct 2018	TenneT, Gasunie, Thyssengas
[30] OYSTER	- <sup>(1)</sup>	Green H <sub>2</sub> prod. with compact PEM electrolyzers (integrated offshore) which adapt to tough conditions	MW	- <sup>(1)</sup>	Offshore wind	- <sup>(1)</sup>	Jan 2021	Element Energy, ITM Power, Ørsted, Siemens Gamesa Renewable Energy

<sup>(1)</sup> Not available data

<sup>(2)</sup> Project announcement data, not necessarily producing H<sub>2</sub> at that time

<sup>(3)</sup> It is not hydrogen production, but hydrogen application

<sup>(4)</sup> 1 GW in 2027, 4 GW in 2030, +10 GW in 2040

<sup>(5)</sup> But in most cases not limited to

<sup>(6)</sup> Date scheduled to start production

<sup>(7)</sup> Start construction in 2022 and production in 2024

<sup>(8)</sup> Now in feasibility study. Decision will be made in 2022

<sup>(9)</sup> It is operating since middle 2021

<sup>(10)</sup> To start in 2022

Table 1. Main current European projects for green H<sub>2</sub> production and uses



Project	Location	Description / Goal	Cap. MW	Prod. tons	Source	Main use <sup>(4)</sup>	Date <sup>(2)</sup>	Companies
[11] [31] H2PORTS	Valencia	Hydrogen station and H <sub>2</sub> supply management in the port	- <sup>(3)</sup>	- <sup>(3)</sup>	- <sup>(3)</sup>	Fuel for operating machines in the port	Jan 2019	Autoridad Portuaria de Valencia, Fundación Valenciaport, Centro Nacional del Hidrógeno, MSC Terminal Valencia, Grupo Grimaldi, Hyster-Yale, Atena, Ballard Power Systems Europa, Enagás
[11] SUN2HY	Móstoles (Madrid)	H <sub>2</sub> production with electro-catalysis (PEC technologies, direct conversion from solar and water to H <sub>2</sub> ) and real implementation in the first plant (Puertollano) of this type without grid connection	- <sup>(1)</sup>	- <sup>(1)</sup>	Solar	- <sup>(1)</sup>	2019	Enagás, Repsol
[11] SEAFUEL	Tenerife	Green H <sub>2</sub> production with wind energy and sea water	- <sup>(1)</sup>	- <sup>(1)</sup>	Wind	Hydrogen vehicles	2017	9 partners and 6 associate members, including companys of all areas. Enagás is an associate member
[11] HIGGS	Participants research centers	International project for H <sub>2</sub> injection in high pressure natural gas networks	- <sup>(3)</sup>	- <sup>(3)</sup>	- <sup>(3)</sup>	Transportation for different uses	Jan 2020	Fundación Hidrógeno de Aragón, Redexis, Tecnalia, DVGW, HSR, ERIG
[11] [32] GREEN HYSLAND	Mallorca	The first project of a Mediterranean country which will be funded by European funds and it is expected to be the first H <sub>2</sub> hub in Southern Europe	7.5	300 year	Solar	Buses, rent-a-car vehicles, power, heat	Jan 2021	Acciona, Enagás y Cemex, Baleares Government, IDAE, Redexis, FHa, Islas Baleares University
[11] [33]-	As Pontes (A Coruña)	The Spanish Gov. wants to create a <i>hub</i> there to produce green H <sub>2</sub>	100	10000 year	Wind	Industry, mobility	Jan 2021	Endesa
[11] [34] GREEN SPIDER	Asturias	Green H <sub>2</sub> production to be used for local consumption and in order to export to Germany and Netherlands	350	- <sup>(1)</sup>	Wind (250 MW) and solar (100 MW)	Steel production	Feb 2021	Naturgy, Enagás
[11] [35]-	Puertollano (Ciudad Real)	The biggest green H <sub>2</sub> production (PEM electrolyzer) plant for industrial use in Europe The next project will be in Palos de la Frontera (Huelva). Between both they get 800 MW electrolysis (20% of national goal for 2030) Iberdrola has also constructed three hydrogen stations (5 MW electrolyzers in each one) in Valencia, Alicante and Murcia whose green H <sub>2</sub> is used in heavy transport	20	- <sup>(1)</sup>	Solar	NH <sub>3</sub> and fertilizer production	Start in 2021	Iberdrola, Fertiberia
[11] -	Huesca	Green H <sub>2</sub> production and grid connection	- <sup>(1)</sup>	- <sup>(1)</sup>	- <sup>(1)</sup>	Mobility (road and rail)	2020	Fundación Hidrógeno de Aragón
[11] [36] E-FUELS BILBAO	Bilbao (Vizcaya)	Use of green H <sub>2</sub> + CO <sub>2</sub> from Petronor oil refinery in order to obtain synthetic fuels It will allow steel or concrete factories to "reuse" the CO <sub>2</sub> produced and become carbon-neutral	- <sup>(3)</sup>	50 synth. fuels barrels day	Wind and CO <sub>2</sub> captured	Synthetic fuels for vehicles, trucks or planes combustion engines	Jun 2020	Repsol, Petronor, Saudi Aramco, Ente Vasco de la Energía (EVE)
[37] Therm. Power Plant Barranco de Tirajana	Barranco de Tirajana (Gran Canarias)	Install renewable energy to feed electrolyzers (energy excess will be used to support the grid). It is a green H <sub>2</sub> production plant	7	- <sup>(1)</sup>	Solar	- <sup>(1)</sup>	Feb 2021	Endesa

Project	Location	Description / Goal	Cap. MW	Prod. tons	Source	Main use <sup>(4)</sup>	Date <sup>(2)</sup>	Companies
[37] Peninsular projects Endesa	Huelva, Teruel, Almería, Tarragona, el Valle del Ebro (Hidrógeno del Cierzo), Compostilla (León), Seseña (Toledo)	Different green H <sub>2</sub> production projects	Up to 250	- <sup>(1)</sup>	Wind or solar	- <sup>(1)</sup>	2021	Endesa
[37] Extra-peninsular projects Endesa	Canarias, Balears, Melilla	Both green H <sub>2</sub> production (Barranco de Tirajana and Granadina, in Canarias, and Alcudia, in Balears) Use in thermal plants fuel substitution with bi-fuel (including H <sub>2</sub> )	Up to 25	Up to 26000 year	Wind or solar	- <sup>(1)</sup>	2021	Endesa
[38] LIFE REWIND	Huesca	PV-Diesel hybrid system as fuel for electric vehicles	- <sup>(3)</sup>	- <sup>(3)</sup>	Solar	Electric vehicles in agriculture works	2017 Ended	Intergia Energía Sostenible, S.L.
[39] -	La Robla (León)	Green H <sub>2</sub> production with the biggest electrolyzer in Spain Export H <sub>2</sub> to North Europe	60	9000 year	Solar	Local consume, injection in gas grid, export to Europe	Dec 2020	Naturgy, Enagás
[40] -	Amorebieta (Vizcaya)	Green H <sub>2</sub> production	<sup>(5)</sup> 20 200	1500 year	- <sup>(1)</sup>	Use in the plant, fuel to heavy transport, export to Europe	<sup>(6)</sup> Dec 2020	Sener, Nortegas, White Summit Capital, Castleton Commodities Internacional (CCI), Bizkaia Energía

<sup>(1)</sup> Not available data  
<sup>(2)</sup> Project announcement data, not necessarily producing H<sub>2</sub> at that time  
<sup>(3)</sup> It is not hydrogen production, but hydrogen application  
<sup>(4)</sup> But in most cases not limited to  
<sup>(5)</sup> First, 20 MW. Expected to be 200 MW before 2030  
<sup>(6)</sup> Start production in 2022

Table 2. Main current Spanish projects for green H<sub>2</sub> production and uses

hydrogen production and exporter countries. Table 2 sums up some of the most important and recent projects in Spain. *Iberdrola* (53 projects), *Endesa* (23 projects), *Enagás* and *Repsol* are the more active companies in the sector in Spain.

It is clear that hydrogen support is getting more and more importance. In fact, there are a lot of more projects that has not been mentioned here. From Table 1 and Table 2 one can state:

- There are so many funds for green hydrogen
- Wind source is more typical in North Europe and solar in Spain
- There is a trend from megawatts (today) to gigawatts (2030)
- Both PEM and alkaline electrolyzers are used, but PEM seems to be more frequent
- Projects are focused on demonstrate in real scale the feasibility of green hydrogen
- It is necessary to reduce production cost and increase system efficiency

The last statement should lead researchers to further investigate electrolysis process, trying to improve electrolyzers. In fact, there are some researches that publish papers or participate in conferences with some news about green hydrogen production. A key part is the process control, where some authors have been working. Basically, one can differentiate between some process variables low-level control like temperature or pressure control (typically carried out by manufacturers), and a high-level one in which one has a complete microgrid with electrolyzers among other elements and wants to manage the demand, regulating the flow of energy and the production or consumption of green hydrogen.

But previous to control the system it is necessary to know electrolyzers and the whole production system well. A MATLAB/Simulink control-oriented PEM electrolyzer model was developed in [41] and some years later, [42] used it to further modelling the entire *Balance of Plant, BoP* of the electrolysis process. More recently, in [43] the authors aim at better understanding the multi-physical phenomenon of H<sub>2</sub> production in water electrolysis, both with PEM and alkaline electrolyzers. They split up the model in different modules: fluid-dynamic (mass flows), thermodynamic (partial pressures), electro-chemical (to connect the input electric power with the output hydrogen flow) and thermal (temperature). For that reason, they develop a simple model of the process based on energy flows which includes ancillary systems, validate it with experimental data and then, scale-up the model for the simulation of a H<sub>2</sub> production infrastructure using the model. The developed model could be used for the development of new control methods and energy management techniques for that process. Anyway, the electrolyzer modelling has been widely treated by the research community, as can be seen in [15], [44], [45], [46], [47], [48], [49] and [50]. In the majority of cases, the model need for a previous identification process in order to estimate all model parameters.

The model developed in [43] shows that in the thermal module of the model there is a heat power term which represents process cooling, so they state that it must be controlled with a proportional valve in order to reach a *setpoint* in temperature. In fact, in [46] that control system is developed. Authors obtain a high-fidelity mathematical model (almost the same as [43]) and expose that the membrane degrades at high temperatures. This last problem with temperatures contrasts with the fact that electrolyzer energy conversion efficiency improves with higher temperatures, so there must be a trade-off. They develop an explicit multi-parametric MPC for controlling the temperature (in particular, differential temperature for taking care of variations). The manipulated variable is the water flowrate entering the electrolyzer. Electrolyzer inlet water temperature and current supplied are considered as disturbances. It is shown that water plays two roles: as product in chemical reaction and as process coolant. Results are validated in a lab-scale electrolyzer. It is proposed for future works to do other classical control schemes for comparison and longer experiments (more time) that better demonstrate membrane degradation and improvements due to control strategy.

The water supplied to the electrolyzer is also part of the control in [47] and [51], where the objective is to maximize the H<sub>2</sub> production with electrolysis using photovoltaic power in a kind of microgrid with solar panels, grid, PEM electrolyzer and load. The first paper tries to increase the performance of the system (more H<sub>2</sub> produced) by including a *DC/DC Buck converter* (controlled digitally via *MPPT*) between the solar panels and the electrolyzer to maximize the quantity of power transferred from the PV to the electrolyzer and by controlling the water flow that enters the electrolyzer (they do not specify how to act upon the water pump). It is important to note that it is derived a relation which shows that the necessary water quantity to produce the maximum H<sub>2</sub> only depends on the available PV power. They do not show experimental results, only deduce a theoretical model and implement it in simulation.

The second paper acts as the first one (it is like its continuation) but in the water flow control uses now the gravity instead of a pump for less energy consumption (in this case they specify how to calculate the current to command the electrovalve). It is an open-loop controller, so if perturbations are considered, it would be necessary to use a closed-loop regulator in order to reject disturbances (they do not consider them). The water flow control simply measures the available PV power and applies a proportional current to the valve in order to obtain the right amount of water flow to maximize H<sub>2</sub> production. The gravity system acts as follows. From electrolyzer, H<sub>2</sub> and O<sub>2</sub> (with electrolytes) are stored in bubblers to be separated. Electrolyte (water) falls to the main tank when a certain level is reached in H<sub>2</sub> or O<sub>2</sub> tanks (logic controller). Then, the main tank (only contains water), supplies water to the electrolyzers, controlled by an electrovalve.

Moreover, in this second paper, a *Power Management Strategy (PMS)* is included in order to better decide the flows, sources and sinks of energy in the microgrid. It is a logical high-level controller whose input is the load power and the output is to decide whether to use the solar panels or the grid as source and whether to allocate PV power to electrolyzer or directly to consumption. Solar radiation and load changes are considered as perturbations in that simple model.

But this power management system could be further improved with more sophisticated techniques. Some years ago (2012), [52] proposed an interesting method which will be highly used since then in other publications of the same authors and most of them are gathered in [2]. They wanted to manage the power in a microgrid with solar panels, PEM electrolyzer, fuel cell, batteries and H<sub>2</sub> storage system in order to satisfy the demand, taking care of equipment operational constraints. Other equipment such as ultracapacitor is included in later publications, as can be seen in [2].

The technique used is to simulate a supervisor MPC. The idea is, assuming that there are low-level equipment control (temperature, flow, pressure, etc.), to develop a high-level MPC controller with restrictions. The MPC formulation is designed to satisfy user power demand optimally and the cost function aims at electrolyzer and battery usage and prevents equipment from damage. The objective variables to control are the battery *State Of Charge (SOC)* and the H<sub>2</sub> storage *Metal Hydride Level (MHL)*. The controller output gives power references for the electrolyzer, the fuel cell and the grid. Net power (power generated by solar panels minus demand power) is considered as disturbance due to its stochastic behavior. Results of [52] are only proven in simulation, but real validation is proven in following works, as can be deduced from [2].

Later, in 2016-2017, authors of [53] developed a non-linear with binary and continuous variables MPC strategy (solved with *Mixed-Integer Quadratic Programming, MIQP*) in order to control alkaline electrolyzers operating points in terms of power. Electrolyzers are, in general, different among them and are fed by wind and wave energy. They also take care of reducing the number of switches between *ON/OFF* states for every electrolyzer, as considered in other previous publications like [54], [55] and [56]. With this and other operating restrictions, they formulate the complete MPC problem. The MPC aims at maximizing H<sub>2</sub> production (consuming the electrolyzer as much renewable energy as available) and taking care of electrolyzers' connections and disconnections. It gives the operating point for each electrolyzer (discrete variable) as outputs, trying to control electrolyzer H<sub>2</sub> production and energy consumption (one can see the ratio H<sub>2</sub> produced/Energy consumption to evaluate electrolyzer performance). Successful results are finally obtained, but again only in simulation.

More recently, in January 2021, a general vision of the whole control process in electrolysis is given in [57], focusing on the high-level controller. It is the first approach which solves both model identification (experimental gray model) and nonlinear MPC control for PEM electrolyzers with *Mixed-Integer Linear Programming, MILP*. They have an available PEM electrolyzer with 4 stacks, supplied by PV panels and the grid, and aim at controlling the DC power supply given to the PEM in order to match the H<sub>2</sub> demand in a fuel cell vehicle fleet. They also have a linearized controller version, with worse results. With the MPC, minimization of production cost is expected. The MPC manipulated variable is the electrolyzer power input and the control variable is the hydrogen production which has to follow the reference of vehicles demand.

The temperature control seems to be internally done (not developed in paper) by the cooling loop with hysteresis and a *PID* for the setpoint. The manipulated variable is a three-way valve and the control variable is the electrolyzer stack temperature. It is done with a *PLC*, which also controls stacks voltage and current (for working at the desired values and protecting from overcurrent) and acts over some actuators (not specified) of the electrolyzer.

They show validation in real electrolyzer and propose some future improvements:

- Higher prediction horizon if deterministic data are known
- Stochastic data instead of deterministic for PV panels
- Improving the model: including tank pressure and periodically refitting parameters
- Include startup/shutdown dynamics in MPC

From all the above publications, it seems to be clear to differentiate between two types of control strategies in hydrogen production systems: high-level and low-level controllers, whose typical characteristics are gathered in Table 3. High-level controllers are focused on managerial aspects of the whole process included in a microgrid. Low-level, centered in electrolyzer process variables control, is usually given by electrolyzer manufacturers. Both high and low-level controller development has not been found in any paper at the same time.

Another conclusion from the analyzed literature is that most of them choose simulation and the software *MATLAB*, although there are other ways such as *PLCs* for logical controllers plus a simulator. Unlike simulation, there are very few real implementations of control methods for this kind of systems. Above all, there is a lack of real implementations of the whole systems, including renewable energy sources like PV panels.

To conclude with hydrogen, it is appropriate to comment here some considerations and trends from the most recent publications about green hydrogen.

Control level	Focused on	Controlled variable	Manipulated variable (output)	Control objective	Disturbances	Examples
High-level	Grid	H <sub>2</sub> production	Electrolyzer input power (PV → Electrolyzer) <sup>(1)</sup>	Maximize H <sub>2</sub> production and/or renewable consumption	Renewable energy generation Power demand	MPC Logical controller
				Minimize H <sub>2</sub> production cost and/or grid power consumption		
				Take care of components physical limits: SOC (batteries), MHL (H <sub>2</sub> storage), etc. Reference (present and future) tracking: H <sub>2</sub> demand		
Low-level	Process	Temperature	Water valve opening Water pump	Reference tracking: operating point from manufacturers	Inlet water temperature and current supplied	PID
		Electrolyzer input power (PV → Electrolyzer)	PWM DC/DC converter switch	Reference tracking: required electrolyzer input power as a function of the goal followed <sup>(2)</sup>	- <sup>(3)</sup>	DC/DC Buck converter controlled digitally via PWM/MPPT <sup>(4)</sup>

<sup>(1)</sup> It gives the reference for low-level controller which is in charge of electrolyzer power supply (between renewable source and electrolyzer)  
<sup>(2)</sup> It comes from the high-level controller  
<sup>(3)</sup> Not data for that  
<sup>(4)</sup> MPPT is used for tracking the maximum power point of the PV panels

Table 3. Summary of control strategies related to electrolyzers

The text of [58] is focused in transportation and distribution of produced green hydrogen. In UK they pretend to use the whole storage capacity of the gas network for hydrogen from renewable energy storage. In Australia, due to the excess of renewable energy production, they are studying how to tech- and cost-efficiently export that energy. The author also states that electrolyzer price is high and will only decrease with economy of scale, so increasing hydrogen production. In conclusion, green hydrogen will play a crucial role in decarbonisation, but there are still managerial and infrastructural challenges.

In [59] they give interesting data of green hydrogen uses: hydrogen fuel cells have an efficiency of about 50%, where 60% is in hydrogen-to-power and 90% in power-to-kinetic energy. They also show a description and the challenges of:

- Production. Electrolysis process needs to improve efficiency (about 50%) and lifetime (<5 years) and need compressors. Some production methods are still being developed, such as photoelectrochemical (PEC) water splitting which can be seen in *SUN2HY* project in Móstoles (Madrid) [11].
- Storage, transportation and distribution.
- End use. They detail the main characteristics of hydrogen-based fuel cell electric vehicles, which are more efficient than gasoline fuel, green and increase autonomy.

Some drawbacks of hydrogen are presented in [60]: low density (high volume to produce, low power output because of air presence), high investment, production and transportation costs and need for big storage space.

Finally, [61] presents green hydrogen as a strong alternative to currently used batteries, whose costs (investment, operation, maintenance and so on) are really high. He highlights the fact that PEM electrolyzers has improved overall hydrogen production process efficiency, but still need improvements. Numbers are: increasing in 60-80% efficiency in power-to-hydrogen processes and more than 25% in hydrogen-to-power processes. He also shows the work to be done with PEM and PEC (photoelectrochemical water splitting) and improvements in course with respect to electrolyzers (focused on new or better materials for the membrane).

Another emerging field nowadays is sustainable mobility, where even hydrogen can have some applications. Novel projects are being developed in fields such as road vehicles, train, maritime or aviation sectors, where

hydrogen could be used as a fuel for some kind of combustion motors or as an electricity generator for electrical motors, using fuel cells (which convert hydrogen and oxygen in water and electricity).

For instance, aviation sector has proposed to reduce 50% CO<sub>2</sub> emissions by 2050. For that objective and a cleaner air in airports, hydrogen is an option as an alternative fuel in even big aircrafts or as main power system via fuel cell (FC) in smaller aircrafts [11] [62]. In course-projects examples for the first one are: *Westküste 100* in the airport of Hamburg [63], *ENABLEH2* in North Europe [64], *Kopernikus* in Germany [65] and *e-Fuels Projects* of the company *Sunfire* [66]. For fuel cell applications, some in course-projects are: *HyFlyer Projects* of *ZeroAvia* [67] [68], *ZEROe* by *Airbus* [69], *Skai* from *Alaka'i* company [70], *BALIS Project* launched by the *German Aerospace Centre (Deutsches Zentrum für Raumfahrt, DLR)* [71] and *Element One* from the company *HES Energy Systems* [72]. Other applications [11] [73] could be as *Auxiliary Power Units, APUs*, (an example of design can be seen in [74]) or as power to airport machinery.

In [75] it is intended to study heavy-duty transport, and specifically maritime, aviation and haulage sectors, in order to decarbonise them seeking for new low-carbon fuels. Electrification, unlike conventional vehicles, seems to be difficult for those sectors because of the big size. The idea is to obtain new alternative fuels which can be liquid, such as biofuels, cryogenic hydrogen or synthetic fuels, or gaseous, such as compressed hydrogen or biomethane. Some of them can be used in current engines and the others need new machines such as fuel cells, batteries or electric motors. Respect to *electrofuels*, such as hydrogen, they say that emissions are higher if only grid electricity is used. But electrolysis with only renewable energies is quite expensive. So, the idea could be to have a good forecast system for renewable energies and consume both from the grid and from the renewable, trying to avoid high-carbon (high-price) grid electricity consumption. This is an idea that could be applied to microgrids if the objectives are economic.

But in the mobility sector, the field where more changes are being carried out is in cars. Now, there is an important support to *Electric Vehicles (EV)* or even *Plug-in Hybrid Electric Vehicles (PHEV)*, which both can be charged from the electrical grid. They contribute to take care of the planet and the contribution is higher if the electricity is taken from renewable resources. This is the idea of [76], where authors present a DC EV fast-charging station with PV generation and grid connection and with the possibility of *Vehicle-to-Grid, V2G*, mode. They described the 3 main power converters (grid-DC bus, PV-DC bus and EV-DC Bus) along with their models and controllers. They implemented a simple rule-based heuristic controller as *Energy Management System, EMS*, based on the DC bus voltage. That control strategy means that four operating modes could be chosen: *PV to EV, PV to Grid, (PV) and Grid to EV, EV to Grid (V2G)*. They finally concluded the use of EVs in balancing electricity network is beneficial, as they are important to support in grid demand and in reactive power compensation, as well as EVs have important impact on health and environment. The results from that work are tested in MATLAB/Simulink simulations but not validated in real experiments.

Another microgrid including EVs is designed and controlled in [77]. Authors presented an optimization method to minimize an economic cost index in using electricity for AC and DC electric vehicles charging stations, which can be connected to the grid, supported by PV panels and batteries. They use a *Multi-Agent Particle Swarm Optimization, MAPSO*, algorithm in order to size the number of batteries and PV panels, as well as to calculate the energy exchanges between grid, PV panels, batteries and EVs. That work does not include V2G mode. They compared three scenarios (without PV, without grid and with all) and the last one seems to be the most cost-effective and sustainable. The load of electric vehicles is taken from a simulation model assuming that the EV arriving the station follow a similar distribution as light-duty vehicles going to gas stations. Moreover, charging times are assumed to follow a normal distribution. The MAPSO algorithm results to be effective, stable, strongly robust, accurate, with convergence speed and can be solved in a reasonable time. Moreover, results were proven in Shanghai.

The previously mentioned work includes a model for EV charging load based on the moments of EVs arrival and their charging duration, and on the maximum power each charger could provide, as well as some already mentioned assumptions. In [78], they propose a scheme to modelling EV charging load profiles which includes scenarios of peak demand, where the grid is not able to deliver the total power required by EVs. The model is based both on real data (such as arrival times and charging duration distributions or maximum charging power for each kind of EV) and assumptions (like the events of high demand in the grid or the behaviour of EV owners while charging, who can stay in the charging station whether for a specific time or for energy targets). The model does not include EV SOC knowledge because this data is not part of the

communication between the electric vehicle and the charging station in the dataset.

The idea of that work is not only to have a method for modelling load profiles and sizing charging stations, but also to highlight the advantages of EVs batteries flexibility. A lot of scenarios can be simulated: number of chargers, demand response events, different arrival time distributions, etc. However, in this case they do not include V2G transactions, which would make it even more flexible. In this case, it is not like a microgrid concept. Instead of having storage units to mitigate the effects of peak demand, the simple proposed solution is to reduce the power destined to charge EVs, affecting charging duration for energy-based EVs.

Once the recent and relevant literature has been explored, one can see that microgrid with hybrid storage including hydrogen and even zero-emissions vehicle charging as a load and as a storage system, have lots of advantages. When different types of power generation, consumption and storage, the problem of energy management becomes difficult, so different kind of control techniques have been proposed in this field [2]:

- **Heuristic methods**, as can be seen in [51] and [76]. One of the most used is the well-known *Hysteresis Band Control*, *HBC*, where the Energy Storage Systems stores or dispatches (also the generators) energy if SOC is between upper and lower thresholds. If more than upper, stop generation or sell to the grid; if less than lower, disconnect loads or purchase from the grid. However, when the number of systems in microgrid increases, the control problem strategy could be extremely difficult, and maybe *Fuzzy Control* techniques could be helpful. Some examples of HBC can be found in [14] and [15].
- **Optimization-Based Methods**, which are based in the minimization of a cost function subject to constraints, so the problem resolution is harder but more versatile than in heuristic cases. It is possible to differentiate between Model Predictive Control and *Metaheuristics*. MPC entails an optimization method, which can be a metaheuristic one, and is based on the model of the system, being able to reject disturbances and model mismatches thanks to the feedback action. Examples of MPC EMS can be found in [52], [53], [54], [55], [56], [57] and extensively in [2]. On the other hand, metaheuristic methods are suitable when nonlinearities, nonconvex problems or in case of huge amount of decision variables, obtaining an approximate solution. There exists different techniques [2]:
  - **Tabu search**: memorizing the optimization process as a human can do.
  - **Genetic Algorithms**: trying to replicate the rules of evolution which living beings follow.
  - **Particle Swarm Optimization**: based on swarm intelligence while searching food. In [77] they implement this strategy for an electric vehicle charging station.
  - **Artificial Neural Networks**: it is a contemporary and emerging field which is used both in forecasting (in [55] was used to predict energy production, consumption and price) and optimization. It is based on neural networks in the brains.





## 3 CONTROL STRATEGY DESIGN

---

In this section, the controllers are designed using MPC techniques. First, the system is briefly described and the general system state space model is derived. Then, the control strategy is explained, describing the details of secondary and tertiary controllers with the formulation of their entire optimization problems. Finally, the software tools employed for the simulations are described with some hints to use them.

### 3.1 System description and modeling

As it has already been commented in section 1, the system to be controlled is a microgrid composed of equipment from different research groups of *Escuela Técnica Superior de Ingeniería de Sevilla*. These components are:

- PV field of 4 kW
- Lead-acid Battery bank of 48 V and capacity of 367 Ah
- PEM Electrolyzer of 1 kW and 0.23 Nm<sup>3</sup>/h
- Metal Hydride Storage Tank of 7 Nm<sup>3</sup>
- PEM Fuel Cell of 1.5 kW
- Ultracapacitor of 63 F
- Consumer load
- Electric vehicle charger and hydrogen recharging point
- Connection to the electrical grid

For the components description and operation details, as well as their equations, the reader is referred to the reference [2]. All the components will be connected to an AC bus through power converters, as can be seen in the scheme of Figure 3. In particular, DC-AC inverters are necessary for the PV panels, fuel cell, battery and ultracapacitor, and an AC-DC rectifier for the electrolyzer. Moreover, for the grid, a transformer and an AC-AC converter are needed. This last converter, as well as the ones of battery and ultracapacitor, must be bidirectional [76]. Anyway, power electronics and the zero-emissions vehicles charging points are out of the scope of this work and are expected to be treated in the future. In fact, the designed controllers in this work obtain at the end the power references to be sent to the power converters, assuming that there exists low-level controllers in the mentioned converters [2]. The EVs and hydrogen-based vehicles are treated as an extra power consumption following a specific demand of power or hydrogen depending on the vehicle, so there is no V2G implementation in this work. In Figure 3, the direction of the current and hydrogen can also be seen.

The modelling of such systems can be done regarding as components dynamics and the energy balance [2]. However, taking into account that generation, storage systems such as the electrolyzer and the fuel cell, and consumption acts faster than second-scale (which is typically the fastest sampling time in an EMS), only dynamics the dynamics of batteries, hydrogen tank and ultracapacitor are considered.

Although equations described in [2] for battery, hydrogen tank and ultracapacitor dynamics are used in the Simulink microgrid implementation, the linearized version are going to be used for control purposes. The convention for power variables will be the same for this work and the same as [2]: positive if providing power to the bus and negative if consuming power from the bus. Selecting the level of energy in the storage systems, i.e. battery SOC, *Level of Hydrogen (LOH)* and ultracapacitor SOC, as the state variables in

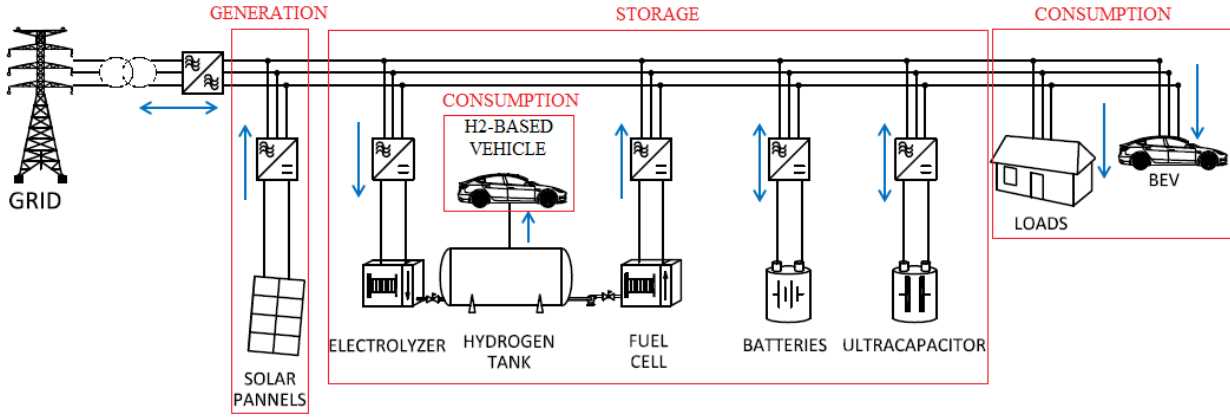


Figure 3. Scheme of the microgrid (Modified image from the original of [2])

percentage (%), the discrete-time linear equations are [2]:

$$SOC_{bat}(t+1) = SOC_{bat}(t) - \frac{\eta_{bat} T_s}{C_{max,bat}} P_{bat}(t) \quad (3-1)$$

$$LOH(t+1) = LOH(t) - 100 \frac{\eta_{H_2} T_s}{V_{max}} P_{H_2}(t) \quad (3-2)$$

$$SOC_{uc}(t+1) = SOC_{uc}(t) - \frac{\eta_{uc} T_s}{C_{max,uc}} P_{uc}(t) \quad (3-3)$$

Where  $t$  is the current time instant,  $T_s$  is the sampling time in hours ( $h$ ),  $C_{max,bat}$  and  $C_{max,uc}$  are the maximum battery and ultracapacitor capacities in  $kWh$ , respectively,  $V_{max}$  is the metal hydride tank maximum volume in  $Nm^3$ , and  $P_i(t)|_{i=bat,H_2,uc}$  are the battery, hydrogen and ultracapacitor power in  $kW$ , respectively.  $\eta_i|_{i=bat,H_2,uc}$  are the efficiencies in those systems in percentage (%) for the battery and ultracapacitor and in  $Nm^3/kWh$  for the hydrogen. These efficiencies can be broken down depending on the sign of  $P_i$  as follows:

$$\eta_i = \begin{cases} \eta_{ch} & \text{if } P_i < 0 \text{ (charging)} \\ \frac{1}{\eta_{disc}} & \text{if } P_i \geq 0 \text{ (discharging)} \end{cases}, \quad i = bat, H_2, uc \quad (3-4)$$

But, if the problem is stated in terms of continuous and binary variables (see next subsections), one can consider that:

$$P_{bat}(t) = P_{bat,disc}(t) - P_{bat,ch}(t) \quad (3-5)$$

$$P_{H_2}(t) = P_{fc}(t) - P_{ez}(t) \quad (3-6)$$

$$P_{uc}(t) = P_{uc,disc}(t) - P_{uc,ch}(t) \quad (3-7)$$

Where the subscripts meaning are: *ch* (charging), *disc* (discharging), *fc* (fuel cell) and *ez* (electrolyzer). It must be remarked that  $P_{bat,disc}(t)$ ,  $P_{bat,ch}(t)$ ,  $P_{fc}(t)$ ,  $P_{ez}(t)$ ,  $P_{uc,disc}(t)$  and  $P_{uc,ch}(t)$  are always positive values.

The equations (3-1), (3-2) and (3-3) can be rewritten as:

$$SOC_{bat}(t+1) = SOC_{bat}(t) + \frac{\eta_{bat,ch} T_s}{C_{max,bat}} P_{bat,ch}(t) - \frac{T_s}{\eta_{bat,disc} C_{max,bat}} P_{bat,disc}(t) \quad (3-8)$$

$$LOH(t+1) = LOH(t) + 100 \frac{\eta_{ez} T_s}{V_{max}} P_{ez}(t) \delta_{ez}(t) - 100 \frac{T_s}{\eta_{fc} V_{max}} P_{fc}(t) \delta_{fc}(t) \quad (3-9)$$

$$SOC_{uc}(t+1) = SOC_{uc}(t) + \frac{\eta_{uc,ch} T_s}{C_{max,uc}} P_{uc,ch}(t) - \frac{T_s}{\eta_{uc,disc} C_{max,uc}} P_{uc,disc}(t) \quad (3-10)$$

Being  $\delta_{ez}(t)$  and  $\delta_{fc}(t)$  two binary variables which indicate the energized state for the electrolyzer and the fuel cell, respectively. If the electrolyzer is working at time instant  $t$ ,  $\delta_{ez}(t)$  will be '1'; if not working,  $\delta_{ez}(t)$  will be '0' (and the same for the fuel cell). They will be further described and formulated in next subsections.

Looking at equations (3-8), (3-9) and (3-10) and taking into account the sign convention, one can see that if the storage system is charging (or the electrolyzer active for the hydrogen case), the energy level will increase. On the contrary, if the storage system is discharging (or the fuel cell is working for the hydrogen case), the energy level will decrease. Those energy levels are defined, as it has already been said in percentages, as the coefficient between the actual capacity and the maximum capacity of each storage device.

For the sake of simplicity, one can define the constants:

$$K_{bat,ch} = \frac{\eta_{bat,ch}}{C_{max,bat}} \quad (3-11)$$

$$K_{bat,disc} = \frac{1}{\eta_{bat,disc} C_{max,bat}} \quad (3-12)$$

$$K_{ez} = \frac{\eta_{ez}}{V_{max}} \quad (3-13)$$

$$K_{fc} = \frac{1}{\eta_{fc} V_{max}} \quad (3-14)$$

$$K_{uc,ch} = \frac{\eta_{uc,ch}}{C_{max,uc}} \quad (3-15)$$

$$K_{uc,disc} = \frac{1}{\eta_{uc,disc} C_{max,uc}} \quad (3-16)$$

With all having units of  $(kWh)^{-1}$ . With these definitios, the dynamics equations state as follows:

$$SOC_{bat}(t+1) = SOC_{bat}(t) + K_{bat,ch} T_s P_{bat,ch}(t) - K_{bat,disc} T_s P_{bat,disc}(t) \quad (3-17)$$

$$LOH(t+1) = LOH(t) + 100 K_{ez} T_s P_{ez}(t) \delta_{ez}(t) - 100 K_{fc} T_s P_{fc}(t) \delta_{fc}(t) \quad (3-18)$$

$$SOC_{uc}(t+1) = SOC_{uc}(t) + K_{uc,ch} T_s P_{uc,ch}(t) - K_{uc,disc} T_s P_{uc,disc}(t) \quad (3-19)$$

Finally, the energy balance must be formulated as it is done in equation (3-20).

$$P_{pv}(t) + P_{grid}(t) + P_{bat}(t) + P_{uc}(t) + P_{fc}(t) - P_{ez}(t) - P_{load}(t) - P_{ev}(t) = 0 \quad (3-20)$$

Where the subscripts mean:  $pv$  (photovoltaic) and  $ev$  (electric vehicle).  $P_{pv}(t)$ ,  $P_{fc}(t)$ ,  $P_{ez}(t)$ ,  $P_{load}(t)$  and  $P_{ev}(t)$  are always positive values, and  $P_{grid}(t)$ ,  $P_{bat}(t)$  and  $P_{uc}(t)$  can have positive or negative sign, depending on the defined sign criterion.

If the total net power, defined as the generation minus the consumption power, is considered as a measurable disturbance  $d$ , the following can be stated:

$$d(t) = P_{generation}(t) - P_{consumption}(t) = P_{pv}(t) - (P_{load}(t) + P_{ev}(t)) \quad (3-21)$$

And the equation (3-20) remains as follows:

$$P_{grid}(t) + P_{bat}(t) + P_{uc}(t) + P_{fc}(t) - P_{ez}(t) + d(t) = 0 \quad (3-22)$$

On the one hand, from equation (3-22), all the terms will be decision variables in the optimization problem to be solved via MPC techniques, except for  $d(t)$ , which will be measured and taken as inputs to the controllers. On the other hand, for equations (3-8), (3-9) and (3-10), some parameters are needed. They are gathered in Table 4, taken from [2], [14], [15] and [79].

Parameter	Representation	Unit	Value
Battery charging efficiency	$\eta_{bat,ch}$	%	90
Battery discharging efficiency	$\eta_{bat,disc}$	%	95
Maximum battery capacity	$C_{max,bat}$	kWh	17.6
Electrolyzer efficiency	$\eta_{ez}$	Nm <sup>3</sup> /kWh	0.23
Fuel cell efficiency	$\eta_{fc}$	kWh/ Nm <sup>3</sup>	1.32
Maximum hydrogen capacity	$V_{max}$	Nm <sup>3</sup>	7
Ultracapacitor charging efficiency	$\eta_{uc,ch}$	%	97
Ultracapacitor discharging efficiency	$\eta_{uc,disc}$	%	99
Maximum ultracapacitor capacity	$C_{max,uc}$	kWh	0.14

Table 4. Parameters for dynamics equations

## 3.2 Controller design

Once the system model has already been formulated, MPC techniques can be used in order to solve the EMS in the microgrid. MPC allows taking care of the system through constraints and the cost function. This can be used, among others, for operational, economical and safety reasons or for reference tracking, depending on the controller. A detailed description of MPC can be seen in [2], [80] and [81]. In this case, as it is proposed in [2], which will be the main reference for all the controllers design, two controllers are designed.

On the one hand, the first controller, known as tertiary controller, is intended to do the scheduling part every hour, taking predictions and energy storage level measurements from the real plant as inputs and calculating the scheduled system state and power, which will be sent to the secondary controller and a part of it will be as feedback for this tertiary controller in order to calculate incremental actions. The energy consumption, production and price predictions are simulated every sample time for the following 24 hours/sampling times (one day), but there is not a predictor implementation, since it is out of the scope of this work.

On the other hand, the secondary controller is dedicated to follow the schedule calculated by the tertiary one, trying to correct power deviations. For that reason, the sampling time is in the second-scale (1 second) in order to catch events such as new vehicle charging (since neither EVs nor hydrogen-based vehicles demand are not included in the forecast). Again, storage level measurements are inputs of the controller, as well as the scheduled outputs of the tertiary controller and the real generation and demand measurements, including EVs charging power. The result of this controller is the power which must be sent to the power converters of all the equipment. These outputs are used as feedback for this secondary controller too, entering as inputs for power variations computations.

An important difference between the two controllers is that in the tertiary one the ultracapacitor is not

included. This is due to ultracapacitors have high specific power but low specific energy, and they act quickly, so they are suitable for correcting power deviations. As they are expected to act more instantaneously, it makes no sense to include the ultracapacitor in an hourly-ahead scheduler MPC. In fact, ultracapacitors help the secondary controller in softening the variations respect to the schedule given by the tertiary controller.

As it is well-known, MPC control calculates the optimal solution for the prediction horizon, but only the first time instant actions are applied, recalculating again for the entire prediction horizon in the next time instant. This is known as *receding horizon* strategy [80] and [81]. For the tertiary controller a prediction horizon of 24 hours is taken, while for the secondary controller, 15 seconds are enough. As the control horizon can be lower than the prediction horizon (see [80] and [81] for further details), for the secondary controller a 5 seconds control horizon has been selected in order to accelerate computations. A scheme of the adopted control strategy is shown in Figure 4. The letter  $\Gamma$  is used to represent energy price, and the subscripts mean: *pred* (prediction), *meas* (measurements), *sch* (schedule) and *ref* (reference).

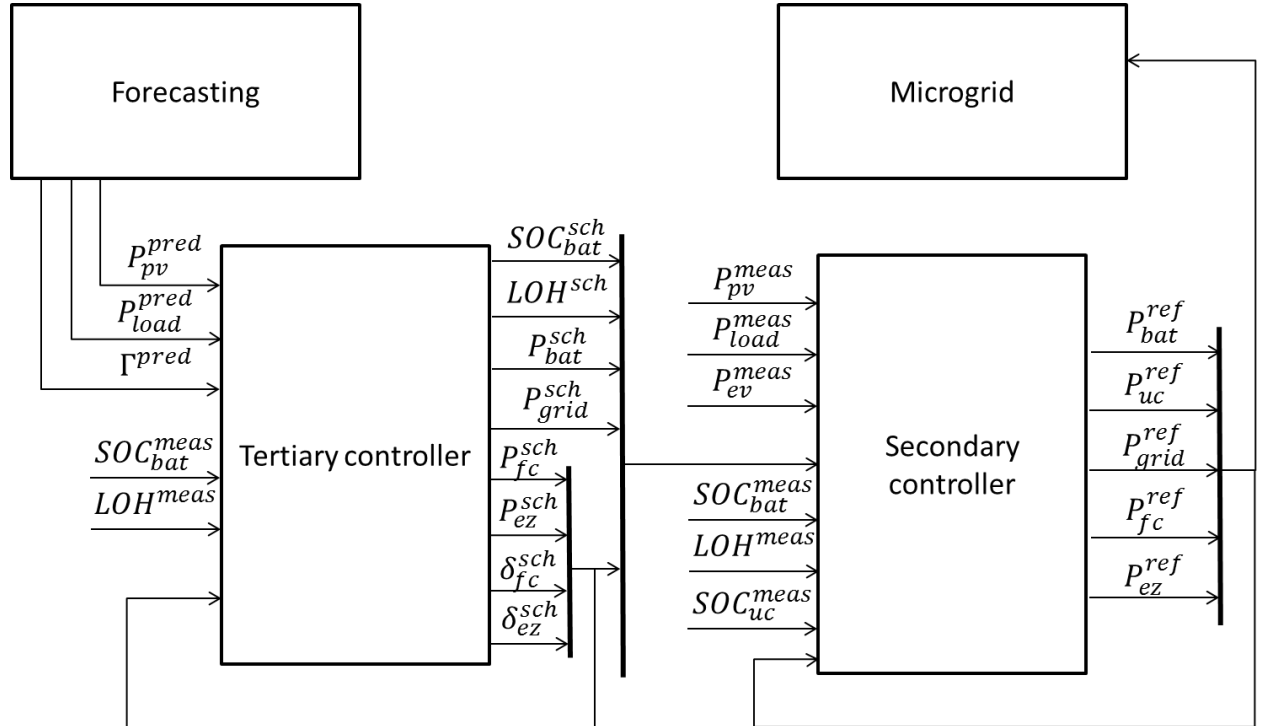


Figure 4. Control strategy

This control strategy coincides with the typical hierarchical control layers, where the tertiary controller can be seen as an economic planner, the secondary controller as a supervisor for sending power references and the primary controllers, not implemented here and acting in the order of milliseconds, are in charge of voltage and frequency deviations correction.

### 3.2.1 Mixed Logical Dynamical Systems

For the tertiary controller design, both continuous and logical variables will be used. The theory of MPC is developed for continuous variables, but it can be extended to hybrid systems, resulting in the so-called *Mixed Logical Dynamical, MLD*, systems. The idea of these systems is to mix the finite state machines techniques with the classical continuous control theory [80]. This topic can be useful for modeling when a system is switched on/off, when it is in a finite state (for example, charging or discharging), and so on.

To construct a MLD system, two steps must be done [2]:

1. Convert any relation which involves logical variables  $\delta \in \{0,1\}$  into linear inequalities, which will be added as constraints to the MPC problem formulation. These transformations are gathered in Table 5, directly taken from [2]. The deduction of all the relationships are based on the work done by [82] and is well-explained in chapter 10 of the book [80]. The relation  $P7$  includes the definition of the mixed product in an auxiliary variable,  $z$ , where both continuous and discrete variables are involved.

	Relation	Logic	MLD inequalities
P1	AND ( $\wedge$ )	$S_3 \Leftrightarrow (S_1 \wedge S_2)$	$-\infty \leq -\delta_1 + \delta_3 \leq 0$ $-\infty \leq -\delta_2 + \delta_3 \leq 0$ $-\infty \leq \delta_1 + \delta_2 - \delta_3 \leq 1$
P2	OR ( $\vee$ )	$S_1 \vee S_2$	$1 \leq \delta_1 + \delta_2 \leq 2$
P3	NOT ( $\sim$ )	$S_2 \equiv \sim S_1$	$1 \leq \delta_1 + \delta_2 \leq 1$
P4	IMPLY ( $\Rightarrow$ )	$[a^T x \leq 0] \Rightarrow [\delta = 1]$	$\epsilon \leq a^T x - (m - \epsilon)\delta \leq \infty$
P5	IMPLY ( $\Rightarrow$ )	$[\delta = 1] \Rightarrow [a^T x \leq 0]$	$-\infty \leq a^T x + M\delta \leq M$
P6	IFF ( $\Leftrightarrow$ )	$[a^T x \leq 0] \Leftrightarrow [\delta = 1]$	$\epsilon \leq a^T x - (m - \epsilon)\delta \leq \infty$ $-\infty \leq a^T x + M\delta \leq M$
P7	Mixed product	$z = \delta \cdot a^T x$	$-\infty \leq z - M\delta \leq 0$ $0 \leq z - m\delta \leq \infty$ $-\infty \leq z - a^T x + m(1 - \delta) \leq 0$ $0 \leq z - a^T x + M(1 - \delta) \leq \infty$

Table 5. Logical relations in a system and their corresponding linear inequalities (Table directly taken from [2]). Nomenclature:  $\delta$  (binary variable),  $S$  (statement represented by  $\delta$ ),  $a$  (vector of parameters),  $x$  (continuous variable),  $\epsilon > 0$  (small tolerance)

2. Modify the classical state space model definition and write the dynamical equations as:

$$x(t+1) = Ax(t) + B_1 u(t) + B_2 \delta(t) + B_3 z(t) \quad (3-23)$$

$$y(t) = Cx(t) + D_1 u(t) + D_2 \delta(t) + D_3 z(t) \quad (3-24)$$

And the systems constraints can be reorder as:

$$E_1 u(t) + E_2 \delta(t) + E_3 z(t) + E_4 x(t) \leq E_5 \quad (3-25)$$

Once the MLD system is available, the optimization MPC problem turns into a *Mixed Integer Programming*, *MIP* [80]. Since the constraints are linear, the problem to solve will be a *Mixed Integer Linear Programming*, *MILP*, if the cost function is linear, or a *Mixed Integer Quadratic Programming*, *MIQP*, if the cost function is quadratic. There exists *branch and bound* techniques which avoid to solve the *Linear Programming*, *LP*, or the *Quadratic Programming*, *QP*, for any combination of logical variable, reducing the number of problems to be solved in the binary tree.

### 3.2.2 Tertiary controller

As it has already been described, this controller takes care every hour of power planning regarding forecasts in energy price, solar generation and consumption (except from EVs charging power) for the following 24 hours [2]. The objective is both economical and operational. On the one hand, the controller aims at minimizing cost of energy purchase and equipment uses and at maximizing the revenue for selling energy to the grid. This scheduler plays a crucial role here, since there are important penalties if the scheduled grid power (purchased or sold) is not finally accomplished. Accurate forecasts help in this task. On the other hand, the components are considered with the objective of extend their lifetimes and not to damage them. Both physical limits and abrupt operating changes are taken into account.

The scheme of the tertiary controller is depicted in Figure 5. As it has already been commented, the output of the controller gives every hour the power and state scheduled for the microgrid components without the ultracapacitor, which will be used in the secondary controller. From those outputs, the hydrogen related are sent as inputs for the next time instant to this tertiary controller with the goal of power variation computations to protect hydrogen equipment. The *SOC* and *LOH* measurements are also taken as input from the components blocks in the simulation and will be taken from real measurements in the future plant implementation. The other inputs are the mentioned predictions.

As in classical MPC, a MIQP optimization problem must be formulated. This takes the form presented in equations (3–26)-(3–34). The problem is composed by the cost function (3–26), system model constraint (3–27)-(3–28), power balance constraint (3–29), physical constraints (3–30)-(3–32) and all the MLD constraints derived from the inclusion of binary variables (3–33)-(3–34). The system model, the cost function and MLD constraints are going to be detailed in the following and the whole MIQP problem will be summarized at the end.

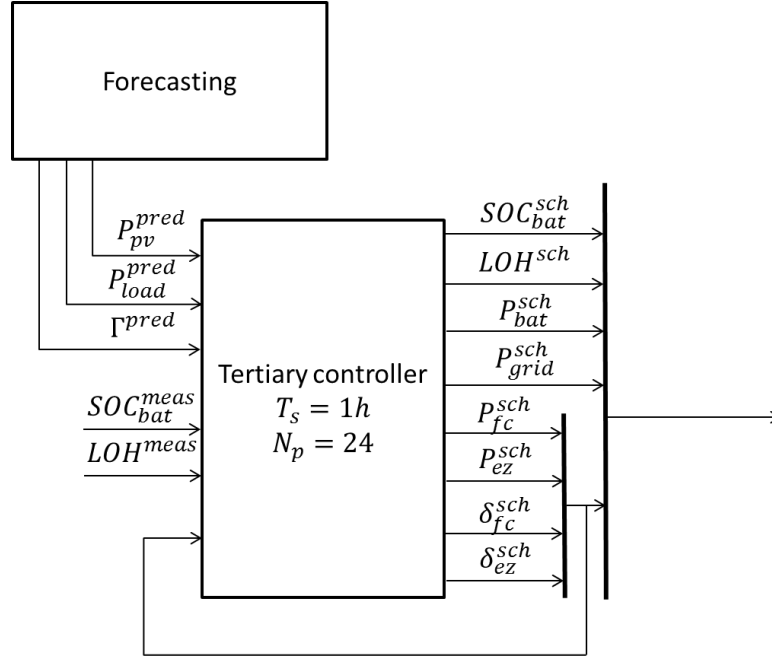


Figure 5. Tertiary controller

$$\min_u J(t) = \sum_{k=1}^{SH} (J_{grid}(t_k|t) + J_{bat}(t_k|t) + J_{H_2}(t_k|t)) \quad (3-26)$$

$$s. t. \quad x(t_k + 1) = Ax(t_k) + B_1u(t_k) + B_2\delta(t_k) + B_3z(t_k) \quad (3-27)$$

$$y(t_k) = Cx(t_k) + D_1u(t_k) + D_2\delta(t_k) + D_3z(t_k) \quad (3-28)$$

$$P_{pv}^{pred}(t_k|t) + P_{grid}(t_k) + P_{bat}(t_k) + P_{fc}(t_k)\delta_{fc}(t_k) - P_{ez}(t_k)\delta_{ez}(t_k) - P_{load}^{pred}(t_k|t) = 0 \quad (3-29)$$

$$P_i^{min} \leq P_i(t_k) \leq P_i^{max} |_{i=bat,fc,ez,grid} \quad (3-30)$$

$$SOC_{bat}^{min} \leq SOC_{bat}(t_k) \leq SOC_{bat}^{max} \quad (3-31)$$

$$LOH^{min} \leq LOH(t_k) \leq LOH^{max} \quad (3-32)$$

$$0 \leq \delta_i(t_k) \leq 1 |_{i=fc,ez} \quad (3-33)$$

$$E_1u(t_k) + E_2\delta(t_k) + E_3z(t_k) + E_4x(t_k) \leq E_5 \quad (3-34)$$

The time notation is chosen indicating that  $t$  is the current time instant and  $t_k$  corresponds to  $k$  instants after the current time ( $t+k$ ). The notation  $(t_k|t)$  refers to the prediction made in instant  $t$  for the time instant  $t+k$ . The superscript schedule (*sch*) has not been included here for simplicity. Now, the terms in equations (3–26)-(3–34) are going to be broken down.

The first step is to know well the model of the system. Vectors for control variable,  $u$ , binary variables,  $\delta$ , and auxiliary variables,  $z$ , are defined in (3–35) and contain the decision variables. The variables in vector  $u$  have already been defined and the variables in vector  $\delta$  and  $z$  will be defined in the following.

$$u(t_k) = \begin{bmatrix} P_{bat}(t_k) \\ P_{fc}(t_k) \\ P_{ez}(t_k) \\ P_{grid}(t_k) \end{bmatrix} \quad \delta(t_k) = \begin{bmatrix} \delta_{bat,ch}(t_k) \\ \delta_{bat,disc}(t_k) \\ \delta_{fc}(t_k) \\ \delta_{ez}(t_k) \\ \delta_{sale}(t_k) \\ \delta_{pur}(t_k) \\ \sigma_{fc}^{on}(t_k) \\ \sigma_{ez}^{on}(t_k) \\ \chi_{fc}(t_k) \\ \chi_{ez}(t_k) \end{bmatrix} \quad z(t_k) = \begin{bmatrix} P_{bat,ch}(t_k) \\ P_{bat,disc}(t_k) \\ z_{fc}(t_k) \\ z_{ez}(t_k) \\ P_{sale}(t_k) \\ P_{pur}(t_k) \\ \theta_{fc}(t_k) \\ \theta_{ez}(t_k) \end{bmatrix} \quad (3-35)$$

As the state,  $x$ , and output of the system,  $y$ , are defined by the same vectors:

$$x(t_k) = y(t_k) = \begin{bmatrix} SOC_{bat}(t_k) \\ LOH(t_k) \end{bmatrix} \quad (3-36)$$

With these definitions, the state space model of the system can be obtained from the subsections 3.1 and 3.2.1, so equations (3–27) and (3–28) are transformed in equations (3–37) and (3–38) as:

$$\begin{bmatrix} SOC_{bat}(t_k + 1) \\ LOH(t_k + 1) \end{bmatrix} = \begin{bmatrix} 1 & 0 \\ 0 & 1 \end{bmatrix} \begin{bmatrix} SOC_{bat}(t_k) \\ LOH(t_k) \end{bmatrix} + \begin{bmatrix} 0 & \dots & 0 \\ 0 & \dots & 0 \end{bmatrix}_{(2,4)} u(t_k) + \begin{bmatrix} 0 & \dots & 0 \\ 0 & \dots & 0 \end{bmatrix}_{(2,10)} \delta(t_k) \\ + \begin{bmatrix} K_{bat,ch} & -K_{bat,disc} & 0 & 0 & 0 & 0 & 0 & 0 \\ 0 & 0 & -K_{fc} & K_{ez} & 0 & 0 & 0 & 0 \end{bmatrix} z(t_k) \quad (3-37)$$

$$\begin{bmatrix} y_1(t_k) \\ y_2(t_k) \end{bmatrix} = \begin{bmatrix} 1 & 0 \\ 0 & 1 \end{bmatrix} \begin{bmatrix} SOC_{bat}(t_k) \\ LOH(t_k) \end{bmatrix} \quad (3-38)$$

Then, as is shown in equation (3–26), the cost function is divided in three terms: grid, battery and hydrogen (which is again divided into fuel cell and electrolyzer). The first term, corresponding to the grid, aims at maximizing the profit in the energy exchange with the grid. The terms  $\Gamma_{sale}^{pred}(t_k|t)$  and  $\Gamma_{pur}^{pred}(t_k|t)$  in €/kWh are assumed to be the same and equal to the energy price forecasting. Taking care with units, the grid cost function is:

$$J_{grid}(t_k|t) = \left( -\Gamma_{sale}^{pred}(t_k|t)P_{sale}(t_k|t) + \Gamma_{pur}^{pred}(t_k|t)P_{pur}(t_k|t) \right) T_s \quad (3-39)$$

For dividing  $P_{grid}$  into  $P_{sale}$  and  $P_{pur}$ , it is necessary to define  $\delta_{sale}$  and  $\delta_{pur}$ , two binary variables which will be active when selling to or purchasing from the main grid, respectively. So, the following relations must be considered:

$$P_{grid}(t_k) = P_{pur}(t_k) - P_{sale}(t_k), \quad P_{pur}(t_k) \geq 0, P_{sale}(t_k) \geq 0 \quad (3-40)$$

$$\delta_{pur}(t_k) + \delta_{sale}(t_k) = 1 \quad (3-41)$$

$$P_{pur}(t_k) = P_{grid}(t_k) \delta_{pur}(t_k) \quad (3-42)$$



$$P_{sale}(t_k) = -P_{grid}(t_k) \delta_{sale}(t_k) \quad (3-43)$$

$$P_{grid}(t_k) \leq 0 \leftrightarrow \delta_{sale} = 1 \quad (3-44)$$

$$P_{grid}(t_k) > 0 \leftrightarrow \delta_{pur} = 1 \quad (3-45)$$

But equations (3-43) and (3-45) are not necessary if equations (3-40) and (3-41) are used. Moreover, equation (3-42) can be transformed in equations (3-46)-(3-49), and equation (3-44) in equations (3-50)-(3-51), using the equivalences of Table 5.

$$-\infty \leq P_{pur}(t_k) - P_{grid}^{max} \delta_{pur}(t_k) \leq 0 \quad (3-46)$$

$$0 \leq P_{pur}(t_k) - P_{grid}^{min} \delta_{pur}(t_k) \leq \infty \quad (3-47)$$

$$-\infty \leq P_{pur}(t_k) - P_{grid}(t_k) + P_{grid}^{min} (1 - \delta_{pur}(t_k)) \leq 0 \quad (3-48)$$

$$0 \leq P_{pur}(t_k) - P_{grid}(t_k) + P_{grid}^{max} (1 - \delta_{pur}(t_k)) \leq \infty \quad (3-49)$$

$$\epsilon \leq P_{grid}(t_k) - (P_{grid}^{min} - \epsilon) \delta_{sale}(t_k) \leq \infty \quad (3-50)$$

$$-\infty \leq P_{grid}(t_k) + P_{grid}^{max} \delta_{sale}(t_k) \leq P_{grid}^{max} \quad (3-51)$$

The next term in the cost function is related with the battery. Assuming that the parameters in Table 6 are known [2], the battery cost function can be written as in equation (3-52). Both terms have economic goals and the second one is related with the fact that batteries suffer at high current ratio. One must take care of units again; i.e. power variables in  $kW$  and sampling time in hours.

Parameter	Representation	Unit	Value
Battery capital cost	$CC_{bat}$	€/kWh	125
Battery life cycles	$Cycles_{bat}$	-	3000
Battery charging degradation cost	$Cost_{degr,ch}$	€/kW <sup>2</sup> h	$10^{-3}$
Battery discharging degradation cost	$Cost_{degr,disc}$	€/kW <sup>2</sup> h	$10^{-3}$

Table 6. Parameters for battery cost function (Taken from [2])

$$J_{bat}(t_k|t) = \frac{CC_{bat}}{2 Cycles_{bat}} (P_{bat,ch}(t_k|t) + P_{bat,disc}(t_k|t)) T_s \quad (3-52)$$

$$+ (Cost_{degr,ch} P_{bat,ch}^2(t_k|t) + Cost_{degr,disc} P_{bat,disc}^2(t_k|t)) T_s$$

As for the battery *SOC* dynamical model exposed in equation (3-37), the variables  $P_{bat,ch}$  and  $P_{bat,disc}$  appear in this cost function. Similar to the case of binary and auxiliary variables for the grid, binary variables  $\delta_{bat,ch}$  and  $\delta_{bat,disc}$  are introduced to indicate that the battery is charging ( $\delta_{bat,ch}$  equal to '1' and  $\delta_{bat,disc}$  equal to '0') or discharging ( $\delta_{bat,disc}$  equal to '1' and  $\delta_{bat,ch}$  equal to '0'). Moreover, as in the case of the grid, the following relations must be fulfilled:

$$P_{bat}(t_k) = P_{bat,disc}(t_k) - P_{bat,ch}(t_k), \quad P_{bat,disc}(t_k) \geq 0, P_{bat,ch}(t_k) \geq 0 \quad (3-53)$$

$$\delta_{bat,disc}(t_k) + \delta_{bat,ch}(t_k) = 1 \quad (3-54)$$

$$P_{bat,disc}(t_k) = P_{bat}(t_k) \delta_{bat,disc}(t_k) \quad (3-55)$$

$$P_{bat,ch}(t_k) = -P_{bat}(t_k) \delta_{bat,ch}(t_k) \quad (3-56)$$

$$P_{bat}(t_k) \leq 0 \leftrightarrow \delta_{bat,ch} = 1 \quad (3-57)$$

$$P_{bat}(t_k) > 0 \leftrightarrow \delta_{bat,disc} = 1 \quad (3-58)$$

In the same way as the grid relations, the use of equations (3-53) and (3-54) avoids the use of equations (3-56) and (3-58). Equation (3-55) is transformed in (3-59)-(3-62), and equation (3-57) in (3-63)-(3-64), using the relationships in Table 5.

$$-\infty \leq P_{bat,disc}(t_k) - P_{bat}^{max} \delta_{bat,disc}(t_k) \leq 0 \quad (3-59)$$

$$0 \leq P_{bat,disc}(t_k) - P_{bat}^{min} \delta_{bat,disc}(t_k) \leq \infty \quad (3-60)$$

$$-\infty \leq P_{bat,disc}(t_k) - P_{bat}(t_k) + P_{bat}^{min} (1 - \delta_{bat,disc}(t_k)) \leq 0 \quad (3-61)$$

$$0 \leq P_{bat,disc}(t_k) - P_{bat}(t_k) + P_{bat}^{max} (1 - \delta_{bat,disc}(t_k)) \leq \infty \quad (3-62)$$

$$\epsilon \leq P_{bat}(t_k) - (P_{bat}^{min} - \epsilon) \delta_{bat,ch}(t_k) \leq \infty \quad (3-63)$$

$$-\infty \leq P_{bat}(t_k) + P_{bat}^{max} \delta_{bat,ch}(t_k) \leq P_{bat}^{max} \quad (3-64)$$

With respect to hydrogen, the last term in the cost function, can be obviously divided in two terms: fuel cell and electrolyzer. First of all, as in the case of battery, for the state space equation of *LOH* in (3-37), new binary and auxiliary variables must be defined. The inclusion of binary variables  $\delta_{fc}$  and  $\delta_{ez}$ , which in their active state mean fuel cell or electrolyzer in energized state (as fuel cell and electrolyzer must not work at the same time, equation (3-67) must be also fulfilled), allows to define the auxiliary variables:

$$z_{fc}(t_k) = P_{fc}(t_k) \delta_{fc}(t_k) \quad (3-65)$$

$$z_{ez}(t_k) = P_{ez}(t_k) \delta_{ez}(t_k) \quad (3-66)$$

$$0 \leq \delta_{fc}(t_k) + \delta_{ez}(t_k) \leq 1 \quad (3-67)$$

Using relation *P7* of Table 5, equation (3-65) is converted to inequalities (3-68)-(3-71), and equation (3-66) in (3-72)-(3-75).

$$-\infty \leq z_{fc}(t_k) - P_{fc}^{max} \delta_{fc}(t_k) \leq 0 \quad (3-68)$$

$$0 \leq z_{fc}(t_k) - P_{fc}^{min} \delta_{fc}(t_k) \leq \infty \quad (3-69)$$

$$-\infty \leq z_{fc}(t_k) - P_{fc}(t_k) + P_{fc}^{min} (1 - \delta_{fc}(t_k)) \leq 0 \quad (3-70)$$

$$0 \leq z_{fc}(t_k) - P_{fc}(t_k) + P_{fc}^{max} (1 - \delta_{fc}(t_k)) \leq \infty \quad (3-71)$$

$$-\infty \leq z_{ez}(t_k) - P_{ez}^{max} \delta_{ez}(t_k) \leq 0 \quad (3-72)$$

$$0 \leq z_{ez}(t_k) - P_{ez}^{min} \delta_{ez}(t_k) \leq \infty \quad (3-73)$$

$$-\infty \leq z_{ez}(t_k) - P_{ez}(t_k) + P_{ez}^{min} (1 - \delta_{ez}(t_k)) \leq 0 \quad (3-74)$$

$$0 \leq z_{ez}(t_k) - P_{ez}(t_k) + P_{ez}^{max} (1 - \delta_{ez}(t_k)) \leq \infty \quad (3-75)$$

The next step is to define some parameters to be used in the hydrogen cost function. They can be seen in Table 7.

Parameter	Representation	Unit	Value
Fuel cell capital cost	$CC_{fc}$	€	30
Fuel cell lifetime	$Hours_{fc}$	h	10000
Fuel cell operation and maintenance cost	$Cost_{o\&m,fc}$	€/h	0.001
Fuel cell startup process degradation cost	$Cost_{start,fc}$	€	0.01
Fuel cell fluctuation power degradation cost	$Cost_{degr,fc}$	€/kW <sup>2</sup>	10000
Electrolyzer capital cost	$CC_{ez}$	€	8.22
Electrolyzer lifetime	$Hours_{ez}$	h	10000
Electrolyzer operation and maintenance cost	$Cost_{o\&m,ez}$	€/h	0.002
Electrolyzer startup process degradation cost	$Cost_{start,ez}$	€	0.123
Electrolyzer fluctuation power degradation cost	$Cost_{degr,ez}$	€/kW <sup>2</sup>	50000

Table 7. Parameters for hydrogen cost function (Taken from [2])

With the previous definition, the hydrogen cost function is:

$$J_{H_2}(t_k|t) = J_{fc}(t_k|t) + J_{ez}(t_k|t) + J_{storage}(t_k|t) + J_{compression}(t_k|t) \quad (3-76)$$

For simplicity reasons, the cost terms associated to storage and compression will not be included. In the case of fuel cell and electrolyzer, the cost functions are the same:

$$J_{fc}(t_k|t) = T_s \left( \frac{CC_{fc}}{Hours_{fc}} + Cost_{o\&m,fc} \right) \delta_{fc}(t_k|t) + Cost_{start,fc} \sigma_{fc}^{on}(t_k|t) + Cost_{degr,fc} \theta_{fc}^2(t_k|t) \quad (3-77)$$

$$J_{ez}(t_k|t) = T_s \left( \frac{CC_{ez}}{Hours_{ez}} + Cost_{o\&m,ez} \right) \delta_{ez}(t_k|t) + Cost_{start,ez} \sigma_{ez}^{on}(t_k|t) + Cost_{degr,ez} \theta_{ez}^2(t_k|t) \quad (3-78)$$

In equations (3-77) and (3-78) there are two new variables for each one. The first one is  $\sigma_i^{on}(t_k)|_{i=fc,ez}$ . It is a logical variable which will be active only in the time instants where the fuel cell or electrolyzer starts working. So, only in the case the binary energized state is active in the current time instant and was not active in the previous one, this variable will be equal to '1':

$$\sigma_i^{on}(t_k) = \delta_i(t_k) \wedge (\sim \delta_i(t_k - 1))|_{i=fc,ez} \quad (3-79)$$

Looking at  $PI$  in Table 5, this equation can be written as:

$$-\infty \leq -\delta_i(t_k) + \sigma_i^{on}(t_k) \leq 0, \quad i = fc, ez \quad (3-80)$$

$$-\infty \leq -(1 - \delta_i(t_k - 1)) + \sigma_i^{on}(t_k) \leq 0, \quad i = fc, ez \quad (3-81)$$

$$-\infty \leq \delta_i(t_k) + (1 - \delta_i(t_k - 1)) - \sigma_i^{on}(t_k) \leq 1, \quad i = fc, ez \quad (3-82)$$

The other new variable is a mixed product which represents the power variations in the fuel cell and electrolyzer, but only in the time instants where the device is energized; i.e. not considering the first time instant when the fuel cell or electrolyzer starts its operation, since an unavoidable larger power variation will occur there. So, being the power variation defined as in equation (3-83),  $\theta_i(t_k)$  variable can be written as in (3-84):

$$\Delta P_i(t_k) = P_i(t_k) - P_i(t_k - 1), \quad i = fc, ez \quad (3-83)$$

$$\theta_i(t_k) = \Delta P_i(t_k) \left( \delta_i(t_k) \wedge (\delta_i(t_k - 1)) \right) = \Delta P_i(t_k) \chi_i(t_k), \quad i = fc, ez \quad (3-84)$$

Where  $\chi_i(t_k)$  is a new auxiliary binary variable which will be active only when the fuel cell or electrolyzer is energized in the current time instant and in the previous one (it must not occur at the same time on both devices, so equation (3-86) must be added). So, equation (3-85) can be transformed in inequalities (3-87)-(3-89). Considering this new auxiliary variable, equation (3-84) can be rewritten as inequalities (3-90)(3-93).

$$\chi_i(t_k) = \delta_i(t_k) \wedge (\delta_i(t_k - 1)), \quad i = fc, ez \quad (3-85)$$

$$0 \leq \chi_{fc}(t_k) + \chi_{ez}(t_k) \leq 1 \quad (3-86)$$

$$-\infty \leq -\delta_i(t_k) + \chi_i(t_k) \leq 0, \quad i = fc, ez \quad (3-87)$$

$$-\infty \leq -\delta_i(t_k - 1) + \chi_i(t_k) \leq 0, \quad i = fc, ez \quad (3-88)$$

$$-\infty \leq \delta_i(t_k) + \delta_i(t_k - 1) - \chi_i(t_k) \leq 1, \quad i = fc, ez \quad (3-89)$$

$$-\infty \leq \theta_i(t_k) - \Delta P_i^{max} \chi_i(t_k) \leq 0, \quad i = fc, ez \quad (3-90)$$

$$0 \leq \theta_i(t_k) - \Delta P_i^{min} \chi_i(t_k) \leq \infty, \quad i = fc, ez \quad (3-91)$$

$$-\infty \leq \theta_i(t_k) - \Delta P_i(t_k) + \Delta P_i^{min} (1 - \chi_i(t_k)) \leq 0, \quad i = fc, ez \quad (3-92)$$

$$0 \leq \theta_i(t_k) - \Delta P_i(t_k) + \Delta P_i^{max} (1 - \chi_i(t_k)) \leq \infty, \quad i = fc, ez \quad (3-93)$$

Finally, to summarize, the following box includes the complete MPC problem formulation.

$$\begin{aligned} \min_u J(t) = & \sum_{k=1}^{SH} \left( \left( -\Gamma_{sale}^{pred}(t_k|t) P_{sale}(t_k|t) + \Gamma_{pur}^{pred}(t_k|t) P_{pur}(t_k|t) \right) T_s \right. \\ & + \frac{CC_{bat}}{2 Cycles_{bat}} \left( P_{bat,ch}(t_k|t) + P_{bat,disc}(t_k|t) \right) T_s \\ & + \left( Cost_{degr,ch} P_{bat,ch}^2(t_k|t) + Cost_{degr,disc} P_{bat,disc}^2(t_k|t) \right) T_s \\ & + T_s \left( \frac{CC_{fc}}{Hours_{fc}} + Cost_{o\&m,fc} \right) \delta_{fc}(t_k|t) + Cost_{start,fc} \sigma_{fc}^{on}(t_k|t) \\ & + Cost_{degr,fc} \theta_{fc}^2(t_k|t) + T_s \left( \frac{CC_{ez}}{Hours_{ez}} + Cost_{o\&m,ez} \right) \delta_{ez}(t_k|t) \\ & \left. + Cost_{start,ez} \sigma_{ez}^{on}(t_k|t) + Cost_{degr,ez} \theta_{ez}^2(t_k|t) \right) \\ \text{s. t.} \quad & \begin{bmatrix} SOC_{bat}(t_k+1) \\ LOH(t_k+1) \end{bmatrix} = \begin{bmatrix} 1 & 0 \\ 0 & 1 \end{bmatrix} \begin{bmatrix} SOC_{bat}(t_k) \\ LOH(t_k) \end{bmatrix} + \begin{bmatrix} 0 & \dots & 0 \\ 0 & \dots & 0 \end{bmatrix}_{(2,4)} u(t_k) + \\ & \begin{bmatrix} 0 & \dots & 0 \\ 0 & \dots & 0 \end{bmatrix}_{(2,10)} \delta(t_k) + \begin{bmatrix} K_{bat,ch} & -K_{bat,disc} & 0 & 0 & 0 & 0 & 0 & 0 \\ 0 & 0 & -K_{fc} & K_{ez} & 0 & 0 & 0 & 0 \end{bmatrix} z(t_k) \\ & \begin{bmatrix} y_1(t_k) \\ y_2(t_k) \end{bmatrix} = \begin{bmatrix} 1 & 0 \\ 0 & 1 \end{bmatrix} \begin{bmatrix} SOC_{bat}(t_k) \\ LOH(t_k) \end{bmatrix} \\ & P_{pv}^{pred}(t_k|t) + P_{grid}(t_k) + P_{bat}(t_k) + z_{fc}(t_k) - z_{ez}(t_k) - P_{load}^{pred}(t_k|t) = 0 \\ & P_i^{min} \leq P_i(t_k) \leq P_i^{max} |_{i=bat,fc,ez,grid} \\ & SOC_{bat}^{min} \leq SOC_{bat}(t_k) \leq SOC_{bat}^{max} \\ & LOH^{min} \leq LOH(t_k) \leq LOH^{max} \\ & 0 \leq \delta_i(t_k) \leq 1 |_{i=fc,ez} \\ & P_{grid}(t_k) = P_{pur}(t_k) - P_{sale}(t_k), \quad P_{pur}(t_k) \geq 0, P_{sale}(t_k) \geq 0 \\ & \delta_{pur}(t_k) + \delta_{sale}(t_k) = 1 \\ & P_{grid}^{min} \delta_{pur}(t_k) \leq P_{pur}(t_k) \leq P_{grid}^{max} \delta_{pur}(t_k) \\ & P_{grid}(t_k) - P_{grid}^{max} (1 - \delta_{pur}(t_k)) \leq P_{pur}(t_k) \leq P_{grid}(t_k) - P_{grid}^{min} (1 - \delta_{pur}(t_k)) \\ & \epsilon + (P_{grid}^{min} - \epsilon) \delta_{sale}(t_k) \leq P_{grid}(t_k) \leq P_{grid}^{max} (1 - \delta_{sale}(t_k)) \end{aligned}$$

$$\begin{aligned}
P_{bat}(t_k) &= P_{bat,disc}(t_k) - P_{bat,ch}(t_k), & P_{bat,disc}(t_k) &\geq 0, P_{bat,ch}(t_k) \geq 0 \\
\delta_{bat,disc}(t_k) + \delta_{bat,ch}(t_k) &= 1 \\
P_{bat}^{min} \delta_{bat,disc}(t_k) &\leq P_{bat,disc}(t_k) \leq P_{bat}^{max} \delta_{bat,disc}(t_k) \\
P_{bat}(t_k) - P_{bat}^{max} (1 - \delta_{bat,disc}(t_k)) &\leq P_{bat,disc}(t_k) \leq P_{bat}(t_k) - P_{bat}^{min} (1 - \delta_{bat,disc}(t_k)) \\
\epsilon + (P_{bat}^{min} - \epsilon) \delta_{bat,ch}(t_k) &\leq P_{bat}(t_k) \leq P_{bat}^{max} (1 - \delta_{bat,ch}(t_k)) \\
0 &\leq \delta_{fc}(t_k) + \delta_{ez}(t_k) \leq 1 \\
P_i^{min} \delta_i(t_k) &\leq z_i(t_k) \leq P_i^{max} \delta_i(t_k), & i &= fc, ez \\
P_i(t_k) - P_i^{max} (1 - \delta_i(t_k)) &\leq z_i(t_k) \leq P_i(t_k) - P_i^{min} (1 - \delta_i(t_k)), & i &= fc, ez \\
-\infty &\leq -\delta_i(t_k) + \sigma_i^{on}(t_k) \leq 0, & i &= fc, ez \\
-\infty &\leq -(1 - \delta_i(t_k - 1)) + \sigma_i^{on}(t_k) \leq 0, & i &= fc, ez \\
-\infty &\leq \delta_i(t_k) + (1 - \delta_i(t_k - 1)) - \sigma_i^{on}(t_k) \leq 1, & i &= fc, ez \\
-\infty &\leq -\delta_i(t_k) + \chi_i(t_k) \leq 0, & i &= fc, ez \\
-\infty &\leq -\delta_i(t_k - 1) + \chi_i(t_k) \leq 0, & i &= fc, ez \\
-\infty &\leq \delta_i(t_k) + \delta_i(t_k - 1) - \chi_i(t_k) \leq 1, & i &= fc, ez \\
0 &\leq \chi_{fc}(t_k) + \chi_{ez}(t_k) \leq 1 \\
\Delta P_i^{min} \chi_i(t_k) &\leq \theta_i(t_k) \leq \Delta P_i^{max} \chi_i(t_k), & i &= fc, ez \\
\Delta P_i(t_k) - \Delta P_i^{max} (1 - \chi_i(t_k)) &\leq \theta_i(t_k) \leq \Delta P_i(t_k) - \Delta P_i^{min} (1 - \chi_i(t_k)), & i &= fc, ez
\end{aligned}$$

### 3.2.3 Secondary controller

This controller is designed with the objective of tracking both power and energy storage level scheduled, given by the tertiary controller every hour. As the secondary controller sampling time is 1 second and this controller has the prediction horizon of 15, one can consider that both the schedule from the tertiary controller and the net power measurements are going to be constant for that prediction horizon. The fact that there exists mismatches between the predictions and the reality, and events like EVs charging or hydrogen-based vehicles charging, makes necessary the inclusion of this controller to cope with all these unforeseen circumstances. Predictions for zero-emission vehicle charging could be included in the tertiary controller for performance improvement, but it has not been considered in this work. Besides references tracking, this controller takes care of equipment including power values, power variations and limits in the energy stored. In particular, one important thing is prevent electrolyzer and fuel cell from high power variations. The main reference for this design is [2].

Inputs and outputs for this controller can be seen in Figure 6. The output of the controller gives every second the power references for the microgrid components (or to its power converters) including the ultracapacitor. All of these outputs will be use as inputs in this secondary controller as in ther tertiary one for power variations computations. The battery and ultracapacitor *SOC* and hydrogen *LOH* measurements are also taken as input from the components blocks in the simulation. Finally, other measurements are taken as inputs, including real solar power generation, real demand power and real EVs charging power. These three last measurements have been simulated based on real data.

In this case, as is usual in MPC, a QP optimization problem must be formulated. This problem, in an initial generic form, takes the form presented in equations (3–26)–(3–34). Then, during this subsection, additional

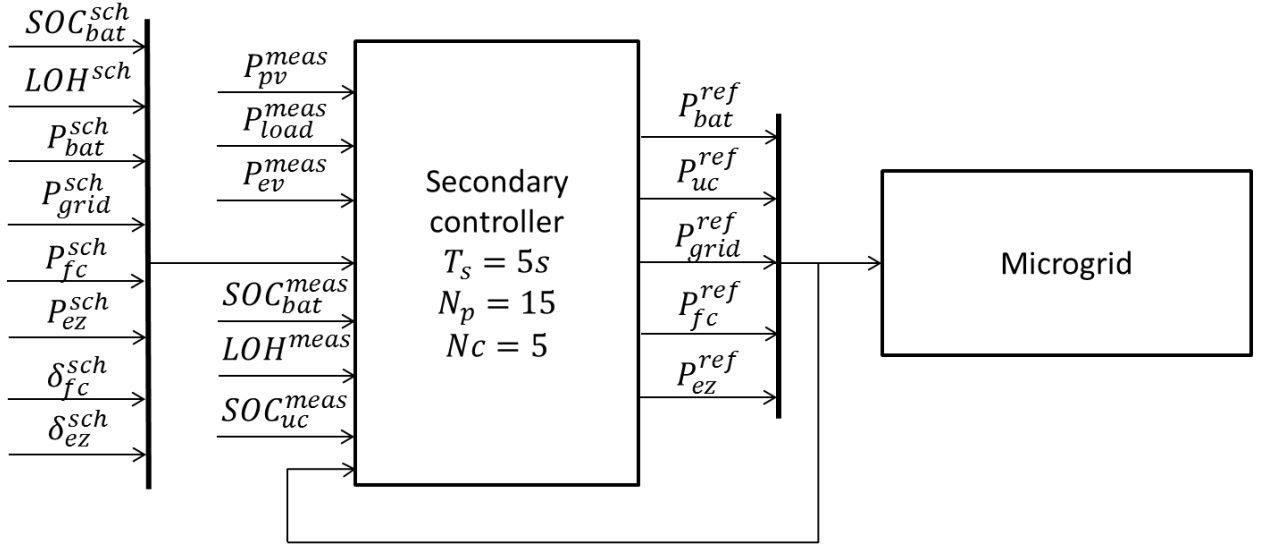


Figure 6. Secondary controller

terms will be added to the cost function, as well as new constraints will be considered. The problem is composed by the cost function (3–94), system model constraint (3–95)–(3–96), power balance constraint (3–97)–(3–98) and physical constraints, composed of power constraints (3–99), power variation constraints (3–100) and output constraints (3–101)–(3–103). The system model, the cost function and the constraints are going to be detailed in the following and the whole QP problem will be summarized at the end.

$$\min_u J(t) = \sum_{k=1}^{N_c} \|u(t_k - 1)\|_{\alpha}^2 + \sum_{k=1}^{N_c} \|\Delta u(t_k - 1)\|_{\lambda}^2 + \sum_{k=1}^{N_p} \|y(t_k) - w(t_k)\|_{\delta}^2 \quad (3-94)$$

$$s. t. \quad x(t_k + 1) = Ax(t_k) + Bu(t_k) + Ed(t_k) \quad (3-95)$$

$$y(t_k) = Cx(t_k) + Du(t_k) \quad (3-96)$$

$$P_{pv}^{meas}(t_k) + P_{grid}(t_k) + P_{bat}(t_k) + P_{uc}(t_k) + P_{H_2}(t_k) - P_{load}^{meas}(t_k) - P_{ev}^{meas}(t_k) = 0 \quad (3-97)$$

$$P_{H_2}(t_k) = P_{fc}(t_k) - P_{ez}(t_k) \quad (3-98)$$

$$P_i^{min} \leq P_i(t_k) \leq P_i^{max} |_{i=bat,fc,ez,grid,uc} \quad (3-99)$$

$$\Delta P_i^{min} \leq \Delta P_i(t_k) \leq \Delta P_i^{max} |_{i=bat,fc,ez,grid,uc} \quad (3-100)$$

$$SOC_{bat}^{min} \leq SOC_{bat}^{meas}(t_k) \leq SOC_{bat}^{max} \quad (3-101)$$

$$LOH^{min} \leq LOH^{meas}(t_k) \leq LOH^{max} \quad (3-102)$$

$$SOC_{uc}^{min} \leq SOC_{uc}^{meas}(t_k) \leq SOC_{uc}^{max} \quad (3-103)$$

Again,  $t_k$  indicates  $k$  time instants after the current time ( $t+k$ ), the superscript reference (*ref*) has not been included for simplicity,  $N_c$  means control horizon,  $N_p$  means prediction horizon, *meas* means measurements, and  $\alpha$ ,  $\lambda$  and  $\delta$  are the weighting term matrices for the cost function. Now, all these equations are going to be broken down.

Firstly, it is important to define the control actions vector,  $u$ . It can be seen in equation (3–104), and in this case

the QP problem does not use these vector components as decision variables. Incremental control actions, defined in equation (3–104) too, will be composed of the decision variables. The meaning of variables in these vectors is easily interpreted.

$$u(t_k) = \begin{bmatrix} P_{H_2}(t_k) \\ P_{grid}(t_k) \\ P_{uc}(t_k) \end{bmatrix} \quad \Delta u(t_k) = \begin{bmatrix} \Delta P_{H_2}(t_k) \\ \Delta P_{grid}(t_k) \\ \Delta P_{uc}(t_k) \end{bmatrix} = \begin{bmatrix} P_{H_2}(t_k) \\ P_{grid}(t_k) \\ P_{uc}(t_k) \end{bmatrix} - \begin{bmatrix} P_{H_2}(t_k - 1) \\ P_{grid}(t_k - 1) \\ P_{uc}(t_k - 1) \end{bmatrix} \quad (3-104)$$

As defined in equation (3–104), the battery power and power variation terms are not included in the control actions vectors. This is due to the fact that equations (3–97) and (3–98) are going to be included in the QP problema by replacing  $P_{bat}$  variable by:

$$P_{bat}(t_k) = -P_{pv}^{meas}(t_k) - P_{H_2}(t_k) - P_{grid}(t_k) - P_{uc}(t_k) + P_{load}^{meas}(t_k) + P_{ev}^{meas}(t_k) \quad (3-105)$$

And defining the disturbance variable as in equation (3–21) in subsection 3.1, equation (3–105) remains as follows:

$$P_{bat}(t_k) = -P_{H_2}(t_k) - P_{grid}(t_k) - P_{uc}(t_k) - d(t_k) \quad (3-106)$$

With this consideration, constraints related to the battery of (3–99) and (3–100) will need further development to be included in the optimization problem. This will be explained at the end of this section. Moreover, considering that no binary variables are going to be used, the system model to be included in the problem is the one in equations (3–1), (3–2) and (3–3); i.e.:

$$SOC_{bat}(t + 1) = SOC_{bat}(t) - \frac{\eta_{bat} T_s}{C_{max,bat}} P_{bat}(t) \quad (3-107)$$

$$LOH(t + 1) = LOH(t) - 100 \frac{\eta_{H_2} T_s}{V_{max}} P_{H_2}(t) \quad (3-108)$$

$$SOC_{uc}(t + 1) = SOC_{uc}(t) - \frac{\eta_{uc} T_s}{C_{max,uc}} P_{uc}(t) \quad (3-109)$$

And taking into account equation (3–106) for replacing  $P_{bat}$ , the battery equation model is transformed into:

$$SOC_{bat}(t + 1) = SOC_{bat}(t) - \frac{\eta_{bat} T_s}{C_{max,bat}} \left( -P_{H_2}(t_k) - P_{grid}(t_k) - P_{uc}(t_k) - d(t_k) \right) \quad (3-110)$$

If model constants definitions are recapped from subsection 3.1 (equations (3–11)-(3–16)):

$$K_{bat,ch} = \frac{\eta_{bat,ch}}{C_{max,bat}} \quad (3-111)$$

$$K_{bat,disc} = \frac{1}{\eta_{bat,disc} C_{max,bat}} \quad (3-112)$$

$$K_{ez} = \frac{\eta_{ez}}{V_{max}} \quad (3-113)$$

$$K_{fc} = \frac{1}{\eta_{fc} V_{max}} \quad (3-114)$$



$$K_{uc,ch} = \frac{\eta_{uc,ch}}{C_{max,uc}} \quad (3-115)$$

$$K_{uc,disc} = \frac{1}{\eta_{uc,disc} C_{max,uc}} \quad (3-116)$$

And new definitions are included, assuming a mean value between the two available ones for the constant of each device:

$$K_{bat} = \frac{\eta_{bat}}{C_{max,bat}} = \frac{K_{bat,ch} + K_{bat,disc}}{2} \quad (3-117)$$

$$K_{H_2} = \frac{\eta_{H_2}}{V_{max}} = \frac{K_{fc} + K_{ez}}{2} \quad (3-118)$$

$$K_{uc} = \frac{\eta_{uc}}{C_{max,uc}} = \frac{K_{uc,ch} + K_{uc,disc}}{2} \quad (3-119)$$

The system model equations remain as follows:

$$SOC_{bat}(t+1) = SOC_{bat}(t) - K_{bat} T_s P_{bat}(t) \quad (3-120)$$

$$LOH(t+1) = LOH(t) - 100 K_{H_2} T_s P_{H_2}(t) \quad (3-121)$$

$$SOC_{uc}(t+1) = SOC_{uc}(t) - K_{uc} T_s P_{uc}(t) \quad (3-122)$$

As the state,  $x$ , and output of the system,  $y$ , are defined by the same vectors:

$$x(t_k) = y(t_k) = \begin{bmatrix} SOC_{bat}(t_k) \\ LOH(t_k) \\ SOC_{uc}(t_k) \end{bmatrix} \quad (3-123)$$

The state space model of the system of equations (3-95) and (3-96) is transformed in equations (3-124) and (3-125) as:

$$\begin{bmatrix} SOC_{bat}(t_k+1) \\ LOH(t_k+1) \\ SOC_{uc}(t_k+1) \end{bmatrix} = \begin{bmatrix} SOC_{bat}(t_k) \\ LOH(t_k) \\ SOC_{uc}(t_k) \end{bmatrix} + \begin{bmatrix} K_{bat} & K_{bat} & K_{bat} \\ -K_{H_2} & 0 & 0 \\ 0 & 0 & -K_{uc} \end{bmatrix} u(t_k) + \begin{bmatrix} K_{bat} \\ 0 \\ 0 \end{bmatrix} d(t_k) \quad (3-124)$$

$$\begin{bmatrix} y_1(t_k) \\ y_2(t_k) \\ y_3(t_k) \end{bmatrix} = \begin{bmatrix} SOC_{bat}(t_k) \\ LOH(t_k) \\ SOC_{uc}(t_k) \end{bmatrix} \quad (3-125)$$

So, identifying terms:

$$A = \begin{bmatrix} 1 & 0 & 0 \\ 0 & 1 & 0 \\ 0 & 0 & 1 \end{bmatrix} \quad B = \begin{bmatrix} K_{bat} & K_{bat} & K_{bat} \\ -K_{H_2} & 0 & 0 \\ 0 & 0 & -K_{uc} \end{bmatrix} \quad E = \begin{bmatrix} K_{bat} \\ 0 \\ 0 \end{bmatrix} \quad (3-126)$$

$$C = \begin{bmatrix} 1 & 0 & 0 \\ 0 & 1 & 0 \\ 0 & 0 & 1 \end{bmatrix} \quad D = \begin{bmatrix} 0 & 0 & 0 \\ 0 & 0 & 0 \\ 0 & 0 & 0 \end{bmatrix}$$

Following reference [2], disturbances can be included as a component of the state, obtaining the augmented state,  $\tilde{x}(t_k)$ :

$$\tilde{x}(t_k) = \begin{bmatrix} x(t_k) \\ d(t_k) \end{bmatrix} \quad (3-127)$$

So, the augmented state space model is transformed in:

$$\tilde{x}(t_k + 1) = \begin{bmatrix} x(t_k + 1) \\ d(t_k + 1) \end{bmatrix} = \begin{bmatrix} A & E \\ 0 & I \end{bmatrix} \begin{bmatrix} x(t_k) \\ d(t_k) \end{bmatrix} + \begin{bmatrix} B \\ 0 \end{bmatrix} u(t_k) \quad (3-128)$$

$$y(t_k) = [C \quad 0] \begin{bmatrix} x(t_k) \\ d(t_k) \end{bmatrix} \quad (3-129)$$

Where  $I$  means the identity matrix of proper dimensions. Moreover, if the incremental power vector  $\Delta u$ , defined in equation (3-104), is wanted to be used as decision variable, the incremental state space model must be used, taking into account that the new state will be composed as follows:

$$\hat{x}(t_k) = \begin{bmatrix} \tilde{x}(t_k) \\ u(t_k - 1) \end{bmatrix} \quad (3-130)$$

Being the incremental control action:

$$\Delta u(t_k) = u(t_k) - u(t_k - 1) \quad (3-131)$$

The incremental state space model remains as:

$$\hat{x}(t_k + 1) = \begin{bmatrix} x(t_k + 1) \\ d(t_k + 1) \\ u(t_k) \end{bmatrix} = \begin{bmatrix} A & E & B \\ 0 & I & 0 \\ 0 & 0 & I \end{bmatrix} \begin{bmatrix} x(t_k) \\ d(t_k) \\ u(t_k - 1) \end{bmatrix} + \begin{bmatrix} B \\ 0 \\ I \end{bmatrix} \Delta u(t_k) \quad (3-132)$$

$$y(t_k) = [C \quad 0 \quad 0] \begin{bmatrix} x(t_k) \\ d(t_k) \\ u(t_k - 1) \end{bmatrix} \quad (3-133)$$

And in compact form, where matrices  $M$ ,  $N$  and  $Q$  are easily identifiable:

$$\hat{x}(t_k + 1) = M\hat{x}(t_k) + N\Delta u(t_k) \quad (3-134)$$

$$y(t_k) = Q\hat{x}(t_k) \quad (3-135)$$

Once the incremental model has been deduced, the optimization problem in (3-94)-(3-103) must be rewritten as a quadratic programming problem in the form of generic equation (3-136). This allows to directly using the solver *quadprog* in *MATLAB*. The cost function in equation (3-94) and the constraints in equations (3-99)-(3-103) must be transformed to have the structure of the ones in equation (3-136). Power balance (equations (3-97) and (3-98)) have already been included in the system model, and this system model (equations (3-95) and (3-96)) will be implicitly included in both the cost function and the output constraints.

$$\begin{aligned} \min_{\mathbf{u}} \quad & \frac{1}{2} \Delta \mathbf{u}^T \mathbf{H}_{qp} \Delta \mathbf{u} + \mathbf{B}_{qp}^T \Delta \mathbf{u} \\ \text{s. t.} \quad & \mathbf{R} \Delta \mathbf{u} \leq \mathbf{c} \end{aligned} \quad (3-136)$$

The first task is to convert the cost function. As pointed in equation (3-94), the cost function is given by:

$$J(t) = \sum_{k=1}^{Nc} \|u(t_k - 1)\|_{\alpha}^2 + \sum_{k=1}^{Nc} \|\Delta u(t_k - 1)\|_{\lambda}^2 + \sum_{k=1}^{Np} \|y(t_k) - w(t_k)\|_{\delta}^2 \quad (3-137)$$

Breaking down these terms, it results in:

$$\begin{aligned} J(t) = & \sum_{k=1}^{Nc} \left( \alpha_1 P_{H_2}^2(t_k - 1) + \alpha_2 P_{grid}^2(t_k - 1) + \alpha_3 P_{uc}^2(t_k - 1) + \lambda_1 \Delta P_{H_2}^2(t_k - 1) \right. \\ & \left. + \lambda_2 \Delta P_{grid}^2(t_k) + \lambda_3 \Delta P_{uc}^2(t_k - 1) \right) \\ & + \sum_{k=1}^{Np} \left( \delta_1 \left( SOC_{bat}(t_k) - SOC_{bat}^{sch}(t_k|t) \right)^2 \right. \\ & \left. + \delta_2 \left( LOH(t_k) - LOH^{sch}(t_k|t) \right)^2 + \delta_3 \left( SOC_{uc}(t_k) - SOC_{uc}^{sch}(t_k|t) \right)^2 \right) \end{aligned} \quad (3-138)$$

But for the problem transformation in equation (3-136), the matricial form is advisable. Detailing these matrices, the cost function remains as:

$$\begin{aligned} J(t) &= [u^T(t_k) \quad u^T(t_k + 1) \quad \cdots \quad u^T(t_k + N_c - 1)] \alpha \begin{bmatrix} u(t_k) \\ u(t_k + 1) \\ \vdots \\ u(t_k + N_c - 1) \end{bmatrix} \\ &+ [\Delta u^T(t_k) \quad \Delta u^T(t_k + 1) \quad \cdots \quad \Delta u^T(t_k + N_c - 1)] \lambda \begin{bmatrix} \Delta u(t_k) \\ \Delta u(t_k + 1) \\ \vdots \\ \Delta u(t_k + N_c - 1) \end{bmatrix} \\ &+ [(y(t_k + 1) - w(t_k + 1))^T \quad \cdots \quad (y(t_k + N_p) - w(t_k + N_p))^T] \delta \left( \begin{bmatrix} y(t_k + 1) \\ \vdots \\ y(t_k + N_p) \end{bmatrix} \right. \\ &\left. - \begin{bmatrix} w(t_k + 1) \\ \vdots \\ w(t_k + N_p) \end{bmatrix} \right) \end{aligned} \quad (3-139)$$

Where the cost function weighting matrices are defined as:

$$\alpha = \begin{bmatrix} \begin{bmatrix} \alpha_1 & \cdots & 0 \\ \vdots & \ddots & \vdots \\ 0 & \cdots & \alpha_m \end{bmatrix} & \cdots & 0 \\ \vdots & \ddots & \vdots \\ 0 & \cdots & \begin{bmatrix} \alpha_1 & \cdots & 0 \\ \vdots & \ddots & \vdots \\ 0 & \cdots & \alpha_m \end{bmatrix} \end{bmatrix} \quad (3-140)$$

$$\boldsymbol{\lambda} = \begin{bmatrix} \begin{bmatrix} \lambda_1 & \cdots & 0 \\ \vdots & \ddots & \vdots \\ 0 & \cdots & \lambda_m \end{bmatrix} & \cdots & 0 \\ \vdots & \ddots & \vdots \\ 0 & \cdots & \begin{bmatrix} \lambda_1 & \cdots & 0 \\ \vdots & \ddots & \vdots \\ 0 & \cdots & \lambda_m \end{bmatrix} \end{bmatrix} \quad (3-141)$$

$$\boldsymbol{\delta} = \begin{bmatrix} \begin{bmatrix} \delta_1 & \cdots & 0 \\ \vdots & \ddots & \vdots \\ 0 & \cdots & \delta_p \end{bmatrix} & \cdots & 0 \\ \vdots & \ddots & \vdots \\ 0 & \cdots & \begin{bmatrix} \delta_1 & \cdots & 0 \\ \vdots & \ddots & \vdots \\ 0 & \cdots & \delta_p \end{bmatrix} \end{bmatrix} \quad (3-142)$$

Where  $m$  and  $p$  indicates for the number of control actions (in this case, three) and for the number of outputs (in this case, three again), respectively.

Denoting:

$$\mathbf{u} = \begin{bmatrix} u(t_k) \\ u(t_k + 1) \\ \vdots \\ u(t_k + N_c - 1) \end{bmatrix} \quad \Delta \mathbf{u} = \begin{bmatrix} \Delta u(t_k) \\ \Delta u(t_k + 1) \\ \vdots \\ \Delta u(t_k + N_c - 1) \end{bmatrix} \quad (3-143)$$

$$\mathbf{y} = \begin{bmatrix} y(t_k + 1) \\ \vdots \\ y(t_k + N_p) \end{bmatrix} \quad \mathbf{w} = \begin{bmatrix} w(t_k + 1) \\ \vdots \\ w(t_k + N_p) \end{bmatrix}$$

The cost function remains as:

$$J(t) = \mathbf{u}^T \boldsymbol{\alpha} \mathbf{u} + \Delta \mathbf{u}^T \boldsymbol{\lambda} \Delta \mathbf{u} + (\mathbf{y} - \mathbf{w})^T \boldsymbol{\delta} (\mathbf{y} - \mathbf{w}) \quad (3-144)$$

As the decision variable is  $\Delta \mathbf{u}$ , both the vector  $\mathbf{u}$  and  $\mathbf{y}$  must be rewritten as a function of  $\Delta \mathbf{u}$ .

For  $\mathbf{u}$ , taking into account:

$$\Delta u(t_k) = u(t_k) - u(t_k - 1) \quad (3-145)$$

The following sequence can be written:

$$\begin{aligned} u(t) &= \Delta u(t) + u(t - 1) \\ u(t + 1) &= \Delta u(t + 1) + \Delta u(t) + u(t - 1) \\ u(t + 2) &= \Delta u(t + 2) + \Delta u(t + 1) + \Delta u(t) + u(t - 1) \\ &\quad \dots \\ u(t + j) &= \Delta u(t + j) + \Delta u(t + j - 1) + \cdots + \Delta u(t) + u(t - 1) \\ &\quad \dots \\ u(t + N_c - 1) &= \Delta u(t + N_c - 1) + \Delta u(t + N_c - 2) + \cdots + \Delta u(t) + u(t - 1) \end{aligned} \quad (3-146)$$

That is, in matrix form:

$$\begin{bmatrix} u(t_k) \\ u(t_k + 1) \\ \vdots \\ u(t_k + N_c - 1) \end{bmatrix} = \begin{bmatrix} I_{m,m} & 0 & \cdots & 0 \\ I_{m,m} & I_{m,m} & \cdots & 0 \\ \vdots & \vdots & \ddots & \vdots \\ I_{m,m} & I_{m,m} & \cdots & I_{m,m} \end{bmatrix} \begin{bmatrix} \Delta u(t_k) \\ \Delta u(t_k + 1) \\ \vdots \\ \Delta u(t_k + N_c - 1) \end{bmatrix} + \begin{bmatrix} I_{m,m} \\ I_{m,m} \\ \vdots \\ I_{m,m} \end{bmatrix} u(t_k - 1) \quad (3-147)$$

Where  $I_{m,m}$  is the identity matrix of size  $m$ . Defining:

$$\mathbf{T} = \begin{bmatrix} I_{m,m} & 0 & \cdots & 0 \\ I_{m,m} & I_{m,m} & \cdots & 0 \\ \vdots & \vdots & \ddots & \vdots \\ I_{m,m} & I_{m,m} & \cdots & I_{m,m} \end{bmatrix} \quad \mathbf{1}_{N_c m, m} = \begin{bmatrix} I_{m,m} \\ I_{m,m} \\ \vdots \\ I_{m,m} \end{bmatrix} \quad (3-148)$$

The vector  $\mathbf{u}$  can be represented as:

$$\mathbf{u} = \mathbf{T} \Delta \mathbf{u} + \mathbf{1}_{N_c m, m} u(t_k - 1) \quad (3-149)$$

On the other side, from the incremental model (equations (3-134) and (3-135)), recursively, one has [80]:

$$\begin{aligned} y(t_k) &= Q \hat{x}(t_k) = Q(M \hat{x}(t_k - 1) + N \Delta u(t_k - 1)) \\ &= Q[M(M \hat{x}(t_k - 2) + N \Delta u(t_k - 2)) + N \Delta u(t_k - 1)] \\ &= Q\{M[M(M \hat{x}(t_k - 3) + N \Delta u(t_k - 3)) + N \Delta u(t_k - 2)] \\ &\quad + N \Delta u(t_k - 1)\} = \dots = Q M^k \hat{x}(t) + \sum_{i=0}^{k-1} Q M^{k-i-1} N \Delta u(t_i) \end{aligned} \quad (3-150)$$

Writing equation (3-150) in matrix form:

$$\mathbf{y} = \mathbf{F} \hat{\mathbf{x}}(t) + \mathbf{H} \Delta \mathbf{u} \quad (3-151)$$

Where  $\hat{\mathbf{x}}(t)$  is the incremental and augmented state in the current time instant, and the matrices are:

$$\mathbf{F} = \begin{bmatrix} QM \\ QM^2 \\ \vdots \\ QM^{N_p} \end{bmatrix} \quad \mathbf{H} = \begin{bmatrix} QN & 0 & \cdots & 0 \\ QMN & QN & \cdots & 0 \\ \vdots & \vdots & \ddots & \vdots \\ QM^{N_p-1}N & QM^{N_p-2}N & \cdots & QM^{N_p-N_c}N \end{bmatrix} \quad (3-152)$$

Therefore, the cost function in equation (3-144) can be rewritten as:

$$\begin{aligned} J(t) &= \left( \mathbf{T} \Delta \mathbf{u} + \mathbf{1}_{N_c m, m} u(t_k - 1) \right)^T \boldsymbol{\alpha} \left( \mathbf{T} \Delta \mathbf{u} + \mathbf{1}_{N_c m, m} u(t_k - 1) \right) + \Delta \mathbf{u}^T \boldsymbol{\lambda} \Delta \mathbf{u} \\ &\quad + \left( \mathbf{H} \Delta \mathbf{u} + (\mathbf{F} \hat{\mathbf{x}}(t) - \mathbf{w}) \right)^T \boldsymbol{\delta} \left( \mathbf{H} \Delta \mathbf{u} + (\mathbf{F} \hat{\mathbf{x}}(t) - \mathbf{w}) \right) \end{aligned} \quad (3-153)$$

Re-organizing terms:

$$\begin{aligned} J(t) &= \Delta \mathbf{u}^T (\mathbf{T}^T \boldsymbol{\alpha} \mathbf{T} + \boldsymbol{\lambda} + \mathbf{H}^T \boldsymbol{\delta} \mathbf{H})^T \Delta \mathbf{u} \\ &\quad + 2 \left( \mathbf{1}_{N_c m, m} u(t_k - 1) \right)^T \boldsymbol{\alpha} \mathbf{T} + (\mathbf{F} \hat{\mathbf{x}}(t) - \mathbf{w}) \boldsymbol{\delta} \mathbf{H} \Delta \mathbf{u} \end{aligned} \quad (3-154)$$

So, looking at const function in the generic form optimization problem of equation (3–136), it is easy to identify terms:

$$\begin{aligned} \mathbf{H}_{qp} &= 2(\mathbf{T}^T \boldsymbol{\alpha} \mathbf{T} + \boldsymbol{\lambda} + \mathbf{H}^T \boldsymbol{\delta} \mathbf{H}) \\ \mathbf{B}_{qp} &= 2 \left( \mathbf{T}^T \boldsymbol{\alpha} \left( \mathbf{1}_{N_c m, m} u(t_k - 1) \right) + \mathbf{H}^T \boldsymbol{\delta} (\mathbf{F} \hat{\mathbf{x}}(t) - \mathbf{w}) \right) \end{aligned} \quad (3-155)$$

Once the cost function has been transformed, the next step is to do the same with the constraints. Restrictions in equations (3–99)-(3–103), except from those for  $P_{bat}$  and  $\Delta P_{bat}$ , can be summarized in vector form as:

$$u_{min} \leq u(t_k) \leq u_{max} \quad (3-156)$$

$$\Delta u_{min} \leq \Delta u(t_k) \leq \Delta u_{max} \quad (3-157)$$

$$y_{min} \leq y(t_k) \leq y_{max} \quad (3-158)$$

Where:

$$u_{min} = \begin{bmatrix} P_{H_2}^{min} \\ P_{grid}^{min} \\ P_{uc}^{min} \end{bmatrix} \quad u_{max} = \begin{bmatrix} P_{H_2}^{max} \\ P_{grid}^{max} \\ P_{uc}^{max} \end{bmatrix} \quad (3-159)$$

$$\Delta u_{min} = \begin{bmatrix} \Delta P_{H_2}^{min} \\ \Delta P_{grid}^{min} \\ \Delta P_{uc}^{min} \end{bmatrix} \quad \Delta u_{max} = \begin{bmatrix} \Delta P_{H_2}^{max} \\ \Delta P_{grid}^{max} \\ \Delta P_{uc}^{max} \end{bmatrix} \quad (3-160)$$

$$y_{min} = \begin{bmatrix} SOC_{bat}^{min} \\ LOH^{min} \\ SOC_{uc}^{min} \end{bmatrix} \quad y_{max} = \begin{bmatrix} SOC_{bat}^{max} \\ LOH^{max} \\ SOC_{uc}^{max} \end{bmatrix} \quad (3-161)$$

Expanding these constraints in the whole prediction and control horizons, one obtains the following:

$$\mathbf{1}_{N_c m, m} u_{min} \leq \mathbf{T} \Delta \mathbf{u} + \mathbf{1}_{N_c m, m} u(t_k - 1) \leq \mathbf{1}_{N_c m, m} u_{max} \quad (3-162)$$

$$\mathbf{1}_{N_c m, m} \Delta u_{min} \leq \Delta \mathbf{u} \leq \mathbf{1}_{N_c m, m} \Delta u_{max} \quad (3-163)$$

$$\mathbf{1}_{N_p p, p} y_{min} \leq \mathbf{F} \hat{\mathbf{x}}(t) + \mathbf{H} \Delta \mathbf{u} \leq \mathbf{1}_{N_p p, p} y_{max} \quad (3-164)$$

Hence, looking at restriction form in equation (3–136), the matrix  $\mathbf{R}$  and vector  $\mathbf{c}$  definitions are:

$$\mathbf{R} = \begin{bmatrix} \mathbf{I}_{N_c m, N_c m} \\ -\mathbf{I}_{N_c m, N_c m} \\ \mathbf{T} \\ -\mathbf{T} \\ \mathbf{H} \\ -\mathbf{H} \end{bmatrix} \quad \mathbf{c} = \begin{bmatrix} \mathbf{1}_{N_c m, m} \Delta u_{max} \\ -\mathbf{1}_{N_c m, m} \Delta u_{min} \\ \mathbf{1}_{N_c m, m} u_{max} - \mathbf{1}_{N_c m, m} u(t_k - 1) \\ -\mathbf{1}_{N_c m, m} u_{min} + \mathbf{1}_{N_c m, m} u(t_k - 1) \\ \mathbf{1}_{N_p p, p} y_{max} - \mathbf{F} \hat{\mathbf{x}}(t) \\ -\mathbf{1}_{N_p p, p} y_{min} + \mathbf{F} \hat{\mathbf{x}}(t) \end{bmatrix} \quad (3-165)$$

Now, with the generic problem written in the right form to use *quadprog* like another QP problems, battery power and incremental power constraints and cost function terms are going to be added to the formulated

problem. In the first place, the battery power constraints are given by:

$$P_{bat}^{min} \leq P_{bat}(t_k) \leq P_{bat}^{max} \quad (3-166)$$

Remembering the power balance given by equation (3-167) and the definitions given by equation (3-168):

$$P_{bat}(t_k) = -P_{H_2}(t_k) - P_{grid}(t_k) - P_{uc}(t_k) - d(t_k) \quad (3-167)$$

$$u(t_k) = \begin{bmatrix} P_{H_2}(t_k) \\ P_{grid}(t_k) \\ P_{uc}(t_k) \end{bmatrix} \quad \hat{x}(t_k) = \begin{bmatrix} SOC_{bat}(t_k) \\ LOH(t_k) \\ SOC_{uc}(t_k) \\ d(t_k) \\ P_{H_2}(t_k - 1) \\ P_{grid}(t_k - 1) \\ P_{uc}(t_k - 1) \end{bmatrix} \quad (3-168)$$

Equation (3-167) can be written as:

$$P_{bat}(t_k) = [-1 \quad -1 \quad -1]u(t_k) + [0 \quad 0 \quad 0 \quad -1 \quad 0 \quad 0 \quad 0]\hat{x}(t_k) \quad (3-169)$$

Expanding for all the time instants of the control horizon:

$$\mathbf{P}_{bat} = \mathbf{aux}_u \mathbf{u} + \mathbf{aux}_x \hat{x}(t_k) \quad (3-170)$$

Being:

$$\mathbf{P}_{bat} = \begin{bmatrix} P_{bat}(t) \\ P_{bat}(t+1) \\ \vdots \\ P_{bat}(t+N_c-1) \end{bmatrix} \quad \mathbf{aux}_x = \begin{bmatrix} [0 & 0 & 0 & -1 & 0 & 0 & 0] \\ [0 & 0 & 0 & -1 & 0 & 0 & 0] \\ \vdots \\ [0 & 0 & 0 & -1 & 0 & 0 & 0] \end{bmatrix} \quad (3-171)$$

$$\mathbf{aux}_u = \begin{bmatrix} [-1 & -1 & -1] & 0 & \dots & 0 \\ 0 & [-1 & -1 & -1] & \dots & 0 \\ \vdots & \vdots & \ddots & \vdots & \dots & \vdots \\ 0 & 0 & \dots & [-1 & -1 & -1] \end{bmatrix}$$

Defining:

$$\mathbf{P}_{bat}^{min} = \begin{bmatrix} P_{bat}^{min} \\ P_{bat}^{min} \\ \vdots \\ P_{bat}^{min} \end{bmatrix}_{N_c,1} \quad \mathbf{P}_{bat}^{max} = \begin{bmatrix} P_{bat}^{max} \\ P_{bat}^{max} \\ \vdots \\ P_{bat}^{max} \end{bmatrix}_{N_c,1} \quad (3-172)$$

Writing vector  $\mathbf{u}$  as a function of  $\Delta \mathbf{u}$ , as pointed in equation (3-149), the restriction (3-166) can be written as:

$$\mathbf{P}_{bat}^{min} \leq \mathbf{aux}_u (\mathbf{T} \Delta \mathbf{u} + \mathbf{1}_{N_c, m, m} u(t_k - 1)) + \mathbf{aux}_x \hat{x}(t_k) \leq \mathbf{P}_{bat}^{max} \quad (3-173)$$

Therefore, adding two more rows to matrix  $\mathbf{R}$  and other two rows to vector  $\mathbf{c}$  of equation (3-165), the battery power constraint is added to the optimization problem.

In the same way, the battery incremental power constraint can be added. This constraint is written as:

$$\Delta P_{bat}^{min} \leq \Delta P_{bat}(t_k) \leq \Delta P_{bat}^{max} \quad (3-174)$$

Following a similar procedure, the incremental battery power, assuming that the disturbance is constant in the whole control horizon, can be expressed as:

$$\begin{aligned} \Delta P_{bat}(t_k) &= P_{bat}(t_k) - P_{bat}(t_k - 1) \\ &= [-1 \quad -1 \quad -1] \Delta u(t_k) - \begin{bmatrix} d(t_k) - d(t_k - 1) \\ 0 \\ \vdots \\ 0 \end{bmatrix} \end{aligned} \quad (3-175)$$

Defining:

$$\Delta \mathbf{P}_{bat}^{min} = \begin{bmatrix} \Delta P_{bat}^{min} \\ \Delta P_{bat}^{min} \\ \vdots \\ \Delta P_{bat}^{min} \end{bmatrix}_{N_c, 1} \quad \Delta \mathbf{P}_{bat}^{max} = \begin{bmatrix} \Delta P_{bat}^{max} \\ \Delta P_{bat}^{max} \\ \vdots \\ \Delta P_{bat}^{max} \end{bmatrix}_{N_c, 1} \quad (3-176)$$

The constraint (3-174) can be written as:

$$\Delta \mathbf{P}_{bat}^{min} \leq \mathbf{a} \mathbf{u}_u \Delta \mathbf{u} - \begin{bmatrix} d(t_k) - d(t_k - 1) \\ 0 \\ \vdots \\ 0 \end{bmatrix} \leq \Delta \mathbf{P}_{bat}^{max} \quad (3-177)$$

The procedure consists again of adding two rows to both the matrix  $\mathbf{R}$  and the vector  $\mathbf{c}$  in equation (3-165).

The next step is to add a term in the cost function which penalizes both the battery power and the battery incremental power. This term is given by:

$$\sum_{k=1}^{N_c} (\alpha_4 P_{bat}^2(t_k - 1) + \lambda_4 \Delta P_{bat}^2(t_k - 1)) \quad (3-178)$$

Recalling that:

$$P_{bat}(t_k) = [-1 \quad -1 \quad -1] u(t_k) + [0 \quad 0 \quad 0 \quad -1 \quad 0 \quad 0 \quad 0] \hat{x}(t_k) \quad (3-179)$$

The first term of (3-178) can be expressed as:

$$\begin{aligned} \alpha_4 P_{bat}^2(t_k) &= P_{bat}(t_k)^T \alpha_4 P_{bat}(t_k) \\ &= \left( u^T(t_k) \begin{bmatrix} -1 \\ -1 \\ -1 \end{bmatrix} + \hat{x}^T(t_k) \begin{bmatrix} 0 \\ 0 \\ 0 \\ -1 \\ 0 \\ 0 \\ 0 \end{bmatrix} \right) \alpha_4 \left( [-1 \quad -1 \quad -1] u(t_k) \right. \\ &\quad \left. + [0 \quad 0 \quad 0 \quad -1 \quad 0 \quad 0 \quad 0] \hat{x}(t_k) \right) \\ &= u^T(t_k) \alpha_{4_{uz}} u(t_k) + 2 \hat{x}^T(t_k) \alpha_{4_{xu}} u(t_k) + \text{constant term in } \Delta u \end{aligned} \quad (3-180)$$

Where:



$$\alpha_{4_{u2}} = \begin{bmatrix} \alpha_4 & \alpha_4 & \alpha_4 \\ \alpha_4 & \alpha_4 & \alpha_4 \\ \alpha_4 & \alpha_4 & \alpha_4 \end{bmatrix} \quad \alpha_{4_{xu}} = \begin{bmatrix} 0 \\ 0 \\ 0 \\ -1 \\ 0 \\ 0 \\ 0 \end{bmatrix} \alpha_4 [-1 \quad -1 \quad -1] \quad (3-181)$$

With a similar procedure, one can develop the following for the second term in (3-178):

$$\begin{aligned} \lambda_4 \Delta P_{bat}^2(t_k) &= \Delta P_{bat}(t_k)^T \lambda_4 \Delta P_{bat}(t_k) = \\ &= \Delta \mathbf{u}^T(t_k) \lambda_{4_{u2}} \Delta \mathbf{u}(t_k) + 2 \Delta \hat{\mathbf{x}}^T(t_k) \lambda_{4_{xu}} \Delta \mathbf{u}(t_k) \\ &+ \text{constant term in } \Delta \mathbf{u} \end{aligned} \quad (3-182)$$

Extending the weighting terms  $\alpha_{4_{u2}}$ ,  $\alpha_{4_{xu}}$ ,  $\lambda_{4_{u2}}$  and  $\lambda_{4_{xu}}$  in order to implement a matrix form:

$$\alpha_{4_{u2}} = \begin{bmatrix} \alpha_{4_{u2}} & 0 & \cdots & 0 \\ 0 & \alpha_{4_{u2}} & \cdots & 0 \\ \vdots & \vdots & \ddots & \vdots \\ 0 & 0 & \cdots & \alpha_{4_{u2}} \end{bmatrix} \quad \alpha_{4_{xu}} = [\alpha_{4_{xu}} \quad \alpha_{4_{xu}} \quad \cdots \quad \alpha_{4_{xu}}] \quad (3-183)$$

$$\lambda_{4_{u2}} = \begin{bmatrix} \lambda_{4_{u2}} & 0 & \cdots & 0 \\ 0 & \lambda_{4_{u2}} & \cdots & 0 \\ \vdots & \vdots & \ddots & \vdots \\ 0 & 0 & \cdots & \lambda_{4_{u2}} \end{bmatrix} \quad \lambda_{4_{xu}} = [\lambda_{4_{xu}} \quad \lambda_{4_{xu}} \quad \cdots \quad \lambda_{4_{xu}}] \quad (3-184)$$

The expression of (3-138) can be expressed in matrix form as:

$$\begin{aligned} & \left( \mathbf{T} \Delta \mathbf{u} + \mathbf{1}_{N_{cm,m}} u(t_k - 1) \right)^T \alpha_{4_{u2}} \left( \mathbf{T} \Delta \mathbf{u} + \mathbf{1}_{N_{cm,m}} u(t_k - 1) \right) \\ & + 2 \hat{\mathbf{x}}^T(t_k) \alpha_{4_{xu}} \left( \mathbf{T} \Delta \mathbf{u} + \mathbf{1}_{N_{cm,m}} u(t_k - 1) \right) + \Delta \mathbf{u}^T \lambda_{4_{u2}} \Delta \mathbf{u} \\ & + 2 \Delta \hat{\mathbf{x}}^T(t_k) \lambda_{4_{xu}} \Delta \mathbf{u} + \text{constant term in } \Delta \mathbf{u} \end{aligned} \quad (3-185)$$

Knowing that:

$$2 \Delta \hat{\mathbf{x}}^T(t_k) \lambda_{4_{xu}} \Delta \mathbf{u} = 2 \Delta d(t_k) \lambda_{4_{xu,small}} \Delta \mathbf{u} = 2(d(t_k) - d(t_k - 1)) \lambda_{4_{xu,small}} \Delta \mathbf{u} \quad (3-186)$$

Where:

$$\lambda_{4_{xu,small}} = [\lambda_4 \quad \lambda_4 \quad \cdots \quad \lambda_4]_{1, N_{cm}} \quad (3-187)$$

The expression (3-185) remains as:

$$\begin{aligned} & \left( \mathbf{T} \Delta \mathbf{u} + \mathbf{1}_{N_{cm,m}} u(t_k - 1) \right)^T \alpha_{4_{u2}} \left( \mathbf{T} \Delta \mathbf{u} + \mathbf{1}_{N_{cm,m}} u(t_k - 1) \right) \\ & + 2 \hat{\mathbf{x}}^T(t_k) \alpha_{4_{xu}} \left( \mathbf{T} \Delta \mathbf{u} + \mathbf{1}_{N_{cm,m}} u(t_k - 1) \right) + \Delta \mathbf{u}^T \lambda_{4_{u2}} \Delta \mathbf{u} \\ & + 2 \Delta d(t_k) \lambda_{4_{xu,small}} \Delta \mathbf{u} + \text{constant term in } \Delta \mathbf{u} \end{aligned} \quad (3-188)$$

The last expression can be rewritten as follows:

$$\begin{aligned}
& \Delta \mathbf{u}^T (\mathbf{T}^T \boldsymbol{\alpha}_{4_{u2}} \mathbf{T} + \lambda_{4_{u2}}) \Delta \mathbf{u} \\
& + 2 \left( (\mathbf{1}_{N_c m, m} u(t_k - 1))^T \boldsymbol{\alpha}_{4_{u2}} \mathbf{T} + \hat{x}^T(t_k) \boldsymbol{\alpha}_{4_{xu}} \mathbf{T} \right. \\
& \left. + 2 \Delta d(t_k) \lambda_{4_{xu, small}} \right) \Delta \mathbf{u} + \text{constant term in } \Delta \mathbf{u}
\end{aligned} \tag{3-189}$$

Therefore, the procedure is finally to add two terms to the matrix  $\mathbf{H}_{qp}$  and three terms to the matrix  $\mathbf{B}_{qp}$  of equation (3-155).

Finally, another term to be added to the cost function is referred to the power reference tracking, in order to take advantages of the schedule done in the tertiary controller.

If the control action vector for references  $\mathbf{u}^{sch}$  and its corresponding matrix  $\mathbf{u}^{sch}$  for the whole control horizon is defined as:

$$\mathbf{u}^{sch}(t_k) = \begin{bmatrix} P_{H_2}^{sch}(t_k) \\ P_{grid}^{sch}(t_k) \\ P_{uc}^{sch}(t_k) \end{bmatrix} \quad \mathbf{u}^{sch} = \begin{bmatrix} \mathbf{u}^{sch}(t) \\ \mathbf{u}^{sch}(t+1) \\ \vdots \\ \mathbf{u}^{sch}(t+N_c-1) \end{bmatrix} \tag{3-190}$$

The term to be added to the cost function is:

$$(\mathbf{u} - \mathbf{u}^{sch})^T \boldsymbol{\gamma} (\mathbf{u} - \mathbf{u}^{sch}) \tag{3-191}$$

Where  $\boldsymbol{\gamma}$  is the weighting term matrix, defined as:

$$\boldsymbol{\gamma} = \begin{bmatrix} \begin{bmatrix} \gamma_1 & \cdots & 0 \\ \vdots & \ddots & \vdots \\ 0 & \cdots & \gamma_m \end{bmatrix} & \cdots & 0 \\ \vdots & \ddots & \vdots \\ 0 & \cdots & \begin{bmatrix} \gamma_1 & \cdots & 0 \\ \vdots & \ddots & \vdots \\ 0 & \cdots & m_p \end{bmatrix} \end{bmatrix} \tag{3-192}$$

So, rewriting the term (3-191):

$$\Delta \mathbf{u}^T \mathbf{T}^T \boldsymbol{\gamma} \mathbf{T} \Delta \mathbf{u} + 2 \left( (\mathbf{1}_{N_c m, m} u(t_k - 1) - \mathbf{u}^{sch})^T \boldsymbol{\gamma} \mathbf{T} \right) \Delta \mathbf{u} + \text{constant term in } \Delta \mathbf{u} \tag{3-193}$$

Again, this can be implemented by adding one term to the matrix  $\mathbf{H}_{qp}$  and another one term to the matrix  $\mathbf{B}_{qp}$  of equation (3-155).

However, as in other terms, the battery power reference tracking is not considered in the cost function. There is a need for further calculations in order to complete the cost function.

The term to be added to the cost function is:

$$(\mathbf{P}_{bat} - \mathbf{P}_{bat}^{sch})^T \boldsymbol{\gamma}_{bat} (\mathbf{P}_{bat} - \mathbf{P}_{bat}^{sch}) \tag{3-194}$$

Where:

$$\mathbf{P}_{bat}^{sch} = \begin{bmatrix} P_{bat}^{sch} \\ P_{bat}^{sch} \\ \vdots \\ P_{bat}^{sch} \end{bmatrix}_{N_c,1} \quad \mathbf{\gamma}_{bat} = \begin{bmatrix} \gamma_{bat} & 0 & \cdots & 0 \\ 0 & \gamma_{bat} & \cdots & 0 \\ \vdots & \vdots & \ddots & \vdots \\ 0 & 0 & \cdots & \gamma_{bat} \end{bmatrix} \quad (3-195)$$

The term (3-194) can be expressed as:

$$\begin{aligned} & \left( \mathbf{aux}_u \left( \mathbf{T} \Delta \mathbf{u} + \mathbf{1}_{N_c, m, m} u(t_k - 1) \right) + \mathbf{aux}_x \hat{x}(t_k) - \mathbf{P}_{bat}^{sch} \right)^T \mathbf{\gamma}_{bat} \left( \mathbf{aux}_u \left( \mathbf{T} \Delta \mathbf{u} \right. \right. \\ & \left. \left. + \mathbf{1}_{N_c, m, m} u(t_k - 1) \right) + \mathbf{aux}_x \hat{x}(t_k) - \mathbf{P}_{bat}^{sch} \right) \end{aligned} \quad (3-196)$$

Re-ordering the terms, one has:

$$\begin{aligned} & \Delta \mathbf{u}^T \left( \mathbf{T}^T \mathbf{aux}_u^T \mathbf{\gamma}_{bat} \mathbf{aux}_u \mathbf{T} \right) \Delta \mathbf{u} \\ & + 2 \left( \left( \mathbf{aux}_u \mathbf{1}_{N_c, m, m} u(t_k - 1) + \mathbf{aux}_x \hat{x}(t_k) \right. \right. \\ & \left. \left. - \mathbf{P}_{bat}^{sch} \right)^T \mathbf{\gamma}_{bat} \mathbf{aux}_u \mathbf{T} \right) \Delta \mathbf{u} + \text{constant term in } \Delta \mathbf{u} \end{aligned} \quad (3-197)$$

Hence, again, this can be implemented by adding one term to the matrix  $\mathbf{H}_{qp}$  and another one term to the matrix  $\mathbf{B}_{qp}$  of equation (3-155).

With all this calculations, the optimization problem to be solved in this secondary controller is summarized in the following box.

Finally, to summarize, the following box includes the complete MPC problem formulation, which can be easily solved using the solver *quadprog* in *MATLAB*.

$$\begin{aligned} & \min_{\Delta \mathbf{u}} \frac{1}{2} \Delta \mathbf{u}^T \mathbf{H}_{qp} \Delta \mathbf{u} + \mathbf{B}_{qp}^T \Delta \mathbf{u} \\ & \text{s. t. } \mathbf{R} \Delta \mathbf{u} \leq \mathbf{c} \end{aligned}$$

Where:

$$\mathbf{R} = \begin{bmatrix} \mathbf{I}_{N_c, m, N_c, m} \\ -\mathbf{I}_{N_c, m, N_c, m} \\ \mathbf{T} \\ -\mathbf{T} \\ \mathbf{H} \\ -\mathbf{H} \\ \mathbf{aux}_u \mathbf{T} \\ -\mathbf{aux}_u \mathbf{T} \\ \mathbf{aux}_u \\ -\mathbf{aux}_u \end{bmatrix} \quad \mathbf{c} = \begin{bmatrix} \mathbf{1}_{N_c, m, m} \Delta u_{max} \\ -\mathbf{1}_{N_c, m, m} \Delta u_{min} \\ \mathbf{1}_{N_c, m, m} u_{max} - \mathbf{1}_{N_c, m, m} u(t_k - 1) \\ -\mathbf{1}_{N_c, m, m} u_{min} + \mathbf{1}_{N_c, m, m} u(t_k - 1) \\ \mathbf{1}_{N_p, p, p} y_{max} - \mathbf{F} \hat{x}(t) \\ -\mathbf{1}_{N_p, p, p} y_{min} + \mathbf{F} \hat{x}(t) \\ \mathbf{P}_{bat}^{max} - \mathbf{1}_{N_c, m, m} u(t_k - 1) - \mathbf{aux}_x \hat{x}(t_k) \\ -\mathbf{P}_{bat}^{min} + \mathbf{aux}_u \mathbf{1}_{N_c, m, m} u(t_k - 1) + \mathbf{aux}_x \hat{x}(t_k) \\ \mathbf{\Delta P}_{bat}^{max} + \begin{bmatrix} d(t_k) - d(t_k - 1) \\ 0 \\ \vdots \\ 0 \end{bmatrix} \\ -\mathbf{\Delta P}_{bat}^{min} - \begin{bmatrix} d(t_k) - d(t_k - 1) \\ 0 \\ \vdots \\ 0 \end{bmatrix} \end{bmatrix}$$

$$\begin{aligned}
 H_{qp} &= 2(T^T \alpha T + \lambda + H^T \delta H + T^T \alpha_{4_{u2}} T + \lambda_{4_{u2}} + T^T \gamma T + T^T \mathbf{aux}_u^T \gamma_{bat} \mathbf{aux}_u T) \\
 B_{qp} &= 2 \left( T^T \alpha \left( \mathbf{1}_{N_{cm,m}} u(t_k - 1) \right) + H^T \delta (F \hat{x}(t) - \mathbf{w}) \right) + 2 \left( \left( \mathbf{1}_{N_{cm,m}} u(t_k - 1) \right)^T \alpha_{4_{u2}} T + \right. \\
 &\quad \left. \hat{x}^T(t_k) \alpha_{4_{xu}} T + 2 \Delta d(t_k) \lambda_{4_{xu,small}} \right)^T + 2 \left( \left( \mathbf{1}_{N_{cm,m}} u(t_k - 1) - \mathbf{u}^{sch} \right)^T \gamma T \right)^T + \\
 &\quad + 2 \left( \left( \mathbf{aux}_u \mathbf{1}_{N_{cm,m}} u(t_k - 1) + \mathbf{aux}_x \hat{x}(t_k) - \mathbf{P}_{bat}^{sch} \right)^T \gamma_{bat} \mathbf{aux}_u T \right)^T
 \end{aligned}$$

### 3.3 Software simulation tools

As it was previously commented, this work only includes simulation, so it is important to have a reliable simulator of the microgrid, as well as a robust tool to solve the optimization problems in which the developed controllers are involved. As a simulation tool, *Simugrid* library is described, and for the optimization problem solver, *Yalmip* tool with the solver *CPLEX*, are going to be described in this subsection. The solver *quadprog* used for the secondary controller is a simple built-in MATLAB function to directly solve quadratic programming problems, so it is not worth to describe more about it.

#### 3.3.1 Simugrid

The microgrid is simulated in *MATLAB/Simulink* using the library *Simugrid*. This library was created by the *Automática y Robótica Industrial* research group from *University of Seville*, for the research project *AGERAR*, which is available online in with the corresponding documentation [83]. In this library, microgrid components are theoretically modelled for control purposes and implemented in Simulink depending on some configurable parameters, which can be obtained from manufacturers or by model and parameters identification techniques with real equipment. Models have been validated and used in other projects and publications. As an example, the *Simugrid* diagram for this work is shown in Figure 7.

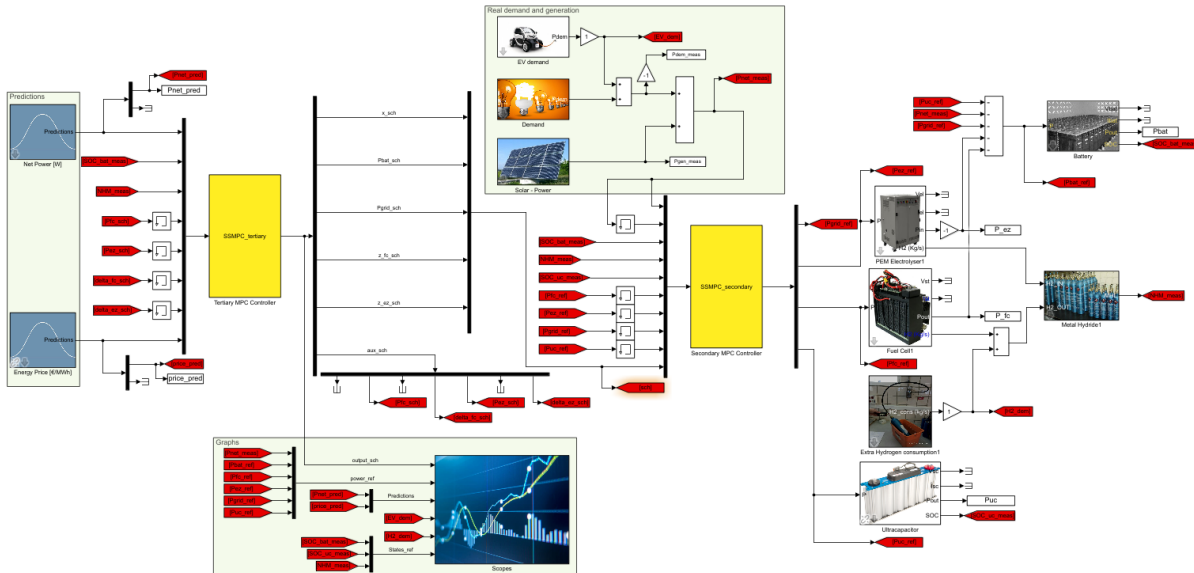


Figure 7. Simugrid complete diagram

The elements used are:

- *Predictions*: to make the net power (generation minus demand) forecast and the price forecast.
- *Solar - Power*: to introduce real PV power generation data.
- *Demand*: to introduce real power consumption data.
- *EV demand*: the same as demand but for electric vehicle charging power. This block has been created

for this work. It takes a MATLAB file *.mat* with the data for EVs charging power, as the block *Demand* does.

- *Scopes*: to analyze all the variables. This block has been created for this work and consists in simple representations of all the variables.
- *Battery*: it simulates the battery dynamic behaviour.
- *Ultracapacitor*: it simulates the ultracapacitor dynamic behaviour.
- *PEM Electrolyzer*: it simulates the electrolyzer dynamic behaviour.
- *Fuel Cell*: it simulates the fuel cell dynamic behaviour.
- *Metal Hydride*: it simulates the hydrogen tank dynamic behaviour.
- *Extra hydrogen consumption*: it simulates an extra hydrogen demand for the hydrogen-based vehicle. This block has been created for this work. It is composed by simple *Step* blocks which allow for a constant hydrogen demand, where its parameters are the constant consumption in *kg/s*, and the initial time and duration of consumption in hours.

The blocks with specific equipment parameters are: battery, ultracapacitor, PEM Electrolyzer, Fuel Cell and Metal Hydride. The others SimuGrid blocks have also parameters but they depend on the scenario one wants to simulate. The principal parameters for the last ones must be given in MATLAB *timeseries* format as it is explained in the SimuGrid documentation [83]. The specific equipment parameters for these first blocks are gathered in Table 8-Table 12, which are obtained from the works of [2], [14], [15] and [79], and correspond to the explained equipment (mainly from the *Hylab*, as explained in section 2).

Parameter	Representation	Unit	Value
Open circuit voltage	$V_{bat,0}$	V	51.58
Maximum capacity	$C_{120,bat}$	Ah	367
Polarization constant	$K_{bat}$	V	0.006215
Amplitude of the exponential zone	$A_{bat}$	V	11.053
Inverse of the time constant in the exponential zone	$B_{bat}$	(Ah) <sup>-1</sup>	2.452
Internal resistance	$R_{bat}$	Ω	0.0838
Charge/Discharge maximum current	$I_{bat}^{max}$	A	52

Table 8. Parameters for battery SimuGrid block

Parameter	Representation	Unit	Value
Capacity	$C_{uc}$	F	63
Internal resistor	$R_{int}$	Ω	0.018
Number of capacitor in series	$N_{uc}^{serie}$	-	1
Number of capacitor in parallel	$N_{uc}^{parallel}$	-	1
Maximum voltage	$V_{uc}^{max}$	V	125
Maximum current	$I_{uc}^{max}$	A	1900

Table 9. Parameters for ultracapacitor SimuGrid block

Parameter	Representation	Unit	Value
Reversible potential at standard conditions	$E_{0,ez}$	V	1.23
Reversible potential coefficient	$K_{1n}$	V/K	$-0.9 \cdot 10^{-3}$
Hydrogen partial pressure	$p_{H_2}$	bar	6.9
Oxygen partial pressure	$p_{O_2}$	bar	1.3
Stack area	$A_{stack}$	cm <sup>2</sup>	212.5
Electrolyzer resistance	$R_{ohm}^{ez}$	$\Omega$	0.00017008
Anode current density	$i_{ao,ez}$	A/cm <sup>2</sup>	$1.0621 \cdot 10^{-6}$
Cathode current density	$i_{co,ez}$	A/cm <sup>2</sup>	$1 \cdot 10^{-3}$
Number of cells in the stack	$N_{ez}^{cell}$	-	6
Electrolyzer temperature	$T_{ez}$	K	298
Maximum input power	$P_{ez}^{max}$	W	1000

Table 10. Parameters for electrolyzer Simugrid block (referred to the cell)

Parameter	Representation	Unit	Value
Reversible potential at standard conditions	$E_{0,fc}$	V	1.046
Reversible potential coefficient	$K_{1t}$	V/K	0.00293
First activation coefficient	$K_{1,act}$	V	0.066098
Second activation coefficient	$K_{2,act}$	A/cm <sup>2</sup>	0.012705
Fuel cell resistance	$R_{ohm}^{fc}$	$\Omega$	0.299
First concentration coefficient	$K_{1,conc}$	V	0.028396
Second concentration coefficient	$K_{2,conc}$	cm <sup>2</sup> /A	8.0011
Stack temperature	$T_{fc}$	K	296
Nominal stack temperature	$T_{fc}^0$	K	296
Effective are of the membrane	$A_{fc}$	cm <sup>2</sup>	61
Number of cells	$N_{fc}^{cell}$	-	60
Maximum current	$I_{fc}^{max}$	A	40

Table 11. Parameters for fuel cell Simugrid block (referred to the cell)

Parameter	Representation	Unit	Value
Hydrogen capacity	$V_{H_2}^{max}$	L	7000
Maximum absorbed/desorbed hydrogen weight fraction	-	% w/w	1.2174

Table 12. Parameters for metal hydride Simugrid block

As alternatives to the use of Simugrid for microgrid simulation, there exist two well-known. One of those is again in MATLAB/Simulink, using *Simscape Electrical* [84] libraries. It allows simulating electrical systems and includes models of microgrid components such as renewable energy generation or energy storage systems. The other alternative is the commercial software *HOMER (Hybrid Optimization Model for Multiple Energy Resources)* [85]. It also includes microgrid equipment models and is suitable for optimizing and analyzing microgrids both in technical and economical ways, as well as a possible connection to MATLAB for testing controllers in the simulated microgrid.

### 3.3.2 Yalmip and CPLEX

The designed tertiary controller is composed of linear constraints and quadratic cost functions, and involves both continuous and binary variables. Hence, as it was described in subsection 3.2.1, a Mixed-Integer Quadratic Programming, MIQP, must be solved. An interesting tool to do that is MATLAB is to use the *toolbox Yalmip*, which was created by *Johan Löfberg* and is well-known due his publication in 2004 [86]. It is a helpful tool which allows easily defining optimization control-related problems and solving it using both internal and external (even commercial) solvers. Among others, this toolbox can solve LP, QP, MILP and MIQP, so it is clear that is suitable for MPC problems.

In the case of MIP problems, as it is stated in [86], Yalmip can solve it by an internal solver based in branch and bound techniques. Currently, this solver is called *BNB* [87]. However, when the problem increases its size and complexity, this solver can be inadequate. An interesting alternative which can be integrated with Yalmip is the solver *CPLEX*, created by the *IBM Company* to solve complicated optimization problems [88]. It is a commercial software, but there exists a free version available for academia.

To use Yalmip-CPLEX to solve the optimization problem, the first things are to download, install and configure MATLAB to use them. Starting with Yalmip, and following the installation tutorial from its webpage [89], the steps are:

- 1- Download and unzip the Yalmip file from <https://github.com/yalmip/yalmip/archive/master.zip>. This corresponds to the latest Yalmip version available in the time of downloading.
- 2- Copy the file in your MATLAB *toolbox* file. For example, assume that this path is: '*C:\Program Files\MATLAB\R2020b\toolbox*'.
- 3- In MATLAB, write the following [90]:

```
>> oldpath = path;
>> path(oldpath, 'C:\Program Files\MATLAB\R2020b\toolbox\YALMIP');
```

- 4- Add all the required directories to the MATLAB path:

```
>> addpath(genpath('C:\Program Files\MATLAB\R2020b\toolbox\YALMIP'));
```

This command has to be executed at the beginning of each time Yalmip is going to be used.

- 5- To test the installation has been done successfully, write the following in MATLAB:

```
>> yalmiptest
```

If no errors appear, the installation has correctly finished.

When running the *yalmiptest* command in MATLAB, one can see a table with the available installed solvers. CPLEX is not included, so it must be externally downloaded and MATLAB must be set up to use it within Yalmip toolbox. Following the guide of [91], the steps to be done are:

- 1- In the webpage <https://www.ibm.com/academic/topic/data-science>, access *Software* → *ILOG CPLEX Optimization Studio* → *Downloads*. Here, one must register using the academia mail.
- 2- Once in the download page, search the version using the instruction “*Access to older versions*” from

[91]. In this case, version 12.10 for Windows 64 bits (CC438ML) was downloaded with the “Quick Start Guide Multiplatform Multilingual (CC437ML)”.

- 3- If you do not have installed a software from IBM called “IBM Download Director”, they require you to install it. To do that, follow the instructions of [https://www-03.ibm.com/isc/esd/dswdown/dldirector/installation\\_en.html](https://www-03.ibm.com/isc/esd/dswdown/dldirector/installation_en.html).
- 4- During de IBM Download Director downloading, Java 8 must be also downloaded. It can be done in the webpage <https://java.com/es/download/>.
- 5- Once IBM Dowload Director and Java 8 have been installed, one must proceed with ILOG CPLEX Optimization Studio installation.
- 6- During the aforementioned installation, Microsoft Visual C++ 2015 Redistributable Update 3 is required to be installed. The executable for that can be obtained by simply clicking in <https://www.microsoft.com/es-es/download/confirmation.aspx?id=53587>.
- 7- Finish the ILOG CPLEX Optimization Studio installation.
- 8- Finally, following the instructions in [92], one must write in MATLAB at the beginning of each time CPLEX is going to be used with Yalmip:

```
>> addpath(genpath('C:\Program Files\MATLAB\R2020b\toolbox\YALMIP'));
% To be able to use YALMIP

>> addpath(genpath('C:\Program Files\IBM\ILOG\CPLEX Studio1210\cplex\matlab\x64_win64')); % To be able to use CPLEX

>> addpath(genpath('C:\Program Files\IBM\ILOG\CPLEX Studio1210\cplex\examples\src\matlab')); % To support navigational links to examples in the online help from within a MATLAB session
```

- 9- Finally, the command *yalmiptest* can be used again and the user can check in the table if CPLEX has correctly been installed.

Once both Yalmip and CPLEX are installed, the important part is to learn how to use Yalmip. There is an extensive official and public tutorial webpage where lot of resources and examples can be found [93]. As can be deduced from [86] and [93], to use Yalmip, the optimization problem must be defined and then used following these steps:

- 6- Define the optimization decision variables using *sdpvar*, or *binvar* for binary variables. They will be used as symbolic variables in the problem definition. An interesting tutorial on how to define them can be found in [94].
- 7- Define the cost function and constraints following Yalmip syntax.
- 8- Decide and establish what are going to be the inputs and outputs for the optimization problem.
- 9- Use the command *optimizer* to define only one time the problem as an object. This command receives as input, in this order: *constraints*, *cost function*, *options*, *inputs*, *outputs*. In the *options*, the solver can be changed; for example, to use CPLEX, one must sent the argument *sdpsettings('solver','cplex')* in the *options* field.
- 10- Call the optimization problem object giving the required inputs to solve it.

As an example, when using the tertiary controller, the optimization problem is created at the beginning only one time (steps 1-4 from above) to reduce compilation overhead. Then, every sampling time (i.e. every hour), the controller inputs (prediction, current state and previous control actions) are sampled and sent to the optimization problem. Once the solver has finished, the control actions are obtained in vector  $u$ ,  $\delta$  and  $z$ . In [95] there is an interesting tutorial on how to use Yalmip to solve MPC problems.



# 4 RESULTS

The controllers are tested in simulation in different scenarios. First, simulations are carried for the tertiary controller and then, for the whole system using both controllers. These simulations include both sunny and cloudy days. All the simulations have the same duration: 86400 seconds or one day. Moreover, the sunny results are also shown for islanded mode in the tertiary controller; i.e. with the microgrid not connected to the main grid. For every simulation, demand and generation power (or net power prediction in the case of tertiary controller) profiles are going to be shown, as well as price prediction for the tertiary controller and EVs charging power and extra hydrogen demand for the secondary controller. The results will be represented in the form of graphs containing the power exchange and the energy storage levels. When binary variables are involved, they will be shown too in order to check the right operation.

## 4.1 Tertiary controller

For the tertiary controller, four simulations have been done. Three of them are in grid-connected mode for sunny day, cloudy day and sunny day with nearly-zero demand. The last of these three is due to the fact that the microgrid can be located in an office or university place where there is no activity on weekends, but solar power is generated anyway. The other simulation is done for the islanded mode for a sunny day. Cloudy days (almost no generation) or days with almost no demand are not considered here because the storage level has some limits and for being in islanded mode there must be both generation and demand. A solution in this case can be the changing to grid-connected mode when the forecasts predict low generation or low demand.

For this controller, the net power (generation minus demand) prediction is directly represented. A common data for all the simulations in grid-connected case is the energy price, which is taken from [96] and in this case from 15<sup>th</sup> November 2021. This day-ahead market energy price can be seen in Figure 8.

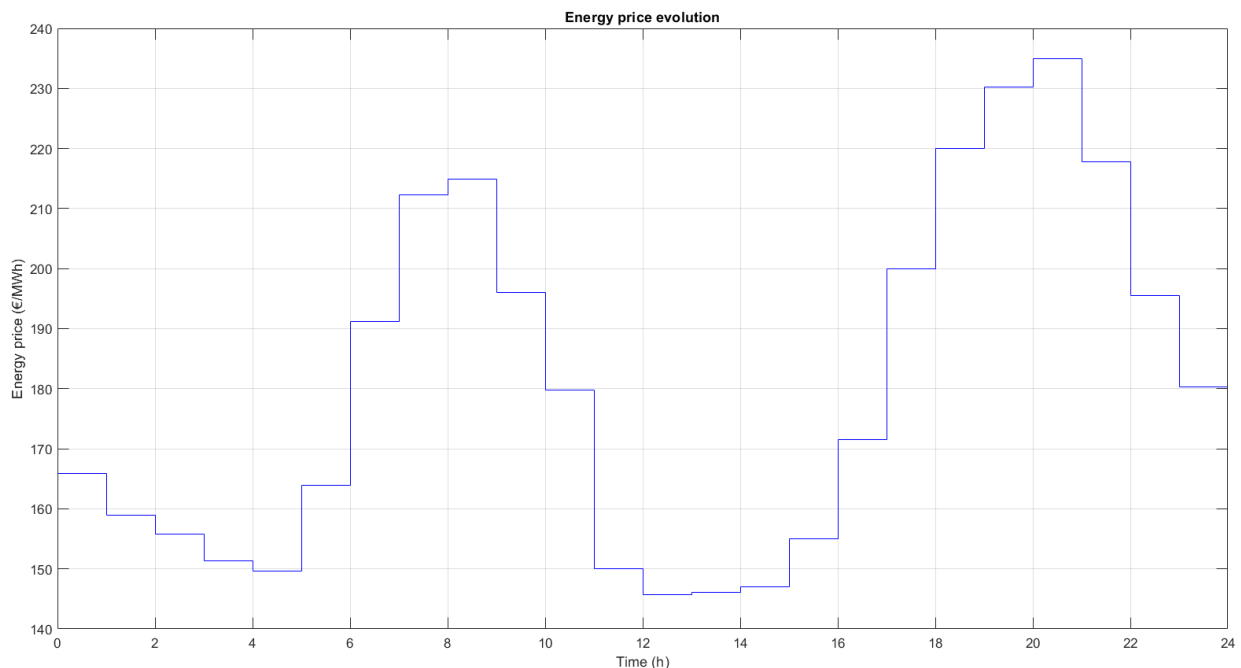


Figure 8. Day-ahead market energy price

Another thing that must be commented is the physical constraints values in order to check in this section that the optimization problem is working properly. They are the same for the four simulations. There are mainly three types of these constraints: for the output, for the control actions and for the incremental control actions. The outputs are constrained as follows:

- Battery:  $SOC_{bat}^{max} = 90\%$ ,  $SOC_{bat}^{min} = 20\%$
- Hydrogen storage:  $LOH^{max} = 90\%$ ,  $LOH^{min} = 10\%$

On the other hand, the control actions, i.e., the power references, are subjected to the following constraints:

- Battery power:  $P_{bat}^{max} = 2.5 \text{ kW}$ ,  $P_{bat}^{min} = -2.5 \text{ kW}$ ,  $\Delta P_{bat}^{max} = 1 \text{ kW/s}$ ,  $\Delta P_{bat}^{min} = -1 \text{ kW/s}$
- Fuel cell power:  $P_{fc}^{max} = 1.2 \text{ kW}$ ,  $P_{fc}^{min} = 0.1 \text{ kW}$ ,  $\Delta P_{fc}^{max} = 0.02 \text{ kW/s}$ ,  $\Delta P_{fc}^{min} = -0.02 \text{ kW/s}$
- Electrolyzer power:  $P_{ez}^{max} = 0.9 \text{ kW}$ ,  $P_{ez}^{min} = 0.1 \text{ kW}$ ,  $\Delta P_{ez}^{max} = 0.02 \text{ kW/s}$ ,  $\Delta P_{ez}^{min} = -0.02 \text{ kW/s}$
- Grid power:  $P_{grid}^{max} = 2.5 \text{ kW}$ ,  $P_{grid}^{min} = -2.5 \text{ kW}$ ,  $\Delta P_{grid}^{max} = 1 \text{ kW/s}$ ,  $\Delta P_{grid}^{min} = -1 \text{ kW/s}$

It is remarkable that the incremental control actions constraints must be multiplied by the sample time in order to be properly applied.

Once all is prepared, firstly, a simulation in the grid-connected and sunny case is analysed. In Figure 9, the power evolution and the storage level can be seen. In the first part of the day, when there is no generation, the demand is covered by purchasing energy to the grid, since the energy price is not too high. Then, since the hour 6, the generation becomes greater than demand and the excess of energy is sold to the grid because the energy price has increased. As the controller considers the predictions for the following 24 hours, it anticipates the fact that energy price will be high between 18 and 21 hours where demand is greater than generation, so at hour 12, it is decided to store some energy excess in the battery for later use. Finally, in the hours of high energy price, both the fuel cell and the battery are used to cope with the demand and to sell some energy to the grid. As the two energy storage systems are near its lower limits in the hour 21, the grid is again used to fulfill the demand regarding as the energy price is decreasing. As can be observed, the electrolyzer and fuel cell are not easily started due to degradation reasons and, when started (in this case the fuel cell), it works at a constant operating point. It is remarkable that all the physical constraints are accomplished and can be seen both in the power and in the storage level graphs.

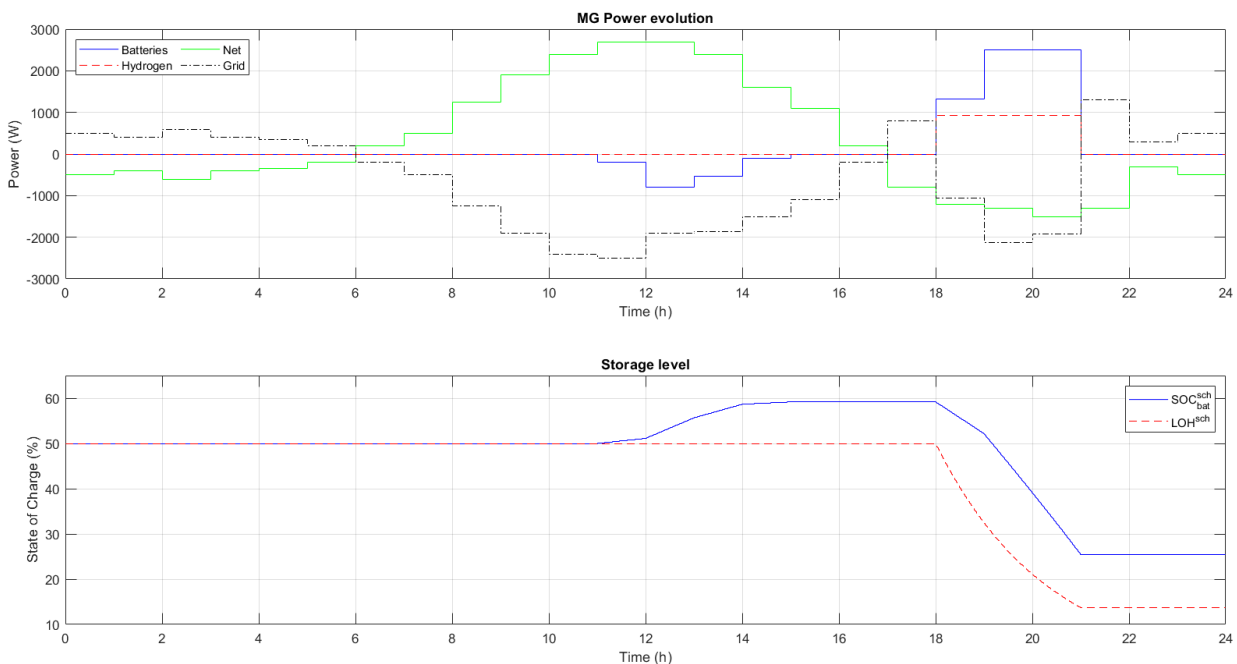


Figure 9. Power evolution and storage level in the sunny and grid-connected case

Only for this first simulation, binary and auxiliary variables are going to be represented and explained to show that they work as desired. In Figure 10, the hydrogen case can be observed. On the left side, first appears the hydrogen power, then the binary variables for the energized state (only active in the three time instants when the fuel cell works), and finally, the auxiliary variable which result from the multiplication of the two previous ones. On the right side, the first graph indicates the time instant when the fuel cell has been activated (hour 18), the third graph the time instant when the fuel cell is active and was active the previous time instant, and the second graph shows the power variation in the time instant of the previous graph.

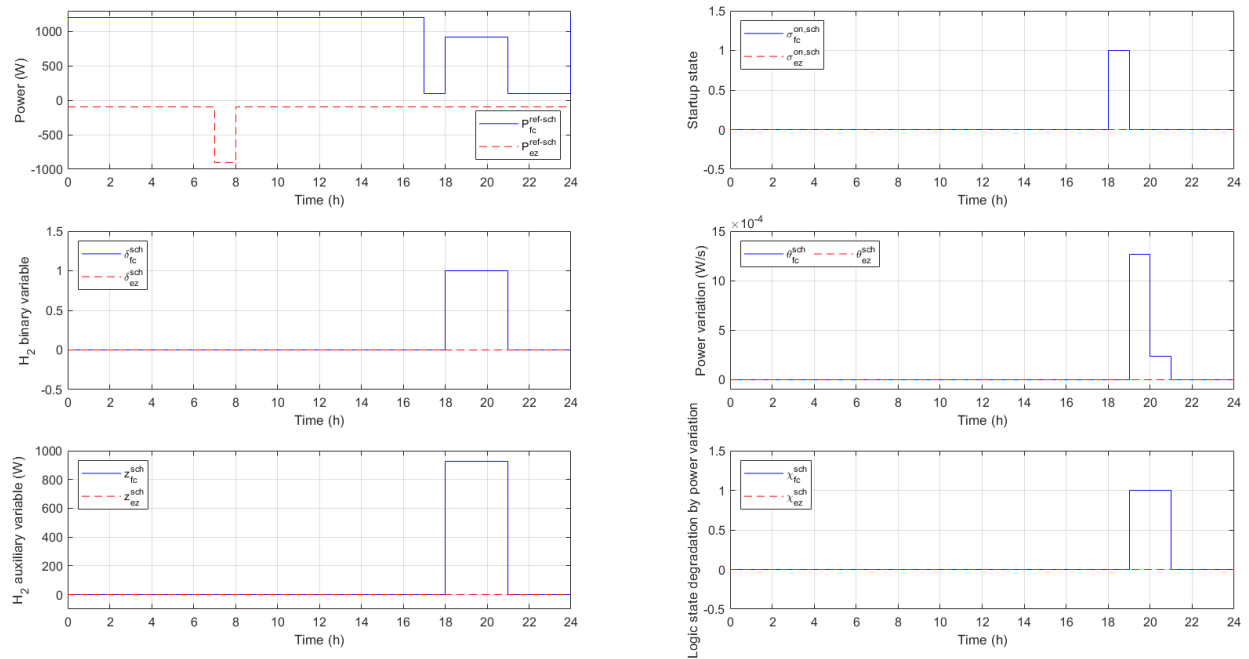


Figure 10. Hydrogen control, binary and auxiliary variables in the sunny and grid-connected case

As in the case of the left side of Figure 10, Figure 11 and Figure 12 represent the control variable, the binary variable indicating the battery charge/discharge mode or the sale to/purchase from the main grid, respectively, and the corresponding auxiliary variables. It can be easily checked that the relations are fulfilled correctly.

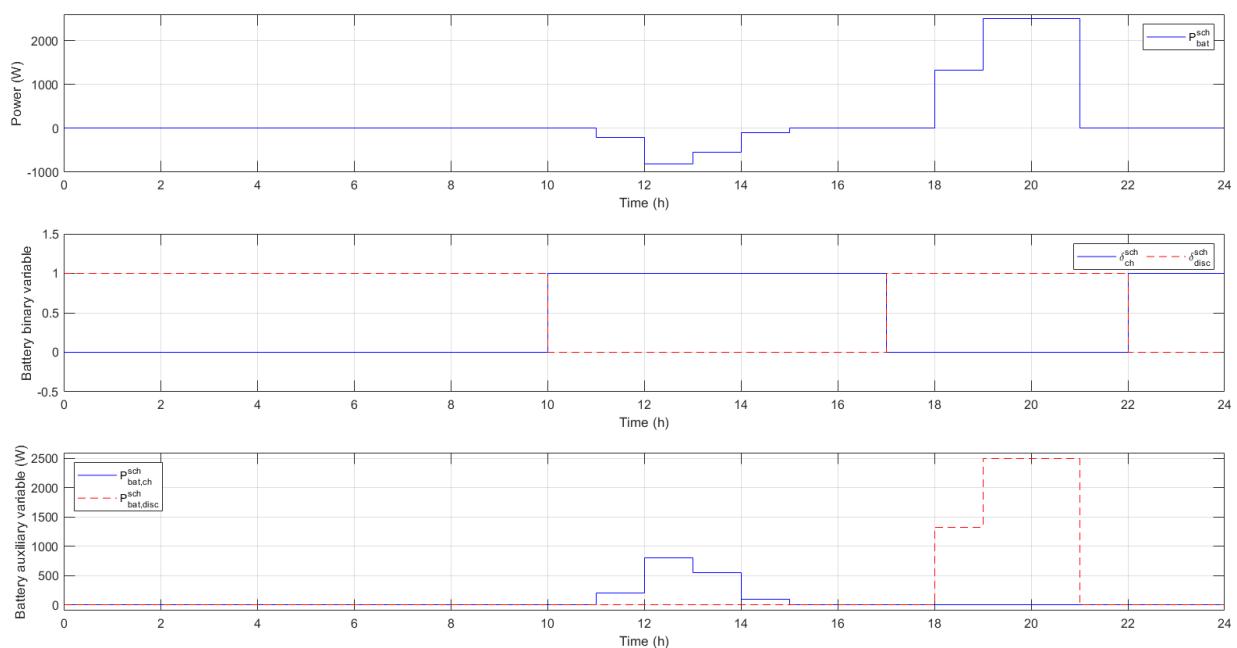


Figure 11. Battery control, binary and auxiliary variables in the sunny and grid-connected case

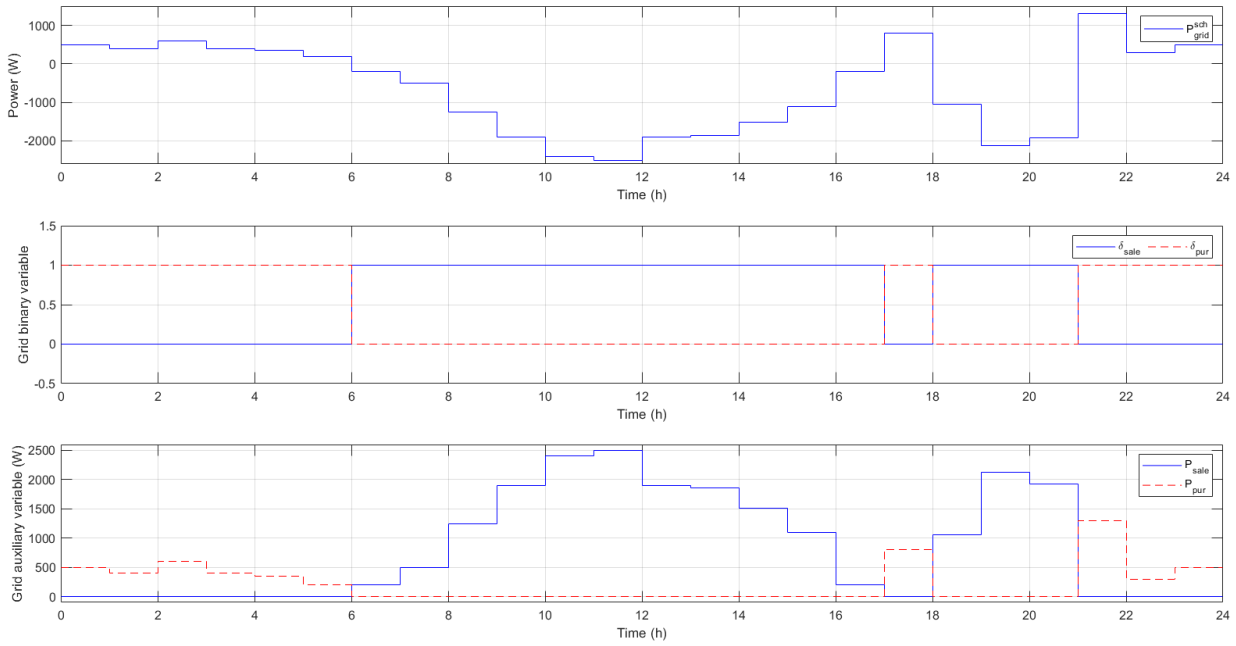


Figure 12. Grid control, binary and auxiliary variables in the sunny and grid-connected case

The second simulation is done again in grid-connected mode but for a cloudy day. Results showing the power scheduled and the storage level can be seen in Figure 13. During all the day, demand is greater than generation, so energy must be supplied from the grid or from the storage systems. Almost all the day, the grid is used to purchase power, except for the hours 18-21, when the energy price is really high. In this time, both fuel cell and battery are used to sell energy and then to obtain an economical benefit. For this reason and due to the price and net power forecast are available for the following 24 hours, at hour 12, the EMS decides to purchase more energy from the grid, in order to have enough energy for selling at hours 18-21. As in the previous simulation, the fuel cell operates without variations and all the described constraints are fulfilled.

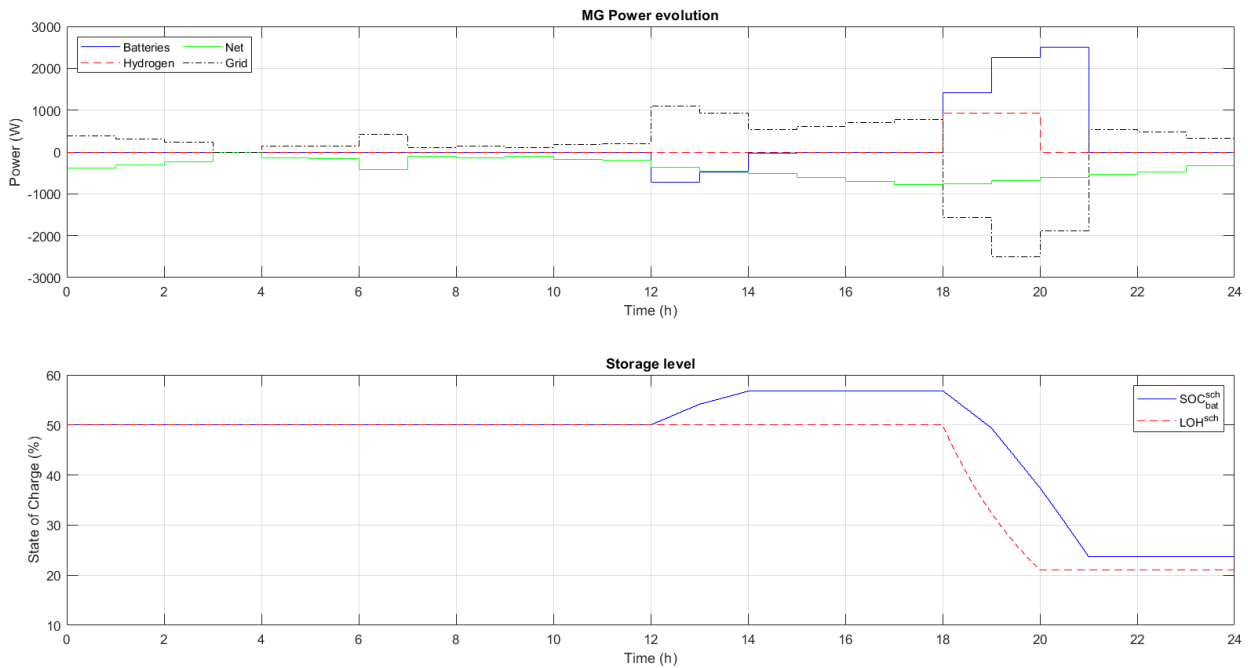


Figure 13. Power evolution and storage level in the cloudy and grid-connected case

Hydrogen control, binary and auxiliary variables are depicted in Figure 14 for this simulation. They are self-explained graphs looking the description made for these variables in the previous simulation. In the same way, these variables are represented for the battery in Figure 15 and for the grid in Figure 16.

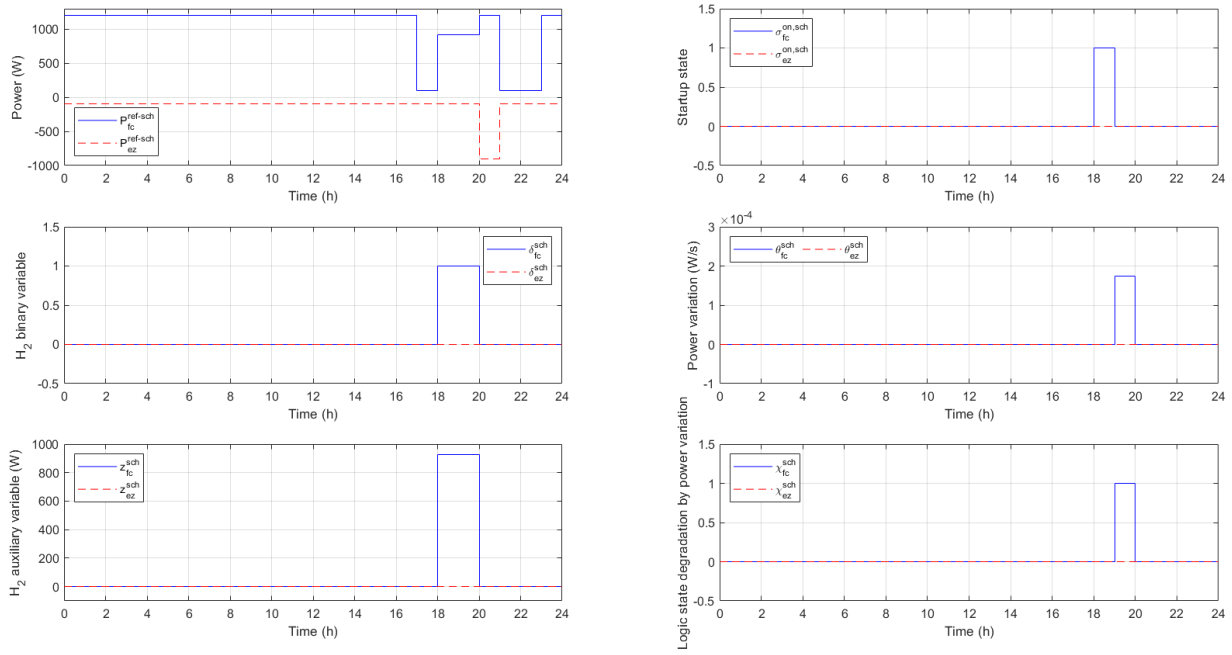


Figure 14. Hydrogen control, binary and auxiliary variables in the cloudy and grid-connected case

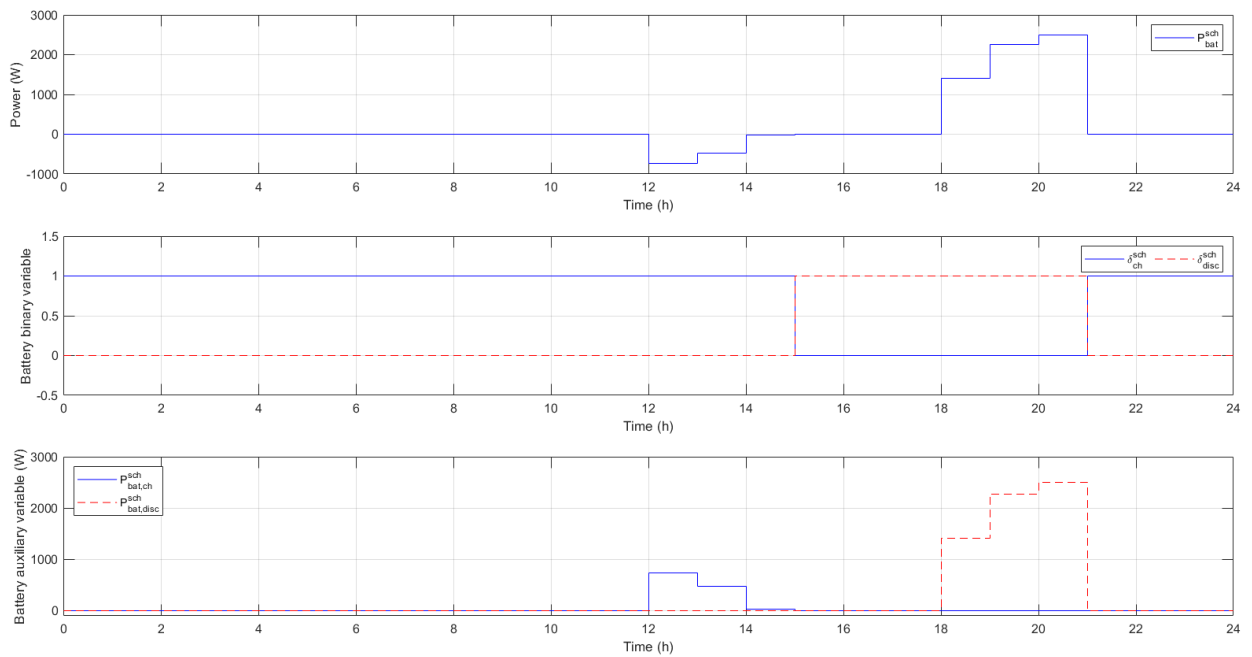


Figure 15. Battery control, binary and auxiliary variables in the cloudy and grid-connected case

From the two described simulation, one can observe that the electrolyzer has not been activated. This is due to the fact that starting the electrolyzer is more expensive than using the battery or the grid and has more degradation aspects. For that reason, a new scenario is simulated where the demand is near zero during all the day. This can correspond with a weekend day in an office or university campus, when there is no activity but generation can be produced. A sunny day is assumed, so the net power is positive in the majority of the day. The power and storage levels can be observed in Figure 17. In that case, the surplus of energy is sold to the grid in the hours when the energy price is higher (mainly in hours 5-12 and 17-22). As a lot of energy is produced and there is no demand, both the battery and the electrolyzer are storing energy at around hour 10. Previously, the battery discharged some energy which was sold to the grid, in order to be ready for the

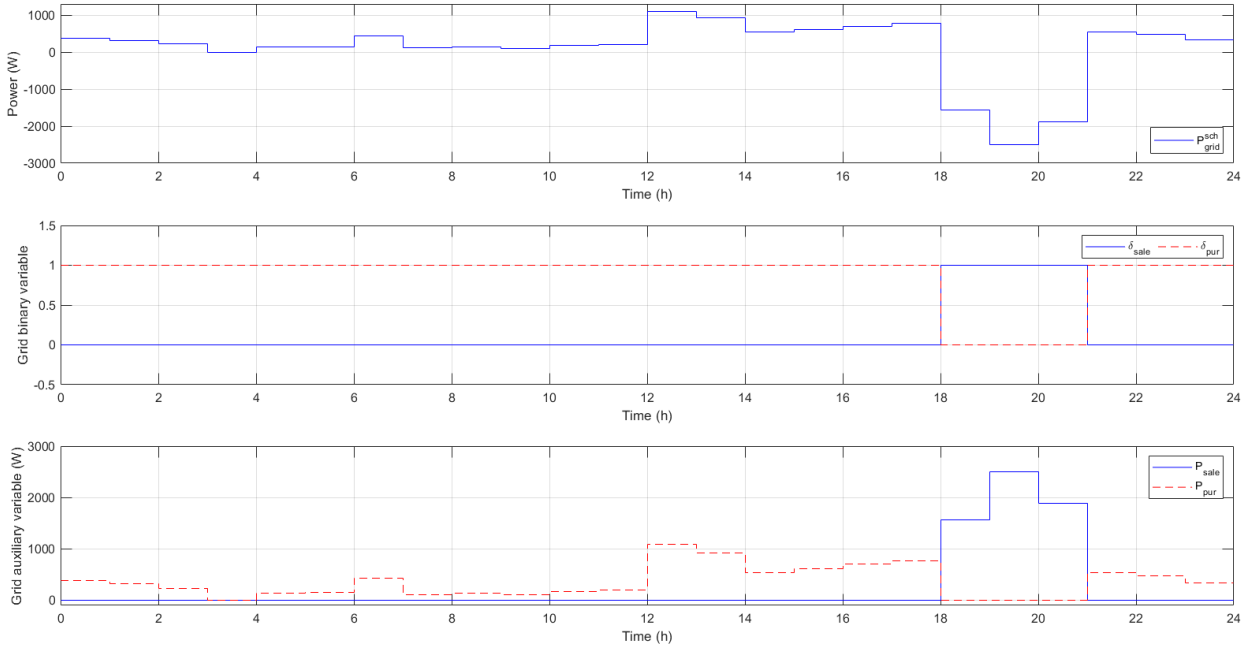


Figure 16. Grid control, binary and auxiliary variables in the cloudy and grid-connected case

charging phase. Finally, between hours 17 and 22, there is neither generation nor consumption, but the EMS decides to sell energy to the grid using the battery and the fuel cell due to the high energy price. Again, all the constraints are accomplished and the hydrogen equipment work at constant operating points.

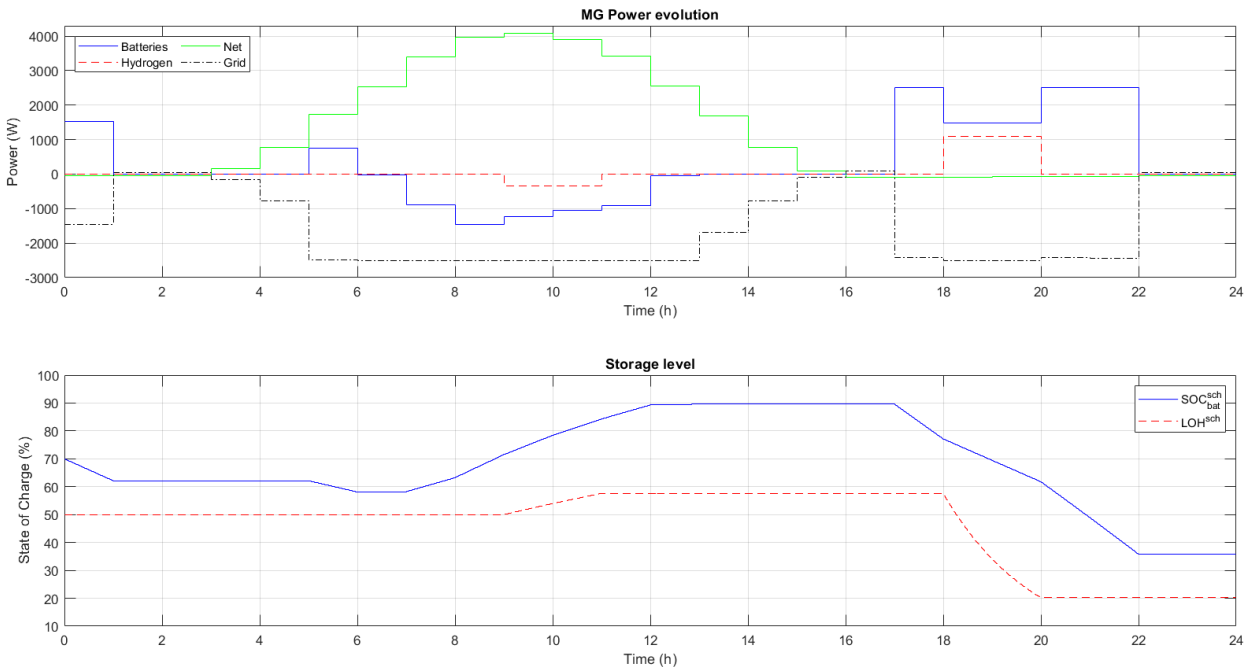


Figure 17. Power evolution and storage level in the sunny and nearly-zero demand day and in grid-connected case

Again, the hydrogen, battery and grid control, binary and auxiliary variables are shown in Figure 18, Figure 19 and Figure 20. In the case of hydrogen, in particular for the electrolyzer, variables can now be checked, as they work as it was expected and the electrolyzer had not been activated in the previous simulations.

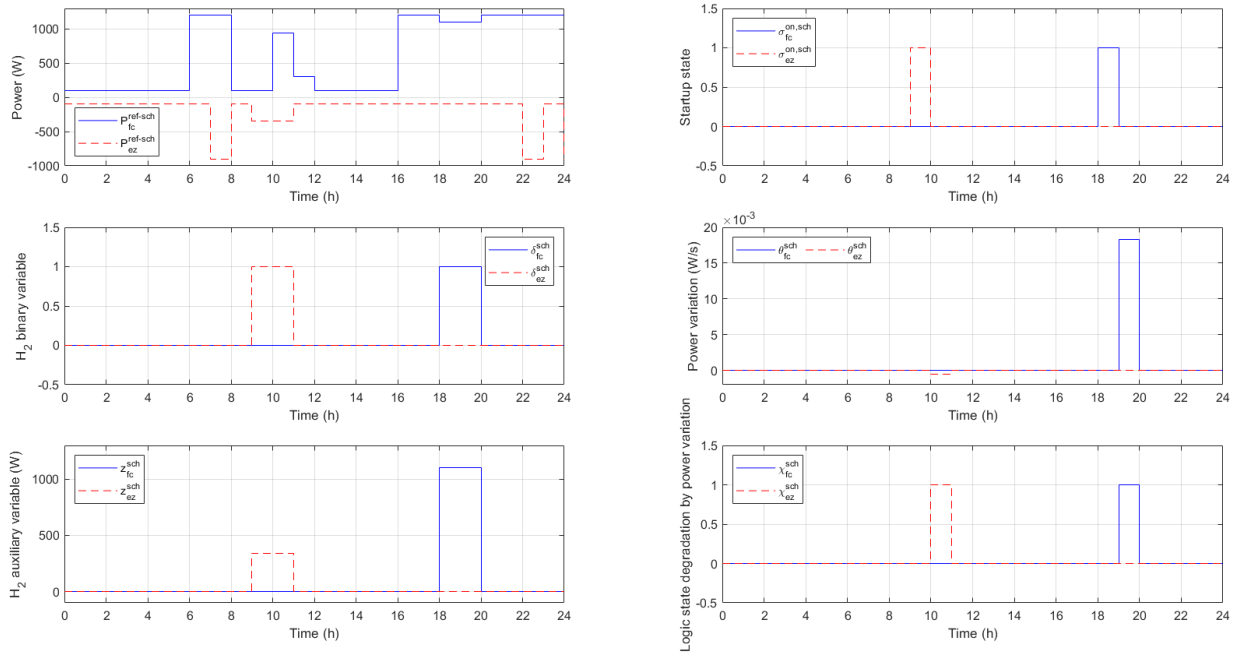


Figure 18. Hydrogen control, binary and auxiliary variables in the sunny and nearly-zero demand day and in grid-connected case

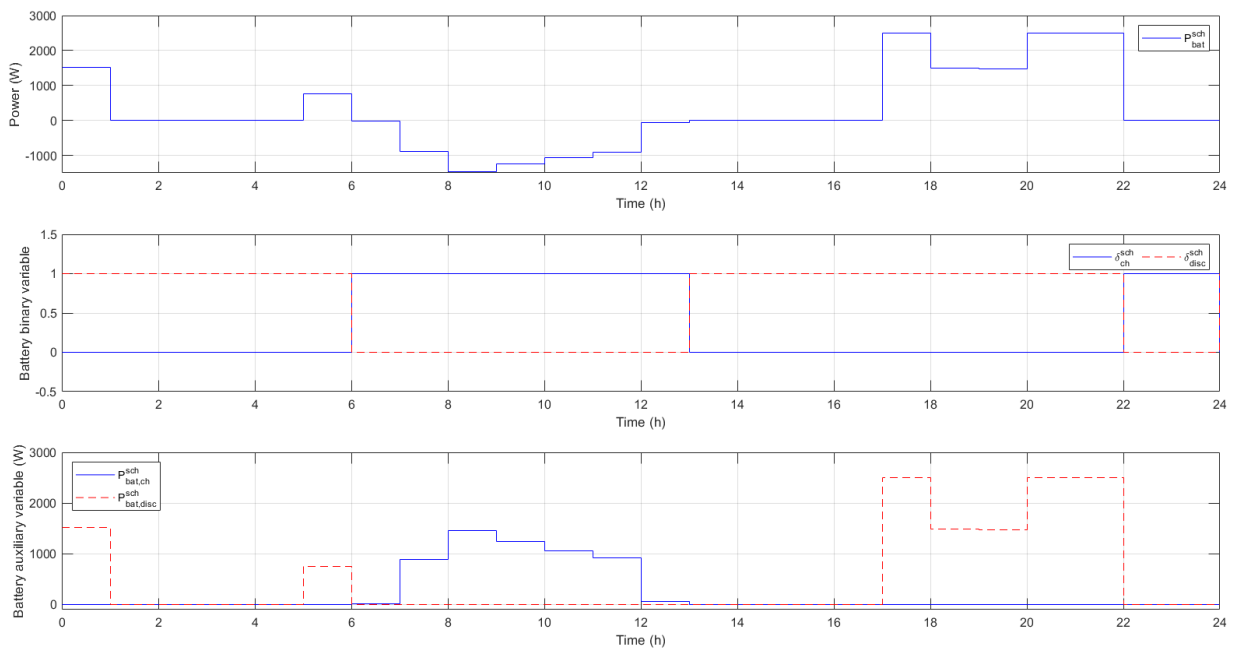


Figure 19. Battery control, binary and auxiliary variables in the sunny and nearly-zero demand day and in grid-connected case

Finally, one simulation for the islanded case is carried out. In islanded mode, the microgrid is expected to be autonomous. But in order to reach this autonomy, both generation and demand must occur because the energy storage devices are not endless. In the case of grid-connected, although it is not recommendable, the grid can give more flexibility. So, when the forecasts predict days with scarcity of generation or demand, the grid could change to grid-connected mode, but this is not considered in this work. Another option is to oversize the energy storage devices considering these special days. In both solutions, the microgrid analysis enters in week simulations and planification and this is out of the scope of this work.

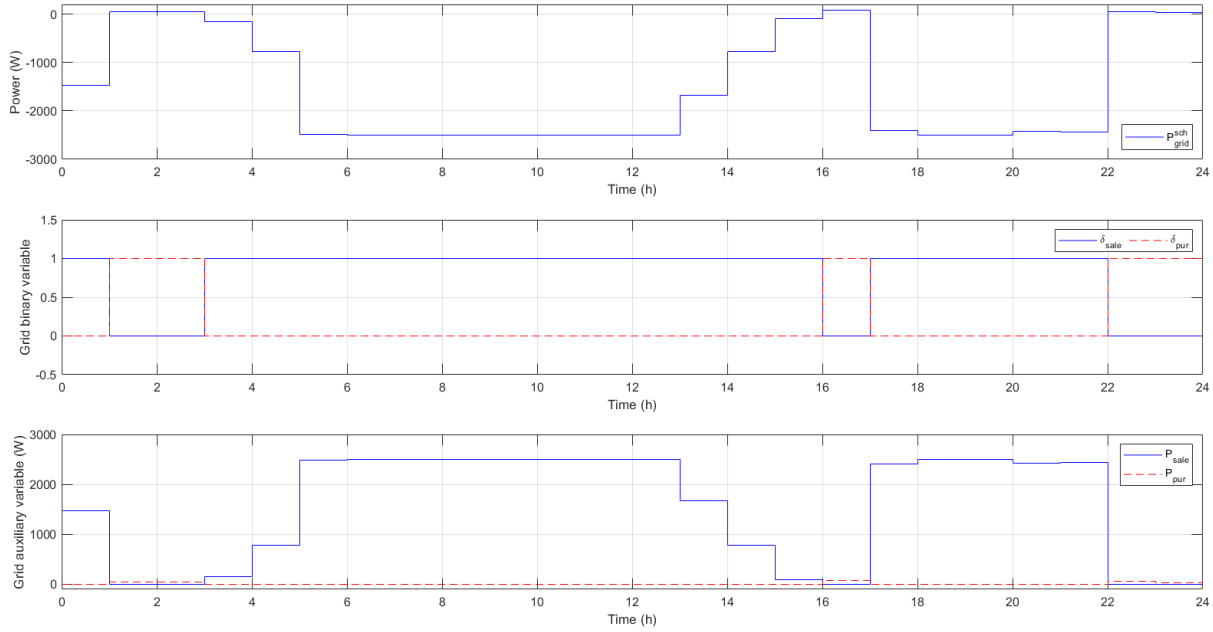


Figure 20. Grid control, binary and auxiliary variables in the sunny and nearly-zero demand day and in grid-connected case

In order to do the simulations with the same net power predictions as in the sunny and grid-connected case, the output constraints must be modified in order to enlarge them. This allows storing more energy in the storage devices as well as obtaining more energy from them. The new output constraints for this simulation are:

- Battery:  $SOC_{bat}^{max} = 95\%$ ,  $SOC_{bat}^{min} = 10\%$
- Hydrogen storage:  $LOH^{max} = 100\%$ ,  $LOH^{min} = 0\%$

In Figure 21, power and storage level evolution are represented. Both at the beginning and at the end of the day there is no generation and the demand is covered using the fuel cell and the battery. In the central part of the day, the generation is enough to cover the demand and energy can be even stored in the form of hydrogen and in the battery. In this case, where the hydrogen is more frequently used than in the grid-connected case,

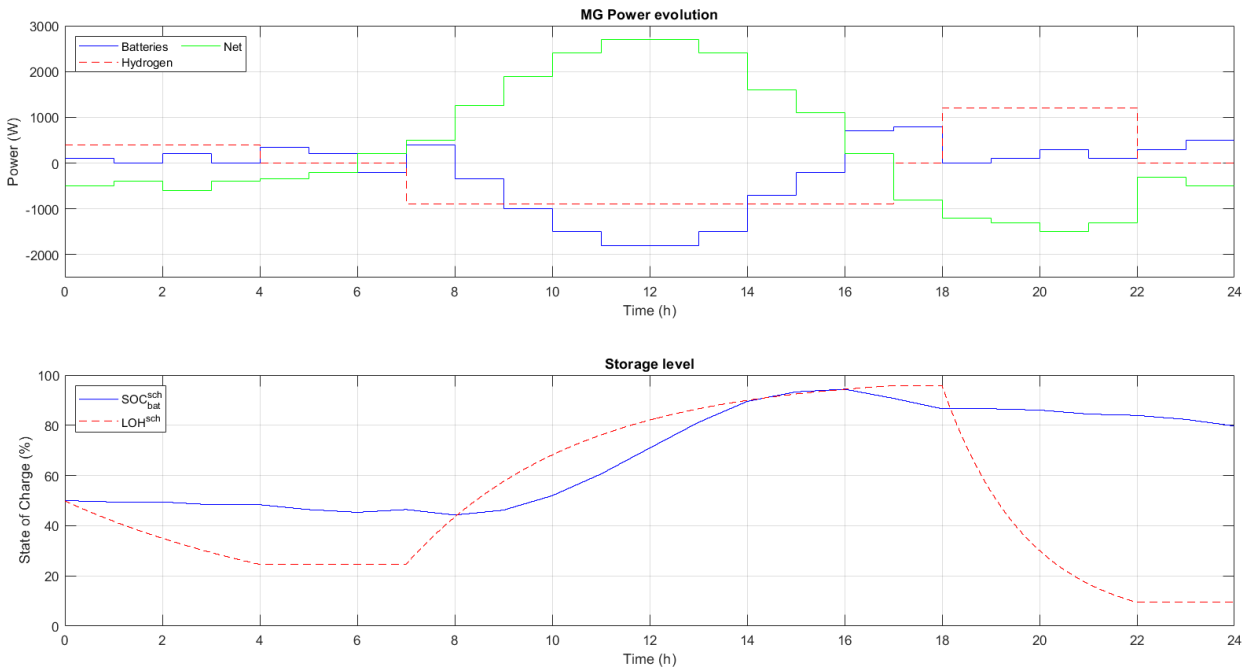


Figure 21. Power evolution and storage level in the sunny and islanded case



one can see that the electrolyzer and fuel cell startups are minimized. Moreover, both devices work at constant operating points. These two last facts are possible due to variations are absorbed by the battery, which suffers less than hydrogen devices. Finally, as in other simulations, all the constraints are fulfilled.

Finally, hydrogen and battery control, binary and auxiliary variables are depicted in Figure 22 and Figure 23, respectively. In this simulation hydrogen activity is greater than in previous cases, so these variables functioning can be better observed.

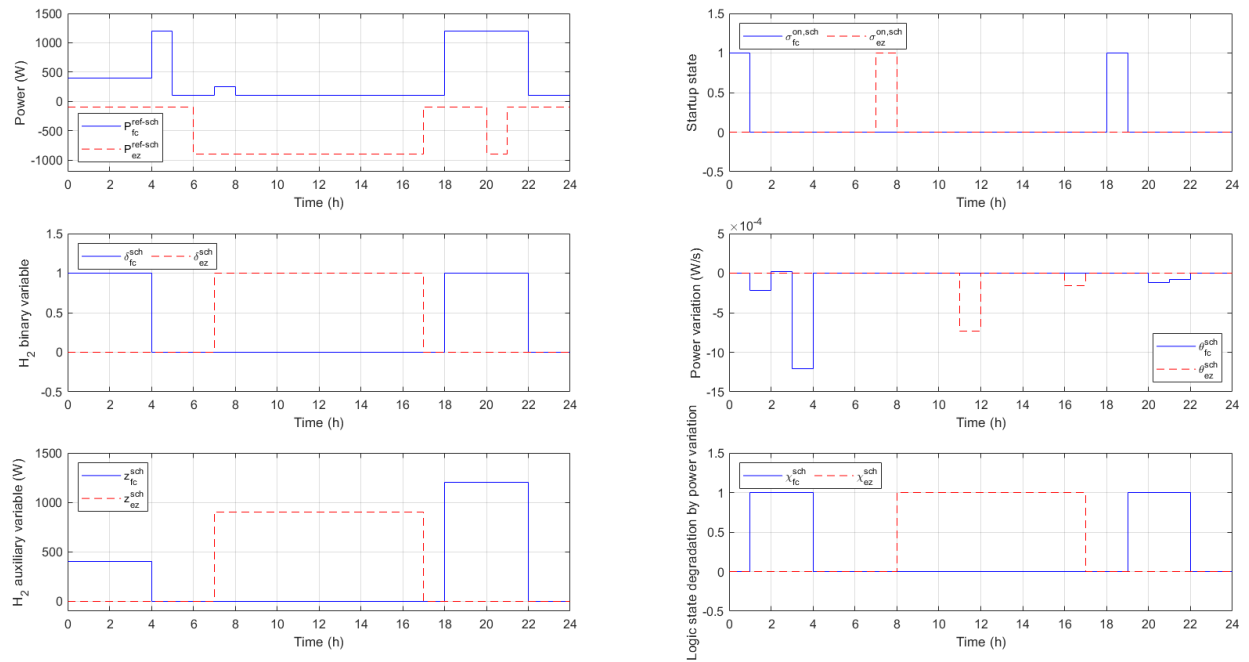


Figure 22. Hydrogen control, binary and auxiliary variables in the sunny and islanded case

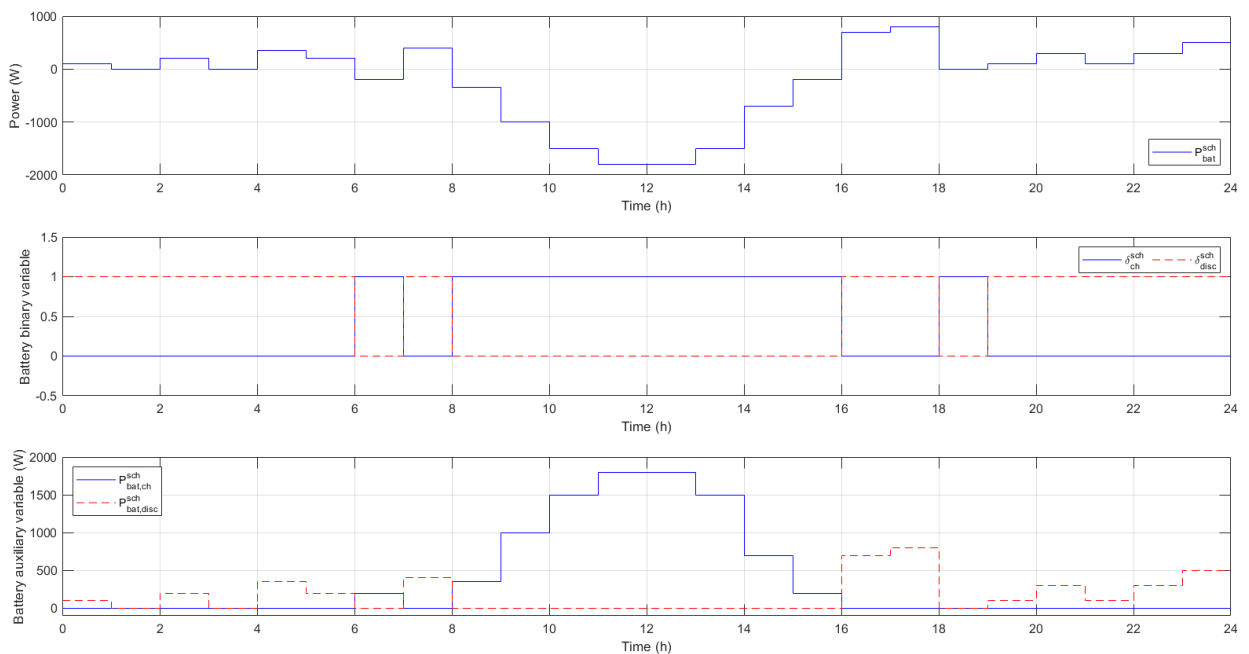


Figure 23. Battery control, binary and auxiliary variables in the sunny and islanded case

## 4.2 Secondary controller

This controller is tested in simulation in the complete system; i.e., together with the tertiary controller. The simulations are almost the same as in the tertiary controller: grid-connected microgrid in sunny and cloudy days. The sunny day with near-zero demand and the sunny day in islanded mode have not been tested here because it was done for the tertiary controller with the unique goal of starting the electrolyzer. For this controller, the net power (generation minus demand) is again directly represented. In the case of real measurements, it can be observed that the net power curve differs from the predicted but has almost the same pattern and shape. The demand, consumption and price predictions are the same data as in the tertiary controller simulations.

The main inclusions in these simulations are the EV charging power and the extra hydrogen consumption for the hydrogen-based vehicles. The same curves are going to be used for all the simulations. For the EVs charging power, it has been assumed that during the day 5 vehicles will be charged. The EV vehicle data are gathered in Table 13. With the data of this table, the EV charging duration is calculated with the expression in equation (4-1), and the EV charging power profile remains as represented in Figure 24.

Vehicle number	Arrival time [0-24 h]	Battery capacity [kWh]	Battery maximum charging power [kW]
1	7	7.68	1.287
2	8	6.5	3.68
3	10	6.5	3.68
4	15	7.68	1.287
5	16	6.5	3.68

Table 13. Data for the EVs charging

$$EV \text{ charging duration } [h] = \frac{Battery \text{ capacity } [kWh]}{Battery \text{ maximum charging power } [kW]} \quad (4-1)$$

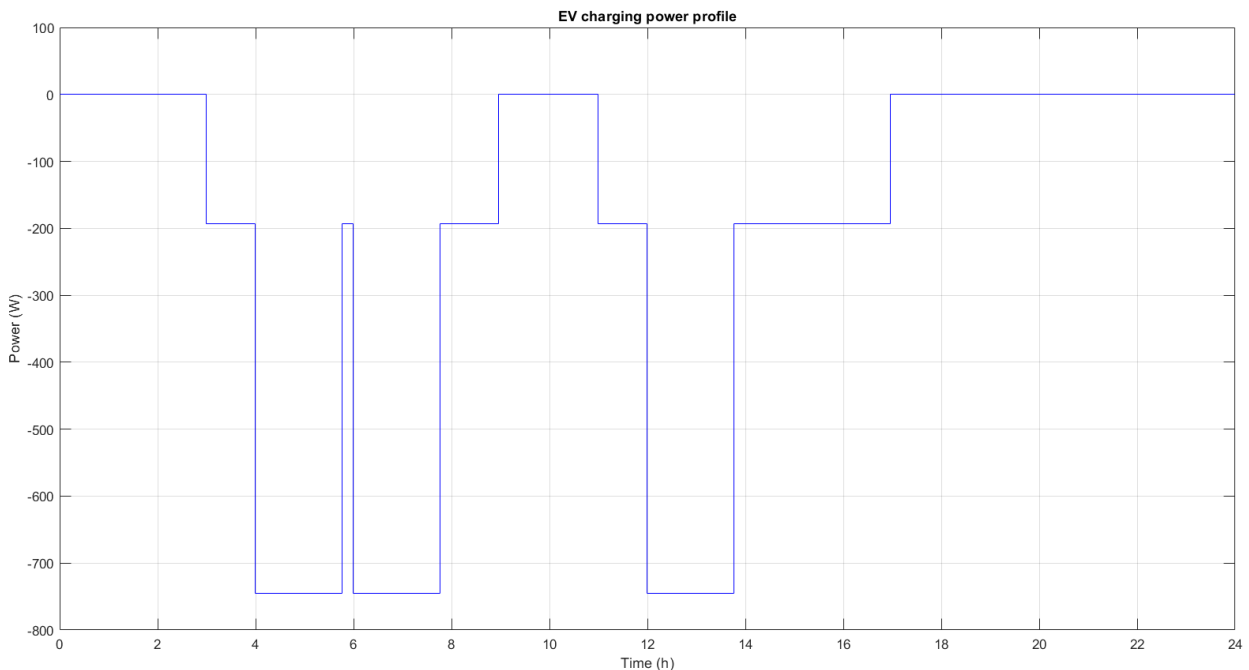


Figure 24. EVs charging power demand profile

The extra hydrogen consumption demand profile is calculated assuming that one of the available metal hydride bottles for the hydrogen-based vehicle in the laboratory is charged one time a day. Following the reference [97], this bottle (called *Ovonic 85G555B*) needs to be charged during 8 hours with hydrogen at 15 bar and its maximum admissible load is 68 g. So, the hydrogen flow (assumed constant during the refilling process) is calculated as follows:

$$H_2 \text{ refilling flow [kg/s]} = \frac{68 \cdot 10^{-3} \text{ [kg]}}{8 \cdot 3600 \text{ [s]}} = 2.36111 \cdot 10^{-6} \text{ [kg/s]} \quad (4-2)$$

Assuming that the hydrogen bottle start its refilling at hour 10, the extra hydrogen consumption profile will be the one in Figure 25.

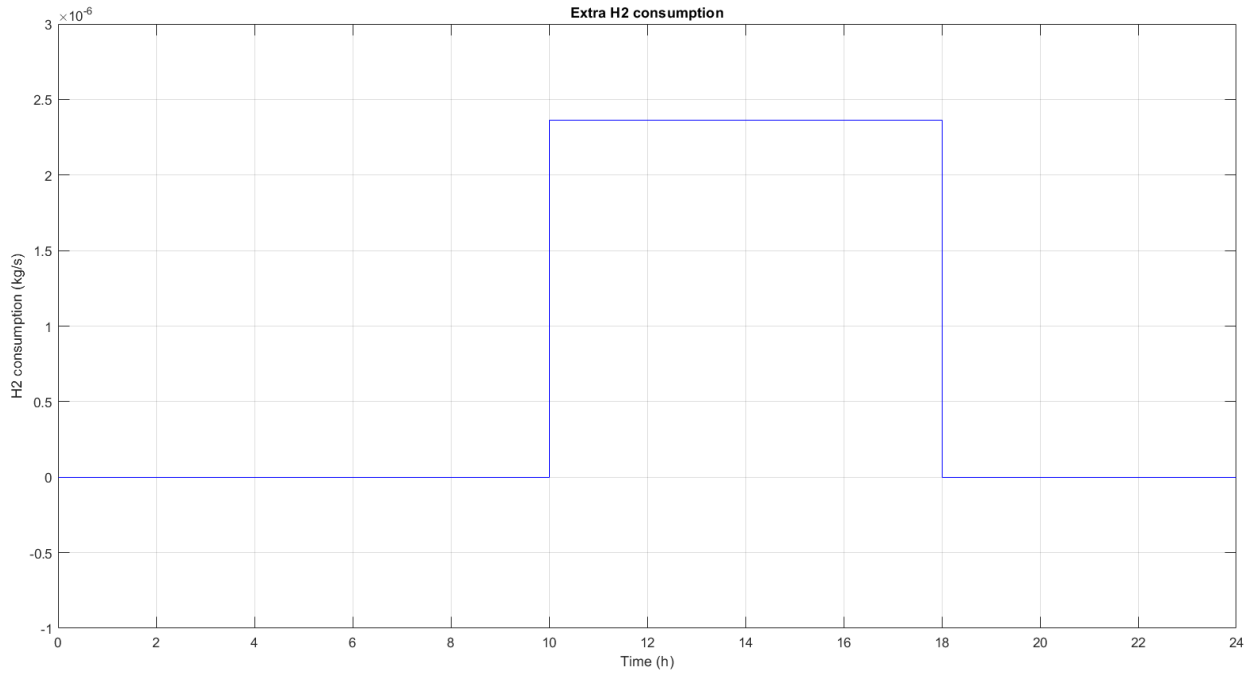


Figure 25. Extra hydrogen consumption profile

With respect to the output, control actions and incremental control actions constraints, the following applies:

- Battery storage level:  $SOC_{bat}^{max} = 90\%$ ,  $SOC_{bat}^{min} = 20\%$
- Hydrogen storage:  $LOH^{max} = 90\%$ ,  $LOH^{min} = 10\%$
- Ultracapacitor storage level:  $SOC_{uc}^{max} = 100\%$ ,  $SOC_{uc}^{min} = 10\%$
- Battery power:  $P_{bat}^{max} = 2.5 \text{ kW}$ ,  $P_{bat}^{min} = -2.5 \text{ kW}$ ,  $\Delta P_{bat}^{max} = 1 \text{ kW/s}$ ,  $\Delta P_{bat}^{min} = -1 \text{ kW/s}$
- Hydrogen power:  $P_{H_2}^{max} = 1.2 \text{ kW}$ ,  $P_{H_2}^{min} = -0.9 \text{ kW}$ ,  $\Delta P_{H_2}^{max} = 0.02 \text{ kW/s}$ ,  $\Delta P_{H_2}^{min} = -0.02 \text{ kW/s}$
- Grid power:  $P_{grid}^{max} = 2.5 \text{ kW}$ ,  $P_{grid}^{min} = -2.5 \text{ kW}$ ,  $\Delta P_{grid}^{max} = 1 \text{ kW/s}$ ,  $\Delta P_{grid}^{min} = -1 \text{ kW/s}$
- Ultracapacitor power:  $P_{grid}^{max} = 3 \text{ kW}$ ,  $P_{grid}^{min} = -3 \text{ kW}$ ,  $\Delta P_{grid}^{max} = 1 \text{ kW/s}$ ,  $\Delta P_{grid}^{min} = -1 \text{ kW/s}$

It is remarkable that the incremental control actions constraints must be multiplied by the sample time in order to be properly applied, as in the case of the tertiary controller.

The cost functions weighting terms for the grid-connected simulation have been chosen following different

considerations. One is clear and it is that hydrogen power variation must have a high weighting term in order to avoid high fluctuations in its operation. The other aspect which is considered of high importance is the grid power schedule tracking, due to the economic penalties imposed by the main grid operator if the schedule exchanges with the grid are not fulfilled. On the contrary, really low weighting terms are given to the state reference tracking for the three storage devices (battery, hydrogen and ultracapacitor), because it is not essential, but only desirable. The other ultracapacitor weighting terms (for power variations, power effort and power reference tracking) are chosen higher than their corresponding for battery, hydrogen and grid, because ultracapacitor is expected to absorb fluctuations, among others. The rest of the weighting terms have an intermediate value and are chosen by tuning the controller in the design phase. Table 14 gathers all the weighting terms included in the cost function and used in the grid-connected simulations.

Weighting term	Equipment	Value
State schedule tracking	Battery	$10^{-8}$
	Hydrogen	$10^{-8}$
	Ultracapacitor	$10^{-4}$
Power schedule tracking	Hydrogen	$10^{-3}$
	Grid	$10^{-2}$
	Ultracapacitor	$10^{-5}$
Control effort (power)	Battery	$10^{-4}$
	Hydrogen	$5 \cdot 10^{-3}$
	Grid	$8 \cdot 10^{-3}$
Incremental control effort (power variations)	Ultracapacitor	$10^{-10}$
	Battery	$10^{-3}$
	Hydrogen	40
	Grid	$10^{-3}$
	Ultracapacitor	$10^{-4}$
	Battery	$10^{-4}$

Table 14. Secondary controller cost function weighting terms for the grid-connected case

The first simulation is the case of grid-connected and sunny day. The power evolution can be seen in Figure 26, being the schedule power given by the tertiary controller the graph on the top, and the reference power given by the secondary controller the graph on the bottom. More or less the power schedule is followed, or at least, the shape of the graph. However, due to the high uncertainty for the zero-emission vehicle recharging, some differences appear. For instance, the grid power follows the same kind of curve, but the values (both sale and purchase power) are usually lower. The battery absorbs the majority of these differences, except for instantaneous moments of change, when the ultracapacitor softens the high variations of power. The ultracapacitor is also always around its power and state references. This state and the battery and hydrogen storage level for both the scheduled and the measured is represented in Figure 27. One can see that the state schedule is approximately fulfilled and that the output constraints, as well as the power constraints are accomplished. Finally, it is remarkable that hydrogen power evolution does not suffer from high power variations.

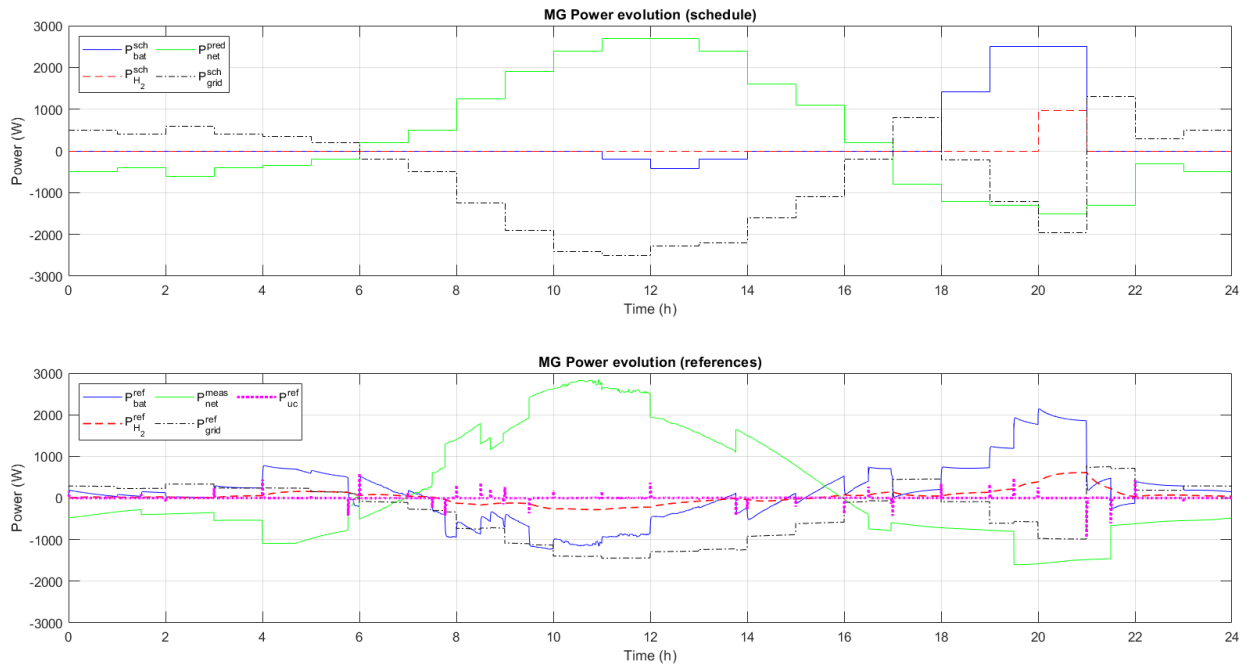


Figure 26. Power evolution in the sunny and grid-connected case. At the top: power schedule given by the tertiary controller; at the bottom: power reference given by the secondary controller

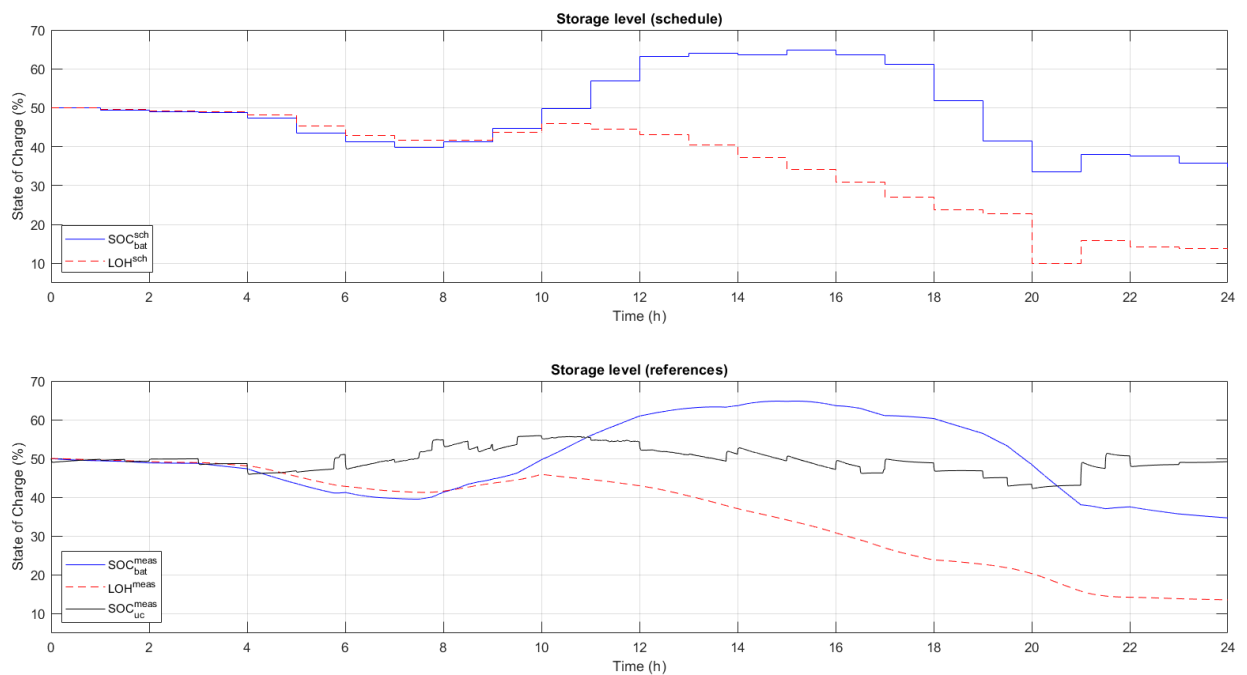


Figure 27. Storage level in the sunny and grid-connected case. At the top: storage level schedule given by the tertiary controller; at the bottom: real storage level measured from the equipment

The last simulation is done for the grid-connected case and a cloudy day. In Figure 28, the power evolution is represented both for the tertiary and the secondary controller, as in the previous simulation. Again, the power schedule is intended to be followed, mainly for the grid power. As in the previous simulation, the ultracapacitor absorbs the instantaneous changes and the battery the bigger discrepancies. The same conclusions can be extracted from Figure 29, where the storage levels are represented. As all the simulations done in this work, the outputs and power constraints are fulfilled, and the hydrogen power variations are not too high.

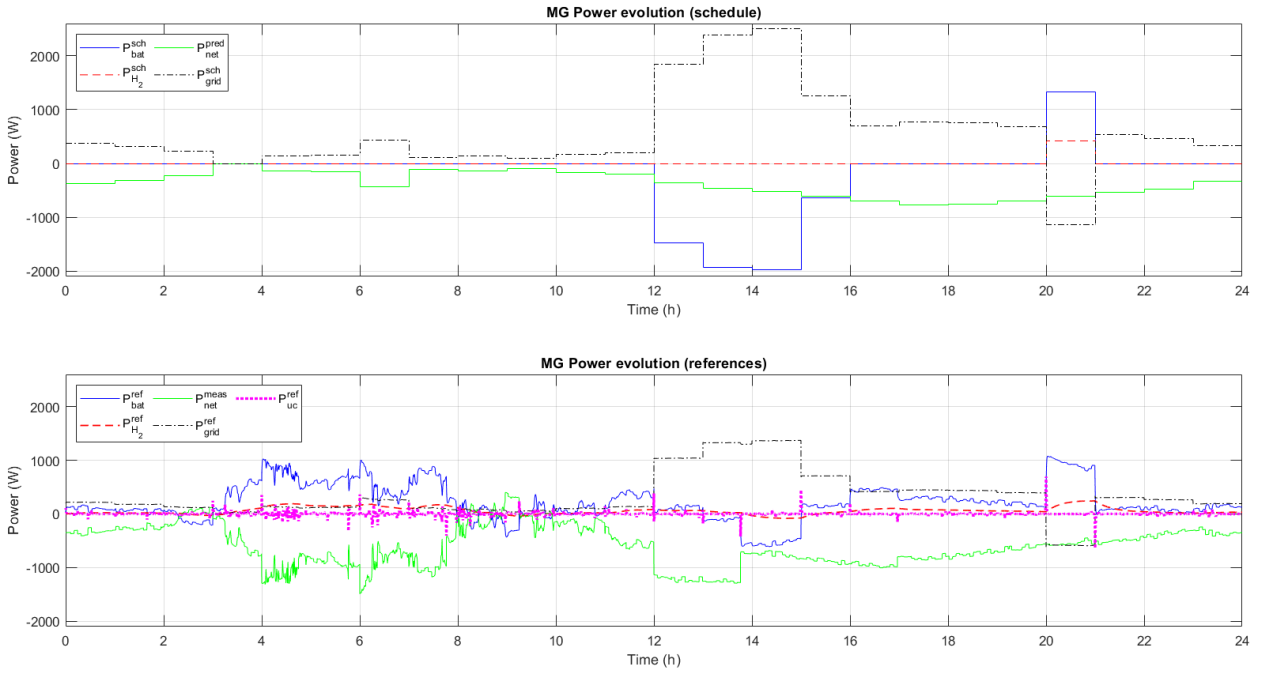


Figure 28. Power evolution in the cloudy and grid-connected case. At the top: power schedule given by the tertiary controller; at the bottom: power reference given by the secondary controller

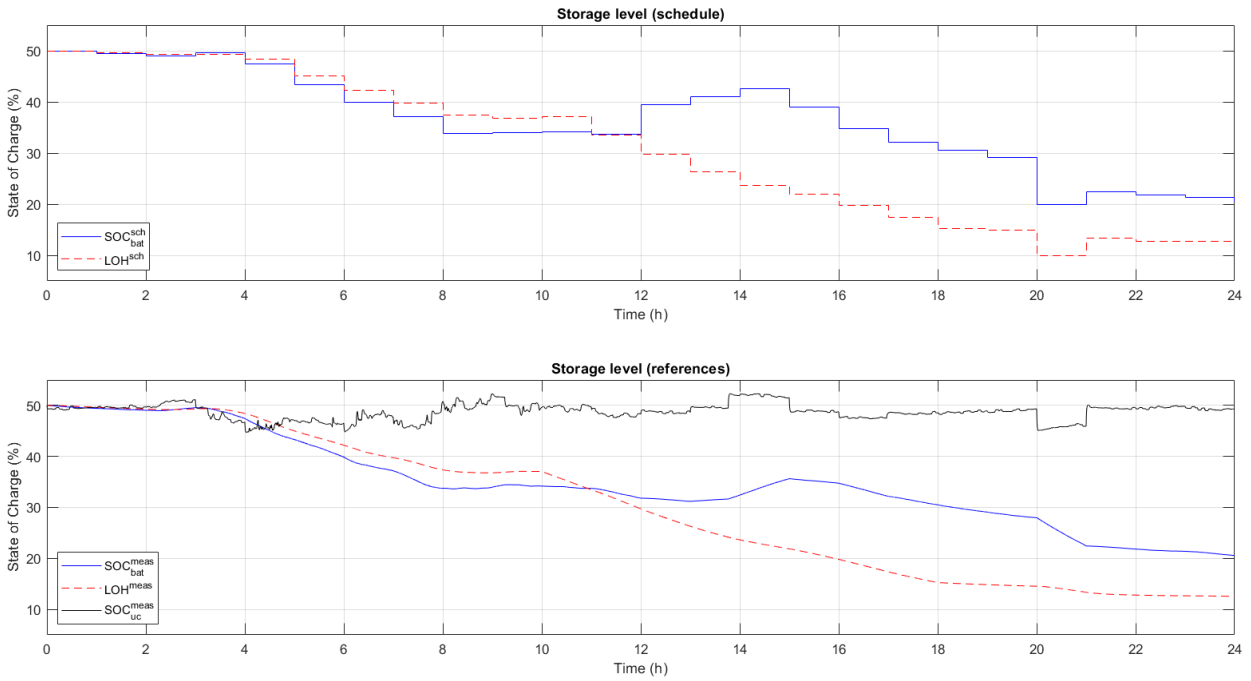


Figure 29. Storage level in the cloudy and grid-connected case. At the top: storage level schedule given by the tertiary controller; at the bottom: real storage level measured from the equipment

# 5 CONCLUSIONS

---

Once the controllers are designed and the simulation results analyzed, one can recap and some conclusions can be extracted from the work. Moreover, some drawbacks and the possible future work are going to be described in order to improve the control strategy and to progress towards the real plan implementation on the zero-emission vehicle charging microgrid.

## 5.1 Conclusions

A microgrid for zero-emission vehicle charging station has been described and modelled in this work in order to design an optimal control strategy based on MPC techniques. Two controllers have been designed and tested in simulation using MATLAB/Simulink: a tertiary controller for the economical, operation and degradation aspects optimization in a MIQP problem (using Yalmip and CPLEX) which gives the schedule every hour to a second controller, and this second controller which acts every second solving a QP problem (using quadprog) to optimally follow the schedule imposed by the tertiary controller and to take care of equipment limitations.

Some simulations have been carried out to test the controllers. Firstly, simulations both in grid connected (with sunny and cloudy days and sunny with near-zero demand day) and in islanded mode of the microgrid have been done to test the tertiary controller alone and to further observe the behaviour of binary variables. Then, the complete system with both controllers is tested under the conditions of grid-connected mode in sunny and cloudy days.

The controllers design gives good results for all the simulations done with the tertiary controller trying to maximize the economical benefit of the microgrid operation while caring about microgrid components lifecycle, and the secondary controller softening the mismatches between the schedules based on forecasts and the real scenario, where there can be many changes. These changes can be in: real power generation, real power demand and real energy price, as well as high variations due to extra power demand for the EVs charging process (which are not considered in the predictions) and the extra hydrogen demand which makes the hydrogen storage to decrease. For this task, the ultracapacitor plays a crucial role by absorbing the rapid change in power from other devices or new events. This is possible due to the high specific power of the ultracapacitor. However, for greater amounts of power deviations, the battery and then the hydrogen are usually used, because the ultracapacitor has a low specific energy.

Therefore, it has been demonstrated that the use of predictive controllers is suitable for having an optimal energy management system in a microgrid, coping with high number of variables, constraints, and size of the problem. These controllers offer a great variety of possibilities in order to design the system with specific requirements. Moreover, the use of two connected controllers as in a typical hierarchical control layer for the industry process seems to be adequate, being them well combined.

Another interesting topic is the use of hybrid energy storage system. The use of batteries, hydrogen storage and the ultracapacitor allows a better optimization strategy to the EMS. The drawbacks of one of these devices are complemented with the advantages of their others. As an example, hydrogen storage has high specific energy but low specific power and the contrary for the ultracapacitor. So, when instantaneous variations in power occur, the ultracapacitor will act, and for longer and bigger energy storage or dispatch, the hydrogen technology must be used. What is more, hydrogen technology suffers if high power variations are applied, so the startup process is intended to be minimized with the tertiary controller and the hydrogen power variations are limited.

## 5.2 Limitations and future work

As well as all the advantages which are extracted from the results analysis, there are also some drawbacks. Firstly, as it was commented during this report, when in islanded mode, the microgrid planning should be done with a longer time horizon (for example a week) in order to better size the equipment or to better plan the power exchanges with other microgrids or the main grid assuming that the islanded mode can be transformed into a connected one. If this aspect is not taken into account, there could be scenarios in islanded mode where the energy storage systems are full and there is a surplus of energy production. This situation can also occur in grid-connected mode, but the grid gives the microgrid more flexibility, although it is not recommended due the economical penalties if the schedule grid power exchange is not fulfilled.

One important aspect to improve the performance of the control strategy is the fact that a secondary controller with both continuous and logical variables can be developed. In this work, for simplicity and for shorter simulations duration, a secondary controller with only continuous variables is designed. Although it is a complete controller, which considers a lot of equipment limitations and some performance requirements, it does not allow considering the startup process for the hydrogen technology (electrolyzer and fuel cell) in order to minimize it. So, in some of the simulations for the secondary controller, one can see that this aspect has not been taken into account in this work.

Another aspect which can be considered in the future for improving this application is to better manage the EV demand. New EVs power demand profiles can be added and tested, or even demand models based on *Gaussian* distributions can be developed. Moreover, implementing a V2G strategy will increase the microgrid flexibility and this will need a specific EV charging management including both binary and continuous variables, as done in the work of [3].

Finally, as it was mentioned at the beginning of this report, this project is wanted to be carried out in a real plant. But for this materialization, some more tasks have to be done. Among others, the energy consumption, production and price forecasts must be implemented with some predictions models, the power electronics converters must be considered and controlled, and more scenarios should be proven. Furthermore, as some of the equipment was used in older projects, new experiments should be made in order to check that their model parameters remain as considered.



# REFERENCES

---

- [1] European Environment Agency. (2019, December) Share of transport greenhouse gas emissions. Data Visualization. [Online]. <https://www.eea.europa.eu/data-and-maps/daviz/share-of-transport-ghg-emissions-2/#tab-dashboard-01>
- [2] Carlos Bordons, Félix García-Torres, and Miguel A. Ridao, *Model Predictive Control of Microgrids*. Spain: Springer, 2020.
- [3] Paulo R.C. Mendes, Luis Valverde Isorna, Carlos Bordons, and Julio E. Normey-Rico, "Energy management of an experimental microgrid coupled to a V2G system," *Journal of Power Sources - ELSEVIER*, vol. 327, pp. 702-713, August 2016.
- [4] United Nations Framework Convention on Climate Change. (2021, November) COP26 Reaches Consensus on Key Actions to Address Climate Change. [Online]. <https://unfccc.int/news/cop26-reaches-consensus-on-key-actions-to-address-climate-change>
- [5] European Commission. A European Green Deal. [Online]. [https://ec.europa.eu/info/strategy/priorities-2019-2024/european-green-deal\\_en](https://ec.europa.eu/info/strategy/priorities-2019-2024/european-green-deal_en)
- [6] European Commission, "Horizon Europe - The EU Research & Innovation Programme 2021-27," Presentation 2021.
- [7] European Environment Agency. (2021, November) Greenhouse gas emissions from transport in Europe. [Online]. <https://www.eea.europa.eu/ims/greenhouse-gas-emissions-from-transport>
- [8] European Environment Agency, "Transport and environment report 2020. Train or plane?," 19, 2020.
- [9] European Environment Agency. (2021, March) Motorised transport: train, plane, road or boat - which is greenest? News. [Online]. <https://www.eea.europa.eu/highlights/motorised-transport-train-plane-road>
- [10] Secretaría de Estado de Energía. Vicepresidencia Cuarta del Gobierno de España, "Estrategia de almacenamiento energético," Ministerio para la Transición Ecológica y el Reto Demográfico (MITERD), Madrid, 2021.
- [11] Vicepresidencia Cuarta del Gobierno de España, "Hoja de ruta del hidrógeno: Una apuesta por el hidrógeno renovable," Ministerio para la Transición Ecológica y el Reto Demográfico (MITERD), Madrid, 2020.
- [12] Gobierno de España. (2021, October) La Moncloa. Presupuestos Generales del Estado 2022. [Online]. <https://www.lamoncloa.gob.es/consejodeministros/Paginas/enlaces/071021-enlace-pge.aspx>
- [13] Gobierno de España. (2021, April) La Moncloa. Pedro Sánchez: "El Plan de Recuperación es el plan económico más ambicioso de la historia reciente de España". [Online]. [https://www.lamoncloa.gob.es/presidente/actividades/Paginas/2021/130421-sanchez\\_recuperacion.aspx](https://www.lamoncloa.gob.es/presidente/actividades/Paginas/2021/130421-sanchez_recuperacion.aspx)
- [14] Luis Valverde, Felipe Rosa, and Carlos Bordons, "Design, Planning and Management of a Hydrogen-

- Based Microgrid," *IEEE Transactions on Industrial Informatics*, vol. 9, no. 3, pp. 1398-1404, August 2013.
- [15] Luis Valverde, Felipe Rosa, Alejandro J. Del Real, Alicia Arce, and Carlos Bordons, "Modeling, simulation and experimental set-up of a renewable hydrogen-based domestic microgrid," *International Journal of Hydrogen Energy - Elsevier*, vol. 38, no. 27, pp. 11672 - 11684, July 2013.
- [16] Iberdrola. Green hydrogen: an alternative that reduces emissions and cares for our planet. [Online]. <https://www.iberdrola.com/sustainability/green-hydrogen>
- [17] Repsol. (2021, January) Repsol joins international consortium to develop cutting-edge renewable hydrogen technology. [Online]. [https://www.repsol.com/imagenes/global/en/PR27012021\\_h24all\\_tcm14-207089.pdf](https://www.repsol.com/imagenes/global/en/PR27012021_h24all_tcm14-207089.pdf)
- [18] CORDIS EU Research Results. European Commission. (2021, January) Fuel Cell Hybrid PowerPack for Rail Applications. [Online]. <https://cordis.europa.eu/project/id/101006633>
- [19] bp. (2020, November) bp y Ørsted crean uno de los mayores proyectos europeos de hidrógeno renovable con base en Alemania. [Online]. [https://www.bp.com/es\\_es/spain/home/noticias/notas-de-prensa/bp\\_y\\_orsted\\_crean\\_uno\\_de\\_los\\_mayores\\_proyectos\\_europeos\\_de\\_hidrogeno\\_renovable\\_con\\_base\\_en\\_alemania.html](https://www.bp.com/es_es/spain/home/noticias/notas-de-prensa/bp_y_orsted_crean_uno_de_los_mayores_proyectos_europeos_de_hidrogeno_renovable_con_base_en_alemania.html)
- [20] North2. (2020, February) North2. Kickstarting the green hydrogen economy. [Online]. <https://www.north2.eu/en/>
- [21] Djewels. (2020, January) Djewels. Pioneering the European renewable eFuels market. [Online]. <https://djewels.eu/>
- [22] ITM Power. (2021, January) Sale to Linde of World's Largest PEM Electrolyser. [Online]. <https://www.itm-power.com/news/sale-to-linde-of-world-s-largest-pem-electrolyser>
- [23] FuelCellsWorks. (2021, January) Green Hydrogen: Air Liquide Electrolysis with H2V. [Online]. <https://fuelcellsworks.com/news/green-hydrogen-air-liquide-electrolysis-with-h2v/>
- [24] Total. (2021, January) Total and Engie partner to develop France's largest site for the production of green hydrogen from 100% renewable electricity. [Online]. <https://www.total.com/media/news/press-releases/total-and-engie-to-develop-france-s-largest-site-of-green-hydrogen>
- [25] Hybridge. Hybridge Project. [Online]. <https://www.hybridge.net/Project/Plan/>
- [26] Port of Rotterdam. (2019, April) BP, Nouryon and Port of Rotterdam partner on green hydrogen study. [Online]. <https://www.portofrotterdam.com/en/news-and-press-releases/bp-nouryon-and-port-of-rotterdam-partner-on-green-hydrogen-study>
- [27] REFHYNE. (2018, January) REFHYNE. Clean Refinery Hydrogen for Europe. [Online]. <https://refhyne.eu/>
- [28] H2Future. (2017, January) H2Future Project. [Online]. <https://www.h2future-project.eu/>
- [29] Tennet. (2018, October) Gasunie, TenneT and Thyssengas reveal detailed, green 'sector coupling' plans using power-to-gas technology. [Online]. <https://www.tennet.eu/news/detail/gasunie-tennet-and-thyssengas-reveal-detailed-green-sector-coupling-plans-using-power-to-gas-tec/>

- [30] CORDIS EU Research Results. European Commission. (2021, January) Offshore hydrogen from shoreside wind turbine integrated electrolyser. [Online]. <https://cordis.europa.eu/project/id/101007168>
- [31] CORDIS EU Research Results. European Commission. (2019, January) Implementing Fuel Cells and Hydrogen Technologies in Ports. [Online]. <https://cordis.europa.eu/project/id/826339>
- [32] CORDIS EU Research Results. European Commission. (2021, January) "GREEN HYSLAND – Deployment of a H2 Ecosystem on the Island of Mallorca". [Online]. <https://cordis.europa.eu/project/id/101007201>
- [33] El periódico de la energía. (2021, January) Endesa iniciará la planta de hidrógeno en As Pontes en 2023 con seis parques eólicos asociados. [Online]. <https://elperiodicodelaenergia.com/endesa-iniciara-la-planta-de-hidrogeno-en-as-pontes-en-2023-con-seis-parques-eolicos-asociados/>
- [34] La Voz de Asturias. (2021, February) Un proyecto de hidrógeno verde pretende crear 1.500 empleos en Asturias. [Online]. <https://www.lavozdeasturias.es/noticia/asturias/2021/02/01/proyecto-hidrogeno-verde-pretende-crear-1500-empleos-asturias/00031612179984619649320.htm>
- [35] Iberdrola. (2020) Iberdrola construirá la mayor planta de hidrógeno verde para uso industrial en Europa. [Online]. <https://www.iberdrola.com/conocenos/lineas-negocio/proyectos-emblematicos/puertollano-planta-hidrogeno-verde>
- [36] Repsol. (2020, June) Repsol desarrollará en España dos grandes proyectos de reducción de emisiones. [Online]. <https://www.repsol.com/es/sala-prensa/notas-prensa/2020/repsol-desarrollara-en-espana-dos-grandes-proyectos-de-reduccion-de-emisiones.cshtml>
- [37] Canarias7. (2021, February) Endesa contempla dos proyectos de hidrógeno verde y el paso de centrales a bi-combustible en Canarias. [Online]. <https://www.canarias7.es/economia/endesa-contempla-proyectos-20210201130152-nt.html>
- [38] Intergia. (2017) Producción de hidrógeno y uso en Vehículo de Hidrógeno – proyecto LIFE REWIND. [Online]. <https://www.intergia.es/portfolio/hidrogeno-life-rewind/>
- [39] Enagás. (2020, December) Enagás y Naturgy impulsan en León la mayor planta de hidrógeno verde de España. [Online]. [https://www.enagas.es/enagas/es/Comunicacion/NotasPrensa/17\\_12\\_2020\\_Acuerdo\\_Naturgy\\_en\\_La\\_Robla](https://www.enagas.es/enagas/es/Comunicacion/NotasPrensa/17_12_2020_Acuerdo_Naturgy_en_La_Robla)
- [40] LibreMercado. (2020, December) Amorebieta acogerá la primera planta de hidrógeno verde de España. [Online]. <https://www.libremercado.com/2020-12-17/espana-planta-hidrogeno-verde-autobuses-6690259/>
- [41] H. Görgün, "Dynamic modelling of a proton exchange membrane (PEM) electrolyzer," *International Journal of Hydrogen Energy*, vol. 31, pp. 29-38, January 2006.
- [42] T. Yigit and O. F. Selamet, "Mathematical modeling and dynamic Simulink simulation of high-pressure PEM electrolyzer system," *International Journal of Hydrogen Energy*, vol. 41, pp. 13901-13914, August 2016.
- [43] P. Fragiaco and M. Genovese, "Modeling and energy demand analysis of a scalable green hydrogen production system," *International Journal of Hydrogen Energy*, vol. 44, pp. 30237-30255, November 2019.

- [44] M. Carmo, D. L. Fritz, J. Mergel, and D. Stolten, "A comprehensive review on PEM water electrolysis," *International Journal of Hydrogen Energy*, vol. 38, pp. 4901-4934, April 2013.
- [45] B. Han, S. M. Steen III, J. Mo, and F. Zhang, "Electrochemical performance modeling of a proton exchange membrane electrolyzer cell for hydrogen energy," *International Journal of Hydrogen Energy*, vol. 40, pp. 7006-7016, June 2015.
- [46] E. N. Pistikopoulos G. S. Ogumerem, "Parametric optimization and control for a smart Proton Exchange," *Journal of Process Control*, vol. 91, pp. 37-49, July 2020.
- [47] R. Aboutni, A. Aziz, N. Benazzi, M. Elhafyani, K. Kassmi S. Dahbi, "Optimised hydrogen production by a photovoltaic-electrolysis system DC/DC converter and water flow controller," *International Journal of Hydrogen Energy*, vol. 41, pp. 20858-20866, December 2016.
- [48] M. Schalenbach, M. Carmo, D. L. Fritz, J. Mergel, and D. Stolten, "Pressurized PEM water electrolysis: Efficiency and gas crossover," *International Journal of Hydrogen Energy*, vol. 38, pp. 14921-14933, November 2013.
- [49] F. Marangio, M. Santarelli, and M. Cali, "Theoretical model and experimental analysis of a high pressure PEM water electrolyser for hydrogen production," *International Journal of Hydrogen Energy*, vol. 34, pp. 1143-1158, February 2009.
- [50] R. García-Valverde, N. Espinosa, and A. Urbina, "Simple PEM water electrolyser model and experimental validation," *International Journal of Hydrogen Energy*, vol. 37, pp. 1927-1938, January 2012.
- [51] S. Dahbi et al., "Management of excess energy in a photovoltaic/grid system by production of clean hydrogen," *International Journal of Hydrogen Energy*, vol. 43, pp. 5283-5299, March 2018.
- [52] C. Bordons, F. Rosa L. Valverde, "Power Management using Model Predictive Control in a hydrogen-based microgrid," in *38th annual conference on IEEE*, 2012, pp. 5669-5676.
- [53] I. Yahyaoui, J. E. Normey-Rico, C. de Prada, F. Tadeo Á. Serna, "Predictive Control for hydrogen production by electrolysis in an offshore platform using renewable energies," *International Journal of Hydrogen Energy*, vol. 42, pp. 12865-12876, April 2017.
- [54] Félix García-Torres and Carlos Bordons, "Optimal economic dispatch for renewable energy microgrids with hybrid storage using Model Predictive Control," in *IECON 2013 - 39th Annual Conference of the IEEE Industrial Electronics Society*, Vienna, Austria, 2013, pp. 7932 - 7937.
- [55] Félix García-Torres and Carlos Bordons, "Optimal Economical Schedule of Hydrogen-Based Microgrids With Hybrid Storage Using Model Predictive Control," *IEEE Transactions on Industrial Electronics*, vol. 62, no. 8, pp. 5195-5207, August 2015.
- [56] Félix García-Torres, Luis Valverde, and Carlos Bordons, "Optimal Load Sharing of Hydrogen-Based Microgrids With Hybrid Storage Using Model-Predictive Control," *IEEE Transactions in Industrial Electronics*, vol. 63, no. 8, pp. 4919 - 4928, March 2016.
- [57] B. Flamm, C. Peter, F. N. Büchi, and J. Lygeros, "Electrolyzer modeling and real-time control for optimized production of hydrogen gas," *Applied Energy*, vol. 281, no. 116031, January 2021.
- [58] P. Mancarella, "Green Hydrogen: A Tale From Two Countries," *IEEE Smart Grid eNewsletter*. *Smart*

*Grid - Green Hydrogen*, February 2021.

- [59] S. M. Bhagavathy and J. Thakur, "Green Hydrogen: Challenges for Commercialization," *IEEE Smart Grid eNewsletter. Smart Grid - Green Hydrogen*, January 2021.
- [60] V. Sooriarachchi, "Green Hydrogen and Transportation Industry – An Overview of High-Speed Railways," *IEEE Smart Grid eNewsletter. Smart Grid - Green Hydrogen*, February 2021.
- [61] D. Houseman, "Curtaiment of Renewables and Hydrogen," *IEEE Smart Grid eNewsletter. Smart Grid - Green Hydrogen*, February 2021.
- [62] Meryem Gizem Sürer and Hüseyin Turan Arat, "State of art of hydrogen usage as a fuel on aviation," *European Mechanical Science*, vol. 2(1), pp. 20-30, 2018.
- [63] Westküste 100. Westküste 100. [Online]. <https://www.westkueste100.de/en/>
- [64] ENABLEH2. ENABLEH2 H2020 Project. [Online]. <https://www.enableh2.eu/>
- [65] Federal Ministry of Education and Research of Germany. Kopernikus Project: P2X. [Online]. <https://www.kopernikus-projekte.de/en/projects/p2x>
- [66] Sunfire. e-Fuel. [Online]. <https://www.sunfire.de/en/e-fuel>
- [67] ZeroAvia. The first practical true zero emission aviation powertrain. [Online]. <https://www.zeroavia.com/>
- [68] EMEC. The European Marine Energy Centre LTD. HyFlyer Projects. [Online]. <http://www.emec.org.uk/projects/hydrogen-projects/hyflyer/>
- [69] AIRBUS. (2020) ZEROe. Towards the world's first zero-emission commercial aircraft. [Online]. <https://www.airbus.com/innovation/zero-emission/hydrogen/zeroe.html>
- [70] Skai. Alaka'i. Hydrogen-Powered VTOL Aircraft. [Online]. <https://www.skai.co/>
- [71] Deutsches Zentrum für Luft- und Raumfahrt (DLR). (2021, January) Project BALIS – DLR is developing and testing fuel cells in the megawatt range for air transport. [Online]. [https://www.dlr.de/content/en/articles/news/2021/01/20210121\\_balis-project-funding.html](https://www.dlr.de/content/en/articles/news/2021/01/20210121_balis-project-funding.html)
- [72] HES Energy Systems. Element One Press Release. [Online]. <https://www.hes.sg/element-one-pr>
- [73] Ahmad Baroutaji, Tabbi Wilberforce, Mohamad Ramadan, and Abdul Ghani Olabi, "Comprehensive investigation on hydrogen and fuel cell technology in the aviation and aerospace sectors," *Renewable and Sustainable Energy Reviews*, vol. 106, pp. 31-40, 2019.
- [74] Zehua Dai, Li Wang, and Shanshui Yang, "Fuel Cell Based Auxiliary Power Unit in More Electric Aircraft," in *IEEE Transportation Electrification Conference and Expo, Asia-Pacific (ITEC Asia-Pacific)*, 2017.
- [75] Nathan Gray, Shane McDonagh, Richard O'Shea, Beatrice Smyth, and Jerry D Murphy, "Decarbonising ships, planes and trucks: An analysis of suitable low-carbon fuels for the maritime, aviation and haulage sectors," *Advances in Applied Energy*, vol. 1, no. 100008, 2021.
- [76] Azhar Ul-Haq, Carlo Cecati, and Essam A. Al-Ammar, "Modeling of a Photovoltaic-Powered Electric Vehicle Charging Station with Vehicle-to-Grid Implementation," *Energies*, vol. 10, no. 1, December

2016.

- [77] Qiongie Dai, Jicheng Liu, and Qiushuang Wei, "Optimal Photovoltaic/Battery Energy Storage/Electric Vehicle Charging Station Design Based in Multi-Agent Particle Swarm Optimization Algorithm," *Sustainability*, vol. 11, no. 7, April 2019.
- [78] Semen Uimonen and Matti Lehtonen, "Simulation of electric Vehicle Charging Stations Load Profiles in Office Buildings Based on Occupancy Data," *Energies*, vol. 13, no. 21, October 2020.
- [79] Maxwell Technologies, "125V Heavy Transport Module Datasheet," Ultracapacitor datasheet.
- [80] Eduardo F. Camacho and Carlos Bordons, *Model Predictive Control*, 2nd ed.: Springer, 2007.
- [81] J. M. Maciejowski, *Predictive Control with Constraints.*: Prentice Hall, 2000.
- [82] Alberto Bemporad and Manfred Morari, "Control of systems integrating logic, dynamics, and constraints," *Automatica*, no. 35, p. 407 427, September 1998.
- [83] Proyecto AGERAR. Simugrid - Proyecto AGERAR. [Online]. <http://institucional.us.es/agerar/simugrid/>
- [84] Mathworks. Simscape Electrical - MATLAB & Simulink. [Online]. <https://es.mathworks.com/products/simscape-electrical.html>
- [85] UL. HOMER - Hybrid Renewable and Distributed Generation System Design Software. [Online]. <https://www.homerenergy.com/index.html>
- [86] Johan Löfberg, "YALMIP: A toolbox for modeling and optimization in MATLAB," in *Computer Aided Control Systems Design, 2004 IEEE International Symposium on*, 2004.
- [87] Johan Löfberg. Solvers - YALMIP. [Online]. <https://yalmip.github.io/allsolvers/>
- [88] IBM. ILOG CPLEX Optimization Studio - IBM. [Online]. <https://www.ibm.com/products/ilog-cplex-optimization-studio>
- [89] Johan Löfberg. (2016, September) Installation - YALMIP. [Online]. <https://yalmip.github.io/tutorial/installation/>
- [90] MathWorks. View or change search path - MATLAB path - MathWorks. [Online]. <https://es.mathworks.com/help/matlab/ref/path.html>
- [91] Xavier Nodet. (2020, July) CPLEX Optimization Studio is free for students and academics! [Online]. <https://community.ibm.com/community/user/datascience/blogs/xavier-nodet1/2020/07/09/cplex-free-for-students?CommunityKey=ab7de0fd-6f43-47a9-8261-33578a231bb7&tab=>
- [92] IBM. (2019) Setting up CPLEX for MATLAB - IBM Documentation. [Online]. <https://www.ibm.com/docs/en/icos/12.10.0?topic=matlab-setting-up-cplex>
- [93] Johan Löfberg. (2016, September) YALMIP. [Online]. <https://yalmip.github.io/tutorials/>
- [94] Johan Löfberg. (2016, September) sdpvar - YALMIP. [Online]. <https://yalmip.github.io/command/sdpvar/>

- 
- [95] Johan Löfberg. (2016, September) Model predictive control - Basics - YALMIP. [Online]. <https://yalmip.github.io/example/standardmpc/>
- [96] OMIE - Iberian Market Operator. (2021, November) OMIE. [Online]. <https://www.omie.es/en>
- [97] Javier Santaolaya Sánchez, "Diseño de Bancada y Sistema de Control para la Integración de Pila de Combustible en un Vehículo," Universidad de Sevilla, Sevilla, Proyecto Fin de Carrera 2017.





# NOMENCLATURE

---

ENGREEN: Laboratory of Engineering for Energy and Environmental Sustainability

MPC: Model Predictive Control

UNFCCC: United Framework Convention on Climate Change

COP26: 26<sup>th</sup> Conference of the Parties

UN: United Nations

NGEU: Next Generation Europe

GHG: Greenhouse Gas

EU: European Union

ESS: Energy Storage System

M€: Million of euros

PV: Photovoltaic

PEM: Polymer Electrolyte Membrane

DC: Direct Current

MW/GW: Mega/Giga-Watts

H<sub>2</sub>: Hydrogen

PEC: Photoelectrochemical

CO<sub>2</sub>: Carbone dioxide

BoP: Balance of Plant

MPPT: Maximum Power Point Tracking

O<sub>2</sub>: Oxygen

PMS: Power Management Strategy

SOC: State of Charge

MHL: Metal Hydride Level

MIQP: Mixed-Integer Quadratic Programming

MILP: Mixed-Integer Linear Programming

PID: Proportional, Integral and Derivative

PLC: Programmable Logic Controller

PWM: Pulse-Width Modulation

FC: Fuel Cell

APU: Auxiliary Power Unit

EV: Electric Vehicle

PHEV: Plug-in Hybrid Electric Vehicle

V2G: Vehicle-to-Grid

EMS: Energy Management System

AC: Alternating Current

MAPSO: Multi-Agent Particle Swarm Optimization

HBC: Hysteresis Band Control

LOH: Level of Hydrogen

MLD: Mixed Logical Dynamical

MIP: Mixed Integer Programming

LP: Linear Programming

QP: Quadratic Programming

HOMER: Hybrid Optimization Model for Multiple Energy Resources